LA-UR-20-26607
Approved for public release; distribution is unlimited.

Title: Charged Particle Transport Libraries Final Report FY2020 Level-2 Milestone #7127

Author(s): Paris, Mark W.
Talou, Patrick
Conlin, Jeremy Lloyd
Gibson, Nathan Andrew
Haeck, Wim
Hale, Gerald M.
Norris, Edward Thomas
Parsons, Donald Kent
Saller, Thomas

Intended for: Report

Issued: 2021-03-04 (rev.1)

To: Patrick Talou, XCP-5, MS F644
Thru: Anna Hayes-Sterbenz, T-2, MS B283
From: Mark Paris, T-2, MS 283
Phone: (505)665-0455
Symbol: LA-UR-20-26607
Date: February 22, 2021

report

ASC/PEM/Nuclear Data Project, Theoretical Division(T-2)

Subject: Charged Particle Transport Libraries Final Report
FY2020 Level-2 Milestone #7127

Authors: M. Paris (Milestone Lead, T-2), P. Talou (Project Lead, XCP-5), J. Conlin (XCP-5), N. Gibson (XCP-5), W. Haeck (XCP-5), G. Hale (T-2), E. Norris (XCP-1), K. Parsons (XCP-5), T. Saller (CCS-2)

Contents

0 Executive summary; main results

Milestone description:
Develop modern Charged Particle Transport (CPT) data libraries (tables) for suite of light elements, including stopping power dE/dx, through a revised version of the Nuclear Data Interface (NDI). Extend upper energy limit of current data files. Document new evaluations and interface in a report.

Completion criteria:

- Develop CP2020 library of CP evaluations (Section 3) ☑;
- Produce dE/dx stopping-power tables (Section 3.4.3) ☑;
- Develop new version of nuclear data interface (NDI) (Section 3.4) ☑;
- Extend upper energy limits of some data files (Section 3.1) ☑;
- Document evaluations and codes (this report) ☑.

Main results:

- **New/updated evaluated angular distributions and cross sections**:
  (i) neutrons (projectile): protons (target) (`n-001_H_001.endf`) and ^{6}Li (`n-003_Li_006.endf`) [Section 3.1.2],
  (ii) protons: protons (`p-001_H_001.endf`) and ^{4}He (`p-002_He_004.endf`) [Section 3.1.4],

(iii) deuterons: ^{3}He (`d-002_He_003.endf`) [Section 3.1.4],

(iv) tritons: ^{4}He (`t-002_He_004.endf`) [Section 3.1.4];

- **New CP2020 continuous-energy (ACE format) library** [Section 3.2.1];
- **New CP2020 multigroup (NDI format) library** [Section 3.2.2];
- **New NDI format and API bindings for CP stopping power (dE/dx)** [Section 3.4.2];
- **Comparison with ECPL-2018 LLNL evaluation charged-particle library** [Section 4.5];
- **Format corrections to CP2011 evaluated (ENDF-6 formatted) data** [Section 3.3];
- **Process CP2011 evaluations with modern (NJOY2016 & NJOY21)** [Section 3.2];
- **Corrections/improvements to processing codes** [Section 3.3].

1 Introduction

This document is the final report on the status and developments of the Charged-Particle Transport (CPT) Level-2 ("CP2020") ASC/PEM Milestone work. (Project Lead: Patrick Talou, XCP-5; Milestone Lead: Mark Paris, T-2; Personnel: J. Conlin, XCP-5; G. Hale, T-2; K. Parsons, XCP-5; T. Saller, CCS-2; Contributors: Nathan Gibson, XCP-5; Wim Haeck, XCP-5; Edward Norris, XCP-1)

This section gives an overview of the CP2020 work partitioned into two subsections: 1) a summary of the code tools used for generating CP (and other) data[1] in Section 1.2; and 2) and library data and codes access information for end users in Section 1.3.

Section 2 gives an overview of the status of previous work on charged-particle (CP) nuclear data, particularly focused on the work of the FY2011 CP Level-2 Milestone[1–3] (CP2011). New work for CP2020 is detailed in the following Section 3. Section 4 discusses testing and validation of the evaluated and processed data for the CP2020 library. Conclusions based on the experience of this Level-2 work and the outlook for future development of CPT-relevant data are given in the final Section 5. Appendices, detailed throughout the report, are provided for further information.

This report, related documentation, codes, and the CPT nuclear data libraries are available via online repository[4].

1.1 Overview of charged-particle nuclear data

The current CP2020 work follows the classification of data types adopted for the CP2011 Level-2 Milestone effort. The CPT data library that was generated for the CP2011 Milestone includes

[1] Appendix B provides a more detailed description of codes used in the evaluation of nuclear data.

four classes of data:

1. evaluated nuclear cross section (NCS) data;
2. continuous-energy (CE) NCS data stored in ACE ('A Compact ENDF') format;
3. multigroup (MG) NCS data, stored in NDI format;
4. charged-particle stopping power (or dE/dx) data, previously hard-coded.

The second two classes (CE and MG data) are derived from the evaluated NCS data, which is stored in the ENDF-6 file format. They are processed through distinct processing chains, as demonstrated in Fig. 1, detailed further below.

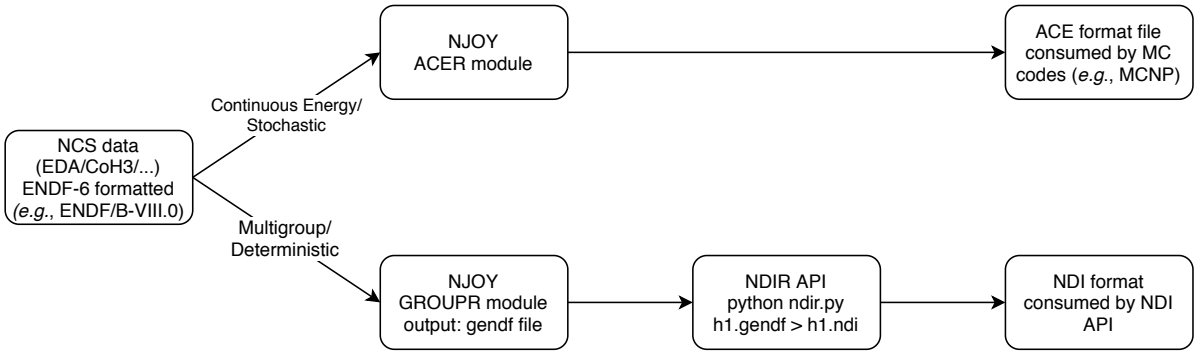

Figure 1: Nuclear data code processing pipeline from evaluated cross section (ENDF) files to CE (upper branch) and MG (lower branch) cross-section representations.

1.1.1 Nuclear cross section data evaluation

The nuclear data pipeline starts at the left-hand side of Fig.1 with the evaluated NCS data for neutron-induced charged-particle production and for charged-particle induced scattering and reactions. The NCS evaluations are produced by developing *models* of the relevant nuclear interaction physics and fitting parameters of these models to the experimentally observed physical data to obtain high-fidelity, continuous energy and angular representations of cross sections and angular distributions.

Ideally, the evaluations should simultaneously describe data from *all* of the scattering and reaction channels that couple to each other (that is, that couple to the same *compound system*) in a manner consistent with fundamental constraints imposed by the quantum theory. (For example, in order to provide evaluated cross sections for the important ^{3}He$(d,p)^4$He fusion reaction, which couples to the ^{5}Li compound system (which has 3 protons and 2 neutrons), the evaluator must provide data not only for this reaction but also for scattering – ^{3}He$(d,d)^3$He, ^{4}He(p,p)^{4}He and the breakup reaction ^{3}He$(d,np)^3$He.) In practice, only a subset of the available data is fit in the evaluations

owing to limitations inherent in the current theoretical models and code tools available to handle these inherently large-scale problems; see Section 5.

The evaluations for the CP2011 and CP2020 Level-2 Milestone efforts have their origin in two sources. Most of the evaluations arise from R-matrix analyses of neutron and charged-particle projectiles, including protons (p), deuterons (d), tritons (t), helium-3 (h), and alpha-particles (α) on light-element target materials (^{1}H, ^{2}H, ^{3}H, ^{3}He, ^{4}He, ^{6}Li, and ^{7}Li) that have been performed by Hale and collaborators in T-2/LANL[5–7]. Since the R-matrix analyses observe quantum mechanical multichannel unitarity (which implies conservation of probability), they are by-far the most accurate representations of the data available. However, the R-matrix approach becomes ponderous at higher energies, where many-body final states are accessed in breakup reactions, and simpler evaluation approaches must be adopted[8]. A few of the projectile sublibraries, taken from the TENDL09 library[9] for CP2011, have been updated to the TENDL19[10] library files for the CP2020 evaluated library. (See Table 1 and Table 4 and their discussion in Sections 2 and 3 for a detailed discussion.)

The evaluated NCS data is encoded in the ENDF-6 format[11] (or usually "ENDF"). The ENDF files provide the underlying nuclear data with emphasis on the differential scattering and reaction observables, which are distributions in energy and angle of particle production probability resulting from two-particle initiated interactions. A complete description of the ENDF format is given in Ref.[11]. We may here only highlight the format in its most broad features. The ENDF format is composed of *tapes* that form a hierarchical data container. As a data container, the tape is composed of *target material* subsections[2], defined by the `MAT` number, for a given projectile sublibrary. The `MAT` sections are further subdivided into *files*, designated by "`MF`" that contain classes of physical interaction information (*e.g.*, `MF=3` contains angle-integrated cross sections, `MF=6` contains coupled energy-angle dependent cross section distributions). Each file is subdivided into reactions specified by the *section* or `MT` number (*e.g.*, for deuteron (d) sublibrary, material ^{3}He (`MAT=325`), `MT=1` is the total cross section $\sigma_{total}(E_d)$, where E_d is the incident deuteron energy in the lab-frame, `MT=2` is the elastic cross section for the process ^{3}He $(d,d)^3$He, etc.).

Throughout this report, two notational conventions are employed to describe an ENDF tape or, equivalently, file. They may be referred to as projectile+target pairs, such as d+^{3}He, or according to their file name: (`d-002_He_003.endf`). In the latter notation, the projectile is abbreviated by a single letter – `n,p,d,t,h,a` for n, p, d, t, ^{3}He, α – and the target is designated by the convention `ZZZ_S_AAA` where `ZZZ` is the nuclear charge and `AAA` is its mass number (number of neutrons plus number of protons).

As part of a 'stretch' objective of the CP2020 Milestone effort, we have commenced an assessment of the LLNL CP data library (ECPL-2018); see Section 4.5.

[2]For the purposes of this work, all tapes contain a single target material.

1.1.2 Processing of evaluated nuclear cross section data

Practical calculations by particle transport codes, reactor physics codes, and other applications, require pointwise and multigroup-averaged nuclear cross section data, which are derived from evaluated (ENDF) data. The LANL NJOY processing code[12] consumes ENDF evaluation files and generate CE/pointwise and MG formatted data files, which are, in turn, consumed by various applications codes. Details of the processing efforts for CP2011 and CP2020, performed with various versions of the NJOY code, are described in the following sections.

1.1.3 Stopping power (dE/dx) data

Energy loss for superthermal charged particles in a plasma is primarily due to drag caused by small-angle, large-distance collisions mediated by Coulomb interactions due to thermal plasma electrons and ions. Previous work, summarized in the CP2011 Level-2 Milestone effort[13–15], have resulted in a variety of robust calculational approaches to energy loss from first-principles calculations. Detailed treatments based on analytical calculations are prohibitive due to the complexity of the theoretical models. Finite-difference approaches using energy-loss or "stopping power" dE/dx tabulated data to calculate the energy loss along charged-particle trajectories has proven to be accurate enough for the purpose of our application needs. Data for $dE/dx(E, \rho, T)$, functions of projectile energy E, plasma density ρ, and target temperature T are available for fourteen light-ion species (charge $1 \leq Z \leq 8$) propagating in plasmas comprised of these species and an additional *generic* target ion species to model energy-loss due to heavy-ion collisions. Differing model assumptions and calculational techniques provide three complete sets of dE/dx for the fourteen projectiles: *i*) RPA-based[16–19] (termed "standard") calculations with large-angle cutoff for MC transport calculations; *ii*) standard (RPA) dE/dx without a large-angle cutoff (non-MC transport); *iii*) field-theoretic calculations[20].

The dE/dx tables have not been changed for CP2020. The present effort includes work to reproduce the tables with the past codes (described in the next section), improve their availability and version-tracking (see Section 1.3.3) and to simplify their interface to improve usability in applications codes. This is done through the development of a new NDI format and advanced programming interface (API), as described in Section 3.4.

1.2 Tools to produce and deliver the libraries

Various codes that are in use for handling data, evaluation and post-processing are described in more detail in Appendix B. Here, we provide a brief summary of their purpose and uses.

1.2.1 Evaluation codes for CP data

Light-element evaluations performed at LANL/T-2 are carried out with a suite of data-handling (C5TOEDA), NCS evaluation (EDA5, EDA6, EDAF90), and post-processing (ENDFORI, SPECT, STEEP) codes. These are described in detail in Section B. Briefly, the data-handling codes are used to convert experimentally observed data from database (EXFOR/CSISRS[21]) formats to the native EDA data format. The evaluation codes express the underlying physics models of scattering and reactions for a accurate parametrization of the experimental data with few parameters.[3] At the completion of the evaluation procedure, `urd` ("unitary reaction data") files are generated from the optimized model parameters. These files encode the scattering and reaction for energy- and angular-dependent probability[4] distributions. We refer "evaluations" to mean the data produced directly by the evaluation codes as encoded in the `urd` files. The post-processing codes consume the `urd` evaluation files and convert them for various purposes. The ENDFORI application converts the evaluation files (`urd`) to ENDF formatted data (collections of which compose ENDF/B libraries); SPECT generates center-of-mass and laboratory frame spectra from the `urd` evaluation files; STEEP converts the scattering and reaction cross sections to thermal, Maxwellian-averaged interaction rates as a function of (ion) temperature.

1.2.2 Processing codes for CP data

Several codes (*e.g.* NJOY [12], AMPX[22], FUDGE[23, 24] and PREPRO[25]) are available to convert ENDF data to CE and MG formatted data. All of the ENDF evaluations for CP2011 and CP2020 have been processed with various versions of NJOY, detailed throughout the report, which provide the CE data in ACE format (via the ACER module[12, p. 499] of NJOY) data files and MG data in NDI format[26, 27], for use with the NDI API, in frequent use by deterministic applications codes at LANL.

In addition to the NJOY processing code, the processing of the ENDF files to MG and CE representations is facilitated by a suite of Python scripts referred to as the "NDVV system," or simply NDVV. These scripts were originally developed[28] as a modular code suite to enable testing of nuclear data libraries and the transport codes – both stochastic and deterministic – that consume the processed CE and MG data. The NDVV system is used in the generation of CP2011 and CP2020 MG representations of neutron-induced CP production data.

[3] The models are constructed to satisfy quantum-mechanical constraints that follow from causality and unitarity, which implies the conservation of probability for two-body–to–two-body reactions.

[4] Actually, the quantum-mechanical amplitudes, which are related to probabilities by taking their modulus squared, are stored.

1.2.3 Stopping power (dE/dx) codes

The stopping power dE/dx is computed in the random-phase approximation (RPA) via the code FermiASCnew[13–19]. The BPS[20] stopping-power theory, developed by Brown, Preston, and Singleton has been coded by Singleton (called clog, see Section 1.3.3).

1.3 Data and codes access summary

The CP2011 and CP2020 processed nuclear data libraries are accessible through both XLAN (ADX network) and HPC (yellow network) connnected computational resources.

1.3.1 CP2011 library access

CP2011 evaluated ENDF files:

- https://xcp-stash.lanl.gov/projects/CPND/repos/milestones/browse/cp2011/data/endfb-cp2011

CP2011 ACE file locations:

- XLAN: `/opt/local/codes/data/nuclear/mc/type1/CP2011`
- HPC: `/usr/projects/data/nuclear/mc/type1/CP2011`

CP2011 NDI formatted data are available from:

- XLAN: NA;
- HPC: `/usr/projects/data/nuclear/ndi/2.2.0alpha/share/sn/cp2011`

1.3.2 CP2020 library access

As of the release date of the final version of this report the CP2020 libraries have not been allocated a directory namespace; please contact the XCP-5 Nuclear Data Team (`nucldata@lanl.gov`; Team Lead, J. Conlin, `jconlin@lanl.gov`) for information on how to obtain the CP2020 cross section data library files.

1.3.3 Codes access

This section contains repository information for available codes.

Evaluation codes:

- Data-handling (EXFOR/CSISRS → EDA): https://github.com/mwparis/c5toeda

Processing code:

- NJOY
  https:www.njoy.io
- NDVV
  https://xcp-stash.lanl.gov/projects/NDT/repos/ndvv/browse

Stopping-power (dE/dx) codes:

- Standard and no-cut (RPA) code:
  https://xcp-stash.lanl.gov/projects/CPND/repos/milestones/browse/cp2011/code
- BPS (field-theoretic) code:
  https://github.com/lanl/clog

2 Status of CP2011 libraries

The context for the CP2020 Level-2 effort is determined by the extensive work performed for the CP2011 Level-2 effort[1–3]. In this section, we discuss of the evaluation and processing efforts to construct the CE and MG libraries for CP2011, accessible as described in Section 1.3.1.

2.1 Origin and content of CP2011 ACE and NDI data libraries

This subsection addresses the source of the CE and MG libraries in terms of their evaluated NCS legacy and serves to clarify and document the evaluated NCS information for the CP2011 Level-2 Milestone work. This endeavor is challenged by a long history of contributions, sometimes documented less than completely, of many evaluators. We provide several tools for the reader that summarize this voluminous database of both the neutron-induced sublibrary (or, more simply, "neutron sublibrary") and the CP-induced sublibraries. These tools include the information in Table 1 and Appendix A.

Table 1 gives a summary of the evaluated NCS ENDF-6 formatted data for the CP2011 work[1, 2]. Note that Tables 1 and 4 represent data only for those target isotopes that are equal to or heavier that the projectile; the ENDF data files themselves are also only so given. This is because the other case of the heavier projectile on a lighter target can be reconstructed from the data given in the tables.

We review some of the material from those memoranda below [see Secs.2.2.1 and 2.2.4]. We detail, in the following subsections, the content of the evaluated NCS, ENDF-6 formatted data for the CP2011 work. The information in Appendix A provides a reaction-by-reaction summary

Projectile\Target	^{1}H	^{2}H	^{3}H	^{3}He	^{4}He	^{6}Li	^{7}Li
n	VII.1^{a,b}	VII.1^{a,b}	VII.1^{a,b,c}	VII.1^{a,b}	VII.1^{d}	2011^{a,b,d}	VII.1^{b,c,d}
p	VII.1	VII.1	2001	VII.1	2011	2001	2001
d		2001	2001	2001	2011	2001	2003
t			2001	2001	2011	2003	TENDL09
$h(^{3}\mathrm{He})$				2001	2011	2001	TENDL09
α					2011	TENDL09	TENDL09

Table 1: CP2011 evaluated nuclear cross section data for scattering and reactions of neutron projectiles and CP projectiles (shown in rows) on light-element isotopes (columns). The entries R.v correspond to the ENDF/B-R.v release and version. The neutron-induced files have superscripts that designate the changes made to the base ENDF/B-R.v release: *a*) ENDF/B-R.v masses were updated; *b*) ENDF/B-R.v `MF/MT` were updated from file `MF=4,5` to an equivalent file `MF=6` designation; *c*) ENDF/B-R.v was augmented to include N-body phase space break-up spectra (but note that there was an update after the CP2011 work to the ENDF-6 manual that corrected the N-body phase space section[29] ; *d*) ENDF/B-R.v has been modified to include additional `MF/MT` data from an updated R-matrix evaluation (see the text in Secs.2.2.1 and 2.2.4 of this report and Ref.[2] for a detailed explanation). The remaining rows detail the ENDF-6 evaluated NCS datafile sources where ENDF/B-R.v library designations are given unless the processed files were local versions in which case they are designated by year (referring to work done in various years by Hale and collaborators). Entries labeled TENDL09 are from TALYS-1.0[9].

comparison of the evaluated NCS data encoded in ENDF/B-VII.1, CP2011, ENDF/B-VIII.0, and CP2020. The CP2011 ENDF library is detailed in this section [Section 2]; CP2020 is discussed in the next, Section 3.

We have reprocessed the CP2011 evaluation (ENDF) files to CE (ACE format) and MG (NDI format) libraries, corresponding to the upper (CE) and lower (MG) branches of Fig. 1. This was accomplished with modern versions of the LANL NJOY16 (the most recent version employed in the CP2011 and CP2020 work is version 2016.60) and NJOY21 (version: 1.0.5) processing codes.

We discuss CE and MG source evaluation files and their processing in the next two subsections. Processing for the CP2020 library, which adheres closely to CP2011 processing but using modern code tools, is discussed in detail in Section 3.2.

2.1.1 CP2011 Charged-particle induced sublibrary evaluations

The charged-particle induced scattering and reaction cross section evaluations, corresponding to charged projectiles $p, d, t, h(^{3}\mathrm{He}), \alpha$, for CP2011 are described in this section. Projectiles are shown in the rows of Table 1; target materials are shown in the columns of this table. (Different notation in rows and columns is in keeping with the conventions in nuclear physics that designate projectiles and targets by differing symbols.) We confine our attention in this section to the entries in Table 1

marked '2011' that were specifically addressed in the CP2011 Level-2 Milestone work. All CP2011 ENDF files are included in Appendix A for convenience.

1. ^{4}He: This section details the status of evaluation work performed for the charged-particle projectile on the ^{4}He target material (`MAT=228`), new for CP2011, and shown in the fifth column of Table 1.

   - p: The p+^{4}He evaluation for CP2011 (see the summary ENDF-digest in Table 85) was based on a LANL EDA R-matrix analysis including elastic, unpolarized and polarized (angular distribution) data for ^{4}He$(p,p)^4$He (for $0.95 < E_p < 23.7$ MeV) and ^{3}He$(d,d)^3$He. Reaction data (^{3}He$(d,p)^4$He) was limited to $E_d < 1.0$ MeV.

   - d: The CP2011 evaluation (Table 14) was based on an R-matrix evaluation[30] of the ^{6}Li compound system that includes elastic unpolarized and polarization differential angular distributions data for ^{4}He$(d,d)^4$He, integrated cross sections for ^{4}He$(d,pn)^4$He for E_d at 10.0, 10.25, and 11.0 MeV.

   - t: The t+^{4}He entrance channel (see Table 119), being part of the ^{7}Li compound system, $\sim$ n+^{6}Li, was significantly updated from the ENDF/B-VII.1 evaluation for CP2011. The R-matrix analysis, also described in the next subsection for the neutron incident sublibrary for the ^{6}Li material [Sec.2.2.3], includes elastic ^{4}He(t,t)^{4}He unpolarized data for $E_t < 18$ MeV and polarization (the A_y analyzing power) for $E_t < 14.2$ MeV angular distribution data. This data extends beyond the three-body break-up threshold at $E_t \approx 11$ MeV; the ^{4}He$(t,n)^6$Li reaction data, for 8.5 MeV $< E_t <$ 14.4 MeV and ^{4}He$(t,n_1)^6$Li $(3^+;0)$ for $E_t = 12.9$ MeV.

   - ^{3}He: The h+^{4}He (see Table 42), (^{7}Be compound system) evaluation was fairly well characterized by the data, like its isospin-$\frac{1}{2}$ partnered compound system ^{7}Li. The R-matrix analysis, based on the three configurations h+^{4}He, p+^{6}Li, and γ+^{7}Be, takes into account elastic ^{4}He(^{3}He,^{3} He)^{4}He angular distributions for unpolarized differential cross section and polarized (A_y) data for 1.72 MeV $< E_{^3\mathrm{He}} <$ 10.8 MeV. Reaction [^{4}He$(h,p)^6$Li] data was strictly unpolarized differential cross section angular distributions for 8.2 MeV $< E_{^3\mathrm{He}} <$ 10.8 MeV and angle integrated cross section capture data to the ^{7}Be ground-state, a reaction of significance in astrophysical and cosmological settings, among others.

   - ^{4}He: The α+^{4}He (see Table 11) which couples to the ^{8}Be compound system, evaluation contains differential cross sections for the elastic scattering of α-particles by ^{4}He at α energies up to 20 MeV. The evaluation was based on an extension, completed by Hale[31], of an R-matrix analysis[32] of reactions in the ^{8}Be system that included the channels α+^{4}He, p+^{7}Li, p+^{7}Li*, n+^{7}Be, n+^{7}Be*, and d+^{6}Li. The analysis included α+^{4}He differential scattering cross section data at energies from 600 keV to 38.4 MeV. The evaluation for α+^{4}He scattering was truncated at 20 MeV, below the threshold for any other reaction. Therefore, the only substantive file included was that for differential elastic α+^{4}He scattering (`MF=6, MT=2`).

2.2 CP2011 processing to continuous energy (CE) and multigroup (MG) formatted data libraries

This section reports on the state and reproducibility of existing CPT CE and MG libraries, as derived from the evaluated NCS data. We have reproduced the capabilities – with new codes – of the CP2011 Milestone work including:

- verified and documented contents of the ENDF-6 NCS data files;
- processed the ENDF-6 data via NJOY21 (version 1.0.5) (to ACE & NDI formats); and
- reproduced stopping power dE/dx tables.

2.2.1 CP2011 Processing to Continuous energy (CE) library data

The CE data, processed according to the upper branch of Fig.1, consists of both elastic scattering and reaction data with charged-particle projectiles: proton (p), deuteron (d), triton (t), helium-3 (^{3}He), and helium-4 (α). Reactions and scatterings induced by ^{6}Li and ^{7}Li are not included in Table 1; we are unaware of any request for this data.

In the next two subsections, we detail the efforts needed to bring the CP2011 evaluated data files into consistency with the new NJOY2016 code versions (NJOY2016.53, NJOY2016.57 and NJOY2016.60). See Section 3.2.1 for further details.

2.2.2 Modifications to CP2011 evaluations

We describe, in this section, format modifications that were required to process the CP2011 ENDF files with modern NJOY code versions and some minor modifications of the NJOY source itself in order to obtain numerically equivalent CE libraries to those produced for CP2011.

The CP2011 charged-particle library of ACE files was issued originally in 2011 and then updated in 2013. The library contains 25 ACE files for incident particles p, d, t, ^{3}He, and ^{4}He onto target nuclei ^{1}H, ^{2}H, ^{3}H, ^{3}He, ^{4}He, ^{6}Li, and ^{7}Li. This library is located on LANL HPC and X-Division (XLAN) computers as detailed in Section 1.3.1 in 5 subdirectories, one for each incident particle.

The evaluation files were processed with NJOY 99.336. Several memos were issued at the time[1, 33, 34].

In 2013, new evaluations provided by Hale[35] were employed for d+^{4}He (`d-002_He_004.endf`) and α+^{4}He (`a-002_He_004.endf`). These replacements were merely re-formatted versions of the originals, and did not constitute new evaluations, but addressed the fact that the original evaluations for d+^{4}He and α+^{4}He did not process correctly.

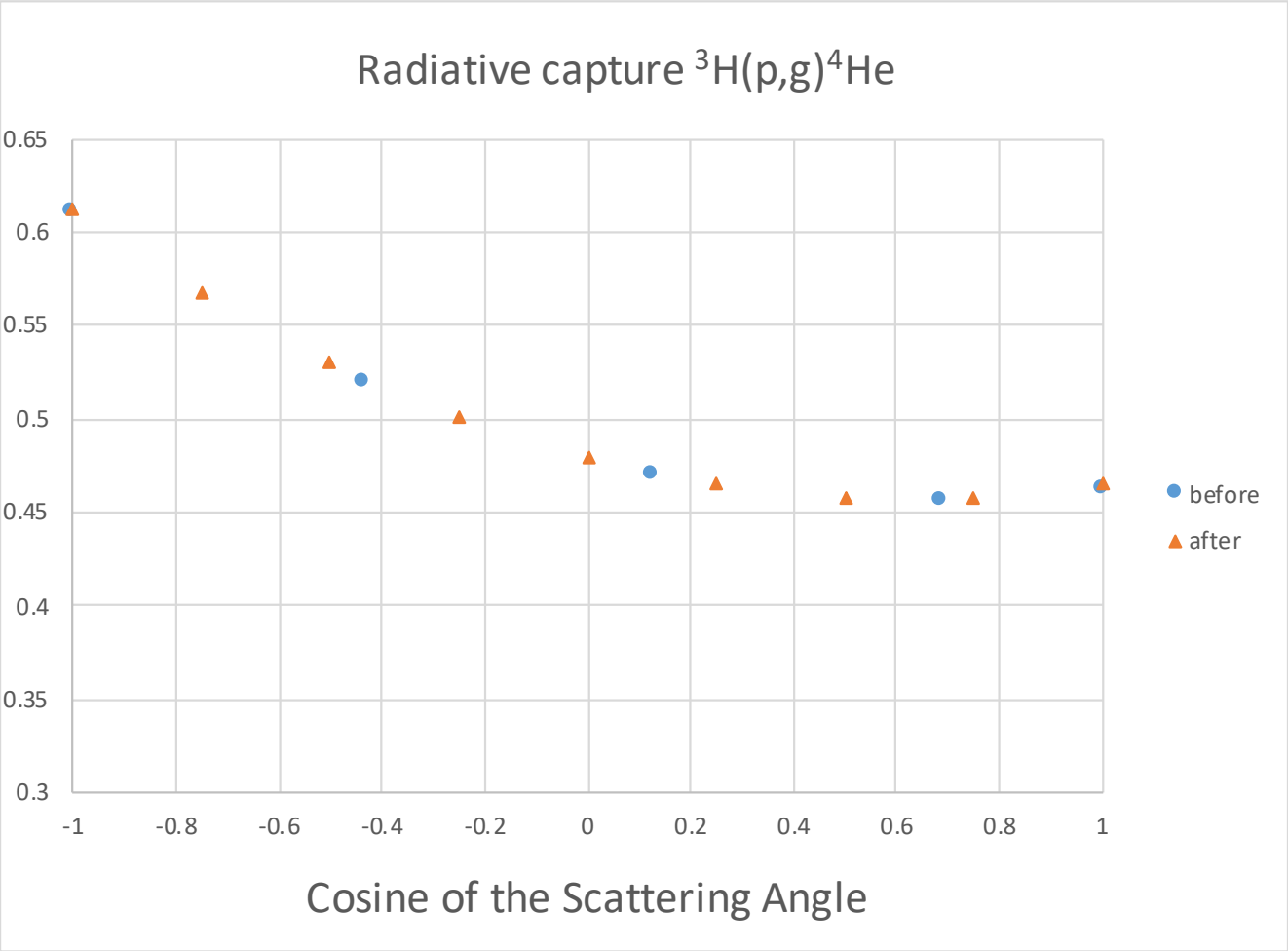

Figure 2: Photon production for $^3\mathrm{H}(p,\gamma)^4\mathrm{He}$ at $E_p = 1.2$ MeV. The 'after' data points reflect the angular distribution data represented in the ACE output file using the finer angular grid determined in the NJOY2012.99 and later versions. The 'before' data points correspond to the more coarse grid used in NJOY versions prior to NJOY2012.99.

As part of the CP2020 Milestone effort, the following question was posed: How would the evaluations used in the previous (2011 and 2013) CP efforts process with the current version of NJOY? Would the resultant ACE files be the same as before?

The short answer is no. However, we have been able to solve most of the discrepancies and characterize them numerically. Fourteen (14) of the twenty-five (25) ACE files changed (as determined by the size/byte-count of the ACE file) when the current version of NJOY (NJOY2016.53) was used for processing. Another ACE file changed (proton onto deuteron, `p-001_H_002.endf`), but still had the same byte count. The purpose of this memo is to document what has changed in NJOY (relative to charged particles) since the earlier CP work.

In a few cases, section dividers and or format corrections were required in the evaluation files, but these changes did not affect the actual charged particle data produced by NJOY. These format changes were confirmed with the utility code, DECE[36], which enforces ENDF-6 format standards.

In some cases, additional manual editing was performed on the ENDF evaluation files to remove data at energies lower than MCNP's[5] hard-coded charged particle energy cut-off of 1 keV. The low-energy data triggers instabilities in NJOY for the angular distribution of the Rutherford scattering and so was removed.

An executable of the NJOY processing code with version number NJOY99.336, the NJOY code version that was used to process the ENDF evaluation files in 2011, was recovered from file storage. During the course of this testing, several versions of NJOY– NJOY2016.53 and NJOY2016.57 – were also used in testing.

Findings

The CP2011 evaluation files were first re-processed using NJOY99.336. Processing with NJOY99.336 produced no substantive changes compared to the processed CP2011 ACE files, which were determined to be otherwise identical by the unix `diff` utility. See findings (1), (3), and (5) below for details on the three cosmetic and understood exceptions.

(1) The p+^{2}H evaluation file has negative Q values for the `MT=102` reaction. This is an error which has been remedied in the CP2020 version of this file (`p-001_H_002.endf`). In previous work on the CP2011 (also in 2013), the ACE file was manually corrected by changing the -5.493539 MeV to 5.493539 MeV in 2 places.

(2) In NJOY2012.99(2017-07-30), the tolerance values for interpolation in subroutine `ptleg2`[38] were changed. The change in these tolerance settings changes the angular grid used by NJOY. Changes to the number of points in the angular grid explains the change in the length of the ACE file. However, the basic ACE data is not altered. It is simply given on a finer (or coarser) angular grid. A sample plot is given in Fig. 2.

A special-purpose version of NJOY (NJOY2016.57) implements the coarser grid from the

[5]MCNP[37] is the LANL stochastic/MC neutronics and charged-particle transport code.

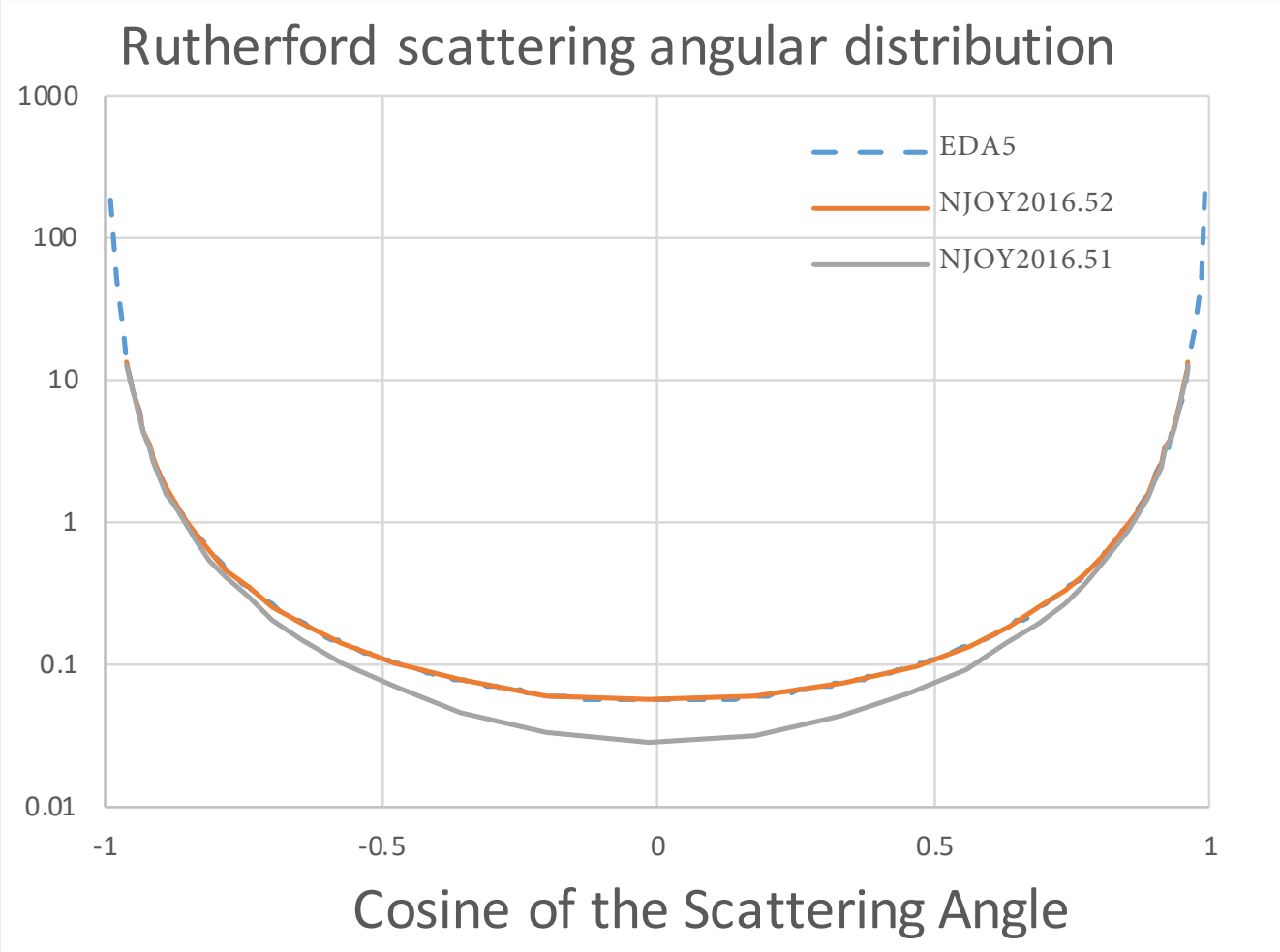

Figure 3: Verification of the bug-fix in NJOY 2016.52 for d+^{2}H at 1 MeV as shown by the agreement between the corrected NJOY 2016.52 code version and code based on the EDA5 evaluation code. The erroneous code in NJOY 2016.51 caused the deviation between the evaluated EDA5 curve and the curve marked NJOY 2016.51.

pre-NJOY2012.99 versions by modifying tolerance settings in the NJOY source code. When the 25 original evaluation files were processed with the special-purpose version of 2016.57, only 5 (not counting p+^{2}H) of the ACE files remained discrepant (by byte-count) from the previously processed CP2011 files. These five files are discussed in findings (3), (4), (5), and (6) – 2 files.

We provide a more detailed comparison in Table 2 of 20 ACE formatted files processed from the format-modified CP2011 ENDF evaluation files with NJOY 2016.57. These files have the same byte- and line-counts but are numerically different. The table characterizes these numerical differences in relative terms[6] The two files are the one produced by NJOY 99.336 and the one produced by a special version of NJOY 2016.57. There are 4 ACE files with relative differences as large as 1%; the differences show up as early as NJOY 2012.39 (dated Sept 2014) – before the `ptleg2` changes in NJOY 2012.99 (dated July 2017).

[6] A python script developed by Gray[39] `fcmp.py`, available in the Milestones repository[4], was used to determine the relative differences in corresponding integer and real numbers in the two ACE files.

Projectile	Target	Max Relative Difference	Comments
α	^{7}Li	< 5.0e-03	Between 99.336 and 2016.57
d	^{3}H	< 1.0e-05	
d	^{3}He	< 1.0e-05	
d	^{6}Li	< 1.0e-05	
d	^{7}Li	< 1.0e-06	
h	^{3}He	< 1.0e-05	
h	^{6}Li	< 1.0e-05	
h	^{7}Li	3 values > 1.0e-02	Between 99.336 and 2016.57
p	^{1}H	< 1.0e-04	
p	^{2}H	< 1.0e-05	Except values related to –Q
p	^{3}H	< 1.0e-05	
p	^{3}He	< 1.0e-05	
p	^{4}He	< 1.0e-05	
p	^{6}Li	< 1.0e-06	
p	^{7}Li	< 1.0e-05	
t	^{3}H	< 1.0e-05	
t	^{3}He	< 1.0e-05	
t	^{4}He	< 1.0e-01	Between 99.336 and 2016.57
t	^{6}Li	< 1.0e-05	
t	^{7}Li	< 1.0e-02	Between 99.336 and 2016.57

Table 2: Numerical precision ACE processing by NJOY2016.57 of CP2011 ENDF files to ACE format compared to previously used version (NJOY99.336) in CP2011.

It is not currently known what caused the problems in the 4 files with relative errors on the order of 1%; they are likely too small to affect any application given other, larger sources of error.

(3) For the h+^{4}He, two of the format settings (concerning how many dictionary entries are present) were incorrect and that some of the MF 6 data was not being read. The format information on the incorrect version of the evaluation file has been fixed.

(4) For α+^{6}Li, the TENDL evaluation contains `MF=3, MT=5` array that was empty (i.e., all zeros). At version 2012.41 (December 2014) coding was added to NJOY to handle this unique situation. None of the other TENDL nor LANL files have empty `MF=3, MT=5` arrays. The new coding omits secondary particle production processing of any `MF=6, MT=5` data when the `MF=3, MT=5` array is empty, so the more current ACE files are reduced in size, but no actual CP data was changed.

(5) For d+^{4}He, the byte-count changed, but the data content did not. Using "`diff --b`" showed

that the differences were blank characters, not numerical data. In fact, the byte count difference was equal to the number of lines. If more modern versions of NJOY (see item 2 above) are used, then some slight differences can also appear in the least significant digit of some of the CP data.

(6) Early in the CP2020 effort a bug (in NJOY2016.51) was detected for identical charged-particle elastic scattering (`MF=6, MT=2, LAW=5`) corrected in NJOY2016.52 (November 2019)[Section 3.3.1]. This affected d+d and for α+^{4}He processing. The resulting corrected angular distribution has been verified Hale and Parsons by comparing the angular distribution for Rutherford (Coulomb-only) elastic scattering, for two energies – 1 keV and 1 MeV. The comparison was made using code developed by Hale, derived from the EDA5 main code, and the two NJOY code versions – NJOY2016.51 (uncorrected) and NJOY2016.52 (corrected). The comparison for one of the energies (1 MeV) is displayed in Fig. 3.

The LTP Issue

The CP2011 p+^{2}H evaluation and all TENDL09 evaluations use option `LTP = 12` for the charged-particle elastic scattering, `LAW=5`. This option is not coded into NJOY (neither during the 2011–2013 time frame nor currently). The NJOY coding in the relevant subroutine `acefc.f90` handles only `LTP = 1` or anything else (intending `LTP =2`). The ENDF-6 format and the NJOY manual[12] include `LTP =12,14` and `15`.

A further complication arises due to a typo in the ENDF-6 formats manual[11] where the terminology `LPT` is used in Section 6.3.1 on elastic scattering. However, everywhere else, the terminology is `LTP`. Kahler[40] originally raised this issue in August, 2011 but the NJOY source code was determined to be correct[34].

2.2.3 CP2011 Neutron-induced sublibrary evaluations

The neutron sublibrary, which has been processed to both CE (ACE) and MG (NDI) NCS representations, corresponding to both the upper (CE) and lower (MG) processing branches of Fig. 1, was based upon the ENDF/B-VII.1 (β4 release) neutron sublibrary; here we focus on the lower (MG) branch. The CP2011 work featured the addition of new evaluations by Hale[2] for neutron-induced CP spectra due to the reaction ^{6}Li$(n,n'd)^4$He and the inclusion of (N-body phase-space – see Ref.[11], Sec.6.2.8 for a detailed description of the `LAW=6` multi-body breakup spectra) information for "all" (meaning neutrons, photons, and charged-particle) emission spectra[7].

The details of changes and extensions of the ENDF/B-VII.1 as described in memorandum [2] for the neutron sublibrary are elaborated upon here. Most of these details are concerned with updating mass parameters (atomic weight ratio (AWR), relative to the neutron) to be consistent with NNDC standards and to restructuring the evaluated data by simply moving already stored

[7]The N-body phase-space spectra is not based upon an R-matrix evaluation. It therefore neglects dynamical information, encoding only the physics of the energy-conserving kinematics of the N-body breakup but neglecting nuclear structure and reaction contributions.

information from one file/section data container (specified by MF/MT) to a physically equivalent file/section; note that this does not represent a change in the evaluated NCS information, it is simply a change of format. This reflects the fact that MF=6 file specification is now the preferred data container specification for both neutron-induced and charged-particle induced reactions.

1. ^{1}H: The MF=4, MT=2 two-body elastic scattering distribution was changed to the MF=6 formalism and the recoil added explicitly, as can be seen from Tables 69 (ENDF/B-VII.1) and 70 (CP2011). The AWR values for the MF=6 MT=102 capture data were updated.

2. ^{2}H: The MF=4 MT=2 two-body elastic scattering distribution was changed to the MF=6 formalism and the recoil added explicitly (see Tables 49 and 50). The MF=6 MT=16 threshold energy was updated to be consistent with the MF=3 value. The AWR values for the MF=6 MT=16 $(n, 2n)$ data were updated. The MF=12 & 14, MT=102 capture photon emission data were converted into a MF=6 formalism and the recoil triton added explicitly.

3. ^{3}H: The AWR for ^{3}Hwas updated throughout the file. The MF=4, MT 2 two-body elastic scattering distribution was changed to the MF=6 formalism and the recoil added explicitly. The MF=4 & 5, MT=16 data state that they were created from an N-body phase space distribution. (These data predate the availability of this law (LAW=6) in the ENDF format.) This distribution has been converted into an MF=6 N-body phase space distribution and the recoil deuteron added explicitly. See Tables 53 and 54.

4. ^{3}He: The AWR for ^{3}He was updated throughout the file. The MF=4 MT=2 two-body elastic scattering distribution was changed to the MF=6 formalism and the recoil added explicitly (see Tables 65 and 66). No emission distribution data were provided in the ENDF/B-VII.1 evaluation for the $^{3}\mathrm{He}(n,\gamma)^{4}\mathrm{He}$, $^{3}\mathrm{He}(n,p)^{3}\mathrm{H}$ or $^{3}\mathrm{He}(n,d)^{2}\mathrm{H}$ reactions. The capture photon is assumed to be an isotropic primary gamma and added using the capture Q-value; the recoil α is also explicitly given. Emissions for the (n,p) and (n,d) channels have been added assuming isotropic center-of-mass two-body scattering.

5. ^{4}He: The MF=4 MT=2 two-body elastic scattering distribution was changed to the MF=6 formalism and the recoil added explicitly; see Tables 73 and 74.

6. ^{6}Li: The $n+^{6}$ Li $\sim^{7}$ Li system R-matrix evaluation was fairly well-developed at energies $E_n \lesssim 4.3$ MeV, the threshold for four-body $(p+2n+^{4}\mathrm{He})$ break-up, for the ENDF/B-VIII.0 evaluated library. The R-matrix analysis contains four two-body configurations, $t+^{4}$He, $n+^{6}$Li, $n+^{6}$Li $(3^{+};0)$[8], and $d+^{5}$He; the χ^2/dof ≈ 1.36 for $\sim 3,800$ data points. It contains differential and integrated cross sections and spectra for total, elastic, inelastic, $(n, 2n\alpha)$, $(n, n'd)$, (n, n_1), capture (n,γ), and charged-particle production information on (n,p) and the important (n, t_0) reaction. This new R-matrix analysis took into account IAEA Standards requirements (in the energy range $E_{n,\mathrm{th}} < E_n < 1$ MeV)[9] and the high-energy region, $E_n > 3.8$ MeV was taken from ENDF/B-VII.1. The MF=4 MT=2 two-body elastic scatter-

[8]Isomeric and resonant configurations of a compound system are denoted by $^{A}Z(J^{\pi};T)$, where A, Z are the number of nucleons and the atomic symbol for Z protons, J, π is the nuclear spin and parity, and T is the isospin.

[9]The thermal neutron energy is $E_{n,\mathrm{th}} = 0.0253$ eV $\leftrightarrow v_{n,\mathrm{th}} \approx 2,200$ m/s at $T \approx 293.15$ K.

ing distribution was changed to the MF=6 formalism and the recoil added explicitly. The ^{6}Li$(n, 2np)^4$He reaction was relabeled from MT=24 to 41 (see Tables 57 and 58) to adhere to the standard convention of describing light particles as emission and recoil as the heavier daughter. The MF=6 MT=41 (^{6}Li$(n, 2np)^4$He) N-body phase space law was assumed for the emission distribution for each particle, consistent with the description employed for MF=4 & 5 neutron distribution. The ^{6}Li$(n, n'd)^4$He (MT=32, referred to in the ENDF-6 manual as (z,nd)) breakup was provided in an R-matrix evaluation (code EDA5; post-processing spectra code SPECT)[41]. It assumes isotropic scattering, neglecting potentially significant anisotropic effects. The MF=4 MT=57 inelastic neutron distribution was converted to the MF=6 formalism; a primary γ-channel was added using the MF=3 Q-value, assumed isotropically distributed, and recoil was added explicitly. The AWR values in the MF=6 MT=105 ^{6}Li$(n, t)^4$He distribution were updated. The capture photon is assumed to be an isotropic primary gamma and added using the capture Q-value; the recoil is also explicitly given. Emission for the ^{6}Li$(n, p)^6$He channel was added assuming isotropic center-of-mass two-body scattering.

7. ^{7}Li: Tables 61 (ENDF/B-VII.1) and 62 (CP2011) summarize the content of ^{7}Lineutron sublibraries. The MF=4 MT=2 two-body elastic scattering distribution was changed to the MF=6 formalism and the recoil added explicitly. The ^{7}Li$(n, 2nd)^4$He and ^{7}Li$(n, 3np)^4$He reactions were relabeled from MT=24 and 25 to MT=11 and 42, respectively, adhering to the standard convention that describes light particles as emission and the recoil as the heaviest daughter The MF=6 MT=11, 16 & 42 N-body phase space law was used to provide emission distributions for each particle; this is consistent with the assumption for the MF=4 & 5 neutron distributions. The ^{7}Li$(n, n't)^4$He MF=4 neutron emission distributions were converted to the MF=6 formalism and breakup t+α emission distributions were added using the N-body phase space law. The MF=12 & 14 capture photon emission data were converted into the MF=6 formalism and the recoil added explicitly. Emissions for the (n,d) channel was added assuming isotropic center-of-mass two-body scattering.

2.2.4 CP2011 Multigroup (MG) processing

The evaluations described in the previous subsection were processed through historically developed standard settings using NJOY99 (version 99.368) corresponding to LANL618 and LANL103 multienergy group structures for neutron and charged-particle files and photon evaluated data, respectively. This procedure is discussed in greater detail in this report; see Section 3.2. Using the procedures described in Section 3.2, we have reproduced the processed libraries identically to the work completed in CP2011. Further, this has been done using new processing code versions of NJOY16 (version 2016.53 [07Nov19]) and NJOY21 (version: 1.0.5), which represents the completion of a primary objective of this Level-2 Milestone.

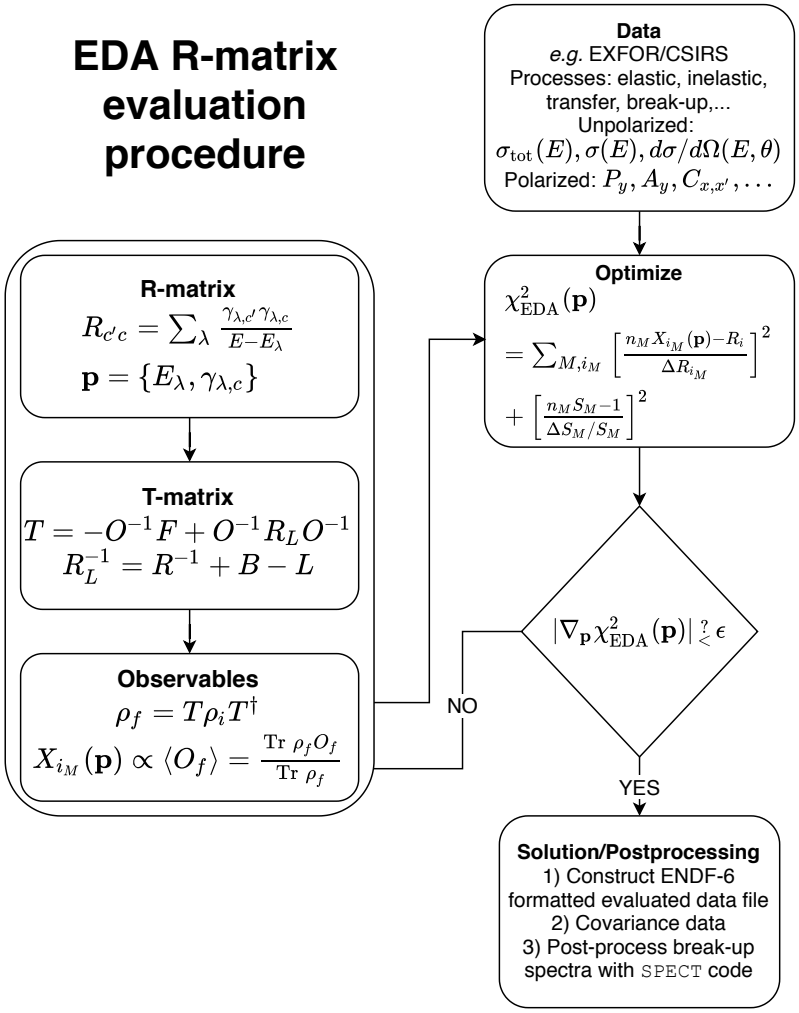

Figure 4: Flowchart for R-matrix evaluation, according to EDA5.

3 CP2020 library

Having outlined the ND pipeline (Fig. 1) and the verification of processing code capabilities of the previous CP2011 NCS libraries, we turn to the new work performed for the CP2020 NCS libraries.

Developments in evaluated ENDF NCS data, the processing of this data into CE and MG formats with modern NJOY code versions (NJOY16 and NJOY21), and a new capability in NDI format and NDI API development for stopping power are detailed in this section.

3.1 CP2020 Evaluated data

Evaluated NCS for CP2020 is being supplied from new evaluation work, extensions of recent evaluations, and evaluated data from the latest, current NNDC evaluated library release, ENDF/B-VIII.0.

The entries in Table 4 display the designations for the updated CP2020 evaluated NCS data.

We first give an overview of the evaluation procedure employed using the LANL R-matrix code EDA5 (see Appendix B). We focus on the ^{5}Li compound system as a concrete example.

3.1.1 R-matrix evaluation: ^{5}Li system example

The flowchart in Fig. 4 shows the course of a typical evaluation. An evaluation begins (at the upper-right portion of the figure) with the observed experimental data. The observables are energy- and/or angle-dependent quantities that may depend on the polarization of the interacting particles (such as the quantities $P_y, A_y, C_{x,x'}, \ldots$[42]) or not (such as $\sigma_{\rm tot}(E), \sigma(E), d\sigma/d\Omega(E,\theta), \ldots$). We emphasize that observables of all known processes observed in all known experiments are included in the data set for a given compound system. For example, the R-matrix evaluation for the compound system ^{5}Li, which couples to the following channels:

$$^5\mathrm{Li} \simeq p \otimes {}^4\mathrm{He} + d \otimes {}^3\mathrm{He} + n \otimes p \otimes {}^3\mathrm{He} + \cdots,$$

includes all of the processes linking these channels for which there is observed experimental data available. (Here the $\otimes$ symbol indicates the direct product in the quantum mechanical Hilbert space.) The processes for which experimental data is available for the ^{5}Li system is show in Table 3.

The top portion of Table 3 shows the channels along with the channel-radius parameters a_c of the R-matrix parametrization and the maximum value of the orbital angular momentum $\ell_{\rm max}$ for the channel. The scattering and reaction processes (collectively "Reactions") of the ^{5}Li compound system are shown in the left column of the lower portion of the table. Energy ranges, numbers of data points and types of observables are shown in the remaining columns of the lower portion.

The R-matrix approach is a phenomenological model, parametrized by the channel-radii, a_c, the level λ energies and reduced widths, E_λ and $\gamma_{\lambda,c}$, respectively.[10] (See Fig. 4.)

Given the data and the model parametrization of the R matrix, we obtain a high-fidelity, simultaneous description of the data by optimizing the χ^2-function:

$$\chi^2_{\rm EDA}(\mathbf{p}) = \sum_{M,i_M} \left[\frac{n_{i_M} X_{i_M}(\mathbf{p}) - R_{i_M}}{\Delta R_{i_M}}\right]^2 + \left[\frac{n_M S_M - 1}{\Delta S_M/S_M}\right]^2. \quad (1)$$

[10] We avoid a description of some technical details of the R-matrix approach such as the *boundary condition* parameters, b_c.[43].

Channel	a_c (fm)	$\ell_{\max}$
d +^{3}He($\frac{1}{2}^+$)	4.8	4
p +^{4}He(0^+)	2.9	4
p +^{4}He*(0^+; 20.2 MeV)	3.4	2
d_0+^{3}He($\frac{1}{2}^+$)	5.1	0

Reaction	Energy Range (MeV)	# Data Points	Observables
^{3}He$(d,d)^3$He	$E_d = 0.32 - 10.0$	2,229	$\sigma(\theta), A_i, A_{ii}$, $C_{i,j}, C_{ij,k}, K_{i,j'k'}, K_{ij,k'l'}$
^{3}He$(d,p)^4$He	$E_d = 0.13 - 10.0$	3,839	$\sigma(E), \sigma(\theta), A_i, A_{ii}$, $C_{i,j}, K_{ij,k'}$
^{3}He$(d,p)^4$He*	$E_d = 3.70 - 6.70$	28	$\sigma(\theta)$
^{4}He$(p,p)^4$He	$E_p = 0.92 - 34.3$	867	$\sigma(E), \sigma(\theta), A_y, P_y$
	Total:	6963	

Table 3: Channel configuration (top) and data summary (bottom) for the ^{5}Li system analysis. The column labeled "Observables" indicates the following data types: $\sigma(E)$, integrated cross section; $\sigma(\theta)$, unpolarized angular distributions (energy-dependence suppressed); A initial-state analyzing power; P final-state polarization; C spin correlation coefficients; K polarization transfer coefficients. (We have suppressed the indices $i, j, \ldots$ which take on values x, y, z for spins/polarization directions in configuration space.) All polarization and spin distributions are angular distributions, which depend on the angle of the outgoing particle. Chi-squared per degree of freedom for the analysis is $\chi^2/\text{dof} \simeq 2.7$ over 7,178 data points, 215 of which were discarded by eliminating individual data points which contribute to $\chi^2 > 40$.

Here, the vector of parameters $\mathbf{p}$ is shorthand for the R-matrix parmeters, $E_\lambda, \gamma_{\lambda,c}$, the $\sum_M$ is over all observed experimental setups M for a given observable type, and i_M indexes the kinematic points (in energy and/or angle) for a particular experimental setup M to measure a single observable type. The X_{i_M} are the calculated values of the observable reaction quantities measured in the an experimental setup M, corresponding to the right-most "Observables" column in Table 3. The observed experimental data are denoted R_{i_M}, along with their corresponding total (systematic and statistical) errors ΔR_{i_M}. Each observable type i_M is assigned an energy-independent normalization constant n_{i_M} to take into account the uncertainties ΔS_{i_M} in the experimentally determined measurement scale S_{i_M}.

Error bands, corresponding to the 90% confidence range of the χ^2-distribution are computed for the evaluated observables (cross sections and angular distributions) and shown as shaded bands, as in Fig. 5, throughout this report.

Projectile\Target	^{1}H	^{2}H	^{3}H	^{3}He	^{4}He	^{6}Li	^{7}Li
n	2020	VIII.0	VIII.0	VIII.0	VIII.0	2020	VIII.0
p	2020	VIII.0	VIII.0	VIII.0	2020	VIII.0	VIII.0
d		VIII.0	VIII.0	2020	VIII.0[a]	VIII.0	VIII.0
t			VIII.0	VIII.0	2020	VIII.0	TENDL19
$h(^{3}\mathrm{He})$				VIII.0	VIII.0	VIII.0	TENDL19
α					VIII.0	TENDL19	TENDL19

Table 4: Updated CP2020 NCS evaluated data entries show designations for evaluated nuclear cross section data for scattering and reactions of neutron projectiles and CP projectiles (shown in rows) on light-element isotopes (columns). The entries ENDF/B-VIII.0 indicate the latest, release version of the NNDC evaluated NCS library. Local, updated versions are designated '2020' and described in the text. The entries labeled TENDL19 are taken from Ref.[10].*a*) Phase space spectra added to this evaluation for CP2020.

3.1.2 Incident neutron sublibrary

The neutron sublibrary, given in top row of Table 4, includes two new evaluations that extend the energy range of various observables. These evaluations, denoted in the table as '2020', are for the nucleon-nucleon (NN) and ^{7}Li(n+^{6}Li) systems.

Note that for all of the evaluated cross section data provided in this section the evaluation's resonance parameters, which would appear in ENDF-6 file/section `MF=2, MT=151`, have not been released in the ENDF/B library due to LANL EDA-code specific issues. This information is important for performing cross-section sensitivity studies of user applications. A proposal to the NNDC Cross Section Evaluation Working Group[44], provisionally approved at the November, 2019 meeting of the CSEWG Formats Committee session, will remedy this long-standing deficiency in the R-matrix evaluated cross section files.

We consider each target nuclide (columns in Table 4) for the neutron-induced reactions the remainder of this subsection.[11]

1. ^{1}H †: This new evaluation for CP2020 is an extension, with respect to the previous ENDF/B-VIII.0 evaluation, of the upper-limit of the incident projectile energy. The previous ENDF/B-VIII.0 evaluation, summarized in Table 71, consists of total, elastic, capture, and deuteron photo-disintegration cross sections, with covariances, up to 20 MeV of the NN system: nn, np, pp, and $d\gamma$ data, simultaneously fit. The CP2020 evaluation, Figs. 5 and 6 extends the incident neutron energy range to 50 MeV and designated in the top row of Table 4 as '2020.'

[11] A dagger (†) after the target nuclide indicates an IAEA Standards[45] cross section, which can indicate significant effort and comprehensive uncertainty quantification in the Standards energy range, here $p(n,n)p$ from 1 keV to 20 MeV.

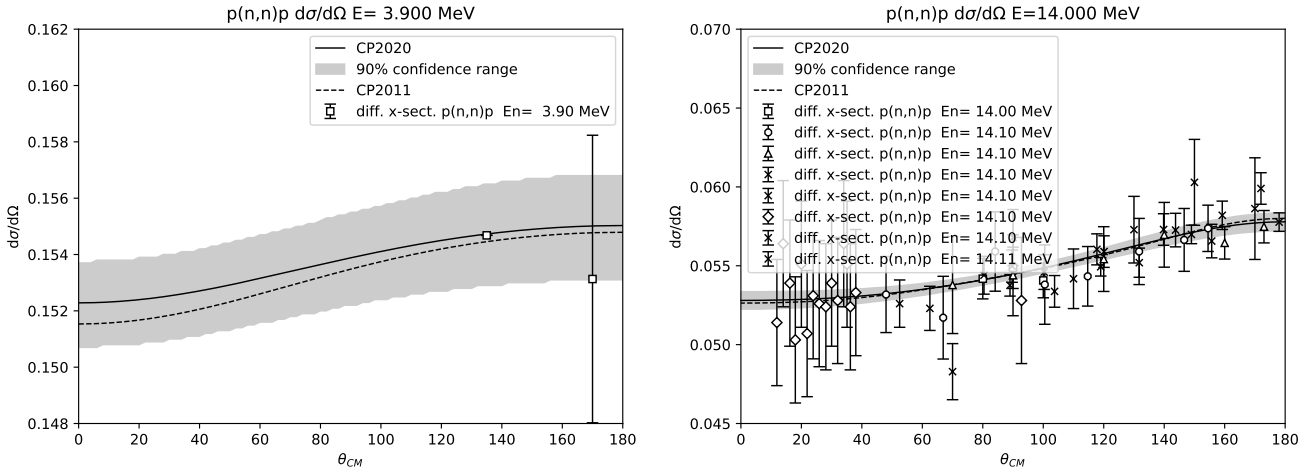

(a) (b)

(c) (d)

Figure 5: The CP2020 differential cross section angular distributions (solid curves), in the center-of-mass frame, compared with those of CP2011 (dashed curves; when available) and the experimentally observed data for the $^{1}\mathrm{H}(n,n)^{1}\mathrm{H}$ reaction. The CP2011 evaluation covered neutron incident laboratory energies from $0 \leq E_n \leq 30$ MeV; the CP2020 fit data up to $E_n \simeq 50$ MeV. Panels (a)–(d) correspond to incident laboratory neutron energies E_n (in MeV) 3.90, 14.0, 23.7, 50.0, respectively. (Both CP2011 and CP2020 have identical high-energy extensions to $E_n \simeq 150$ MeV.)

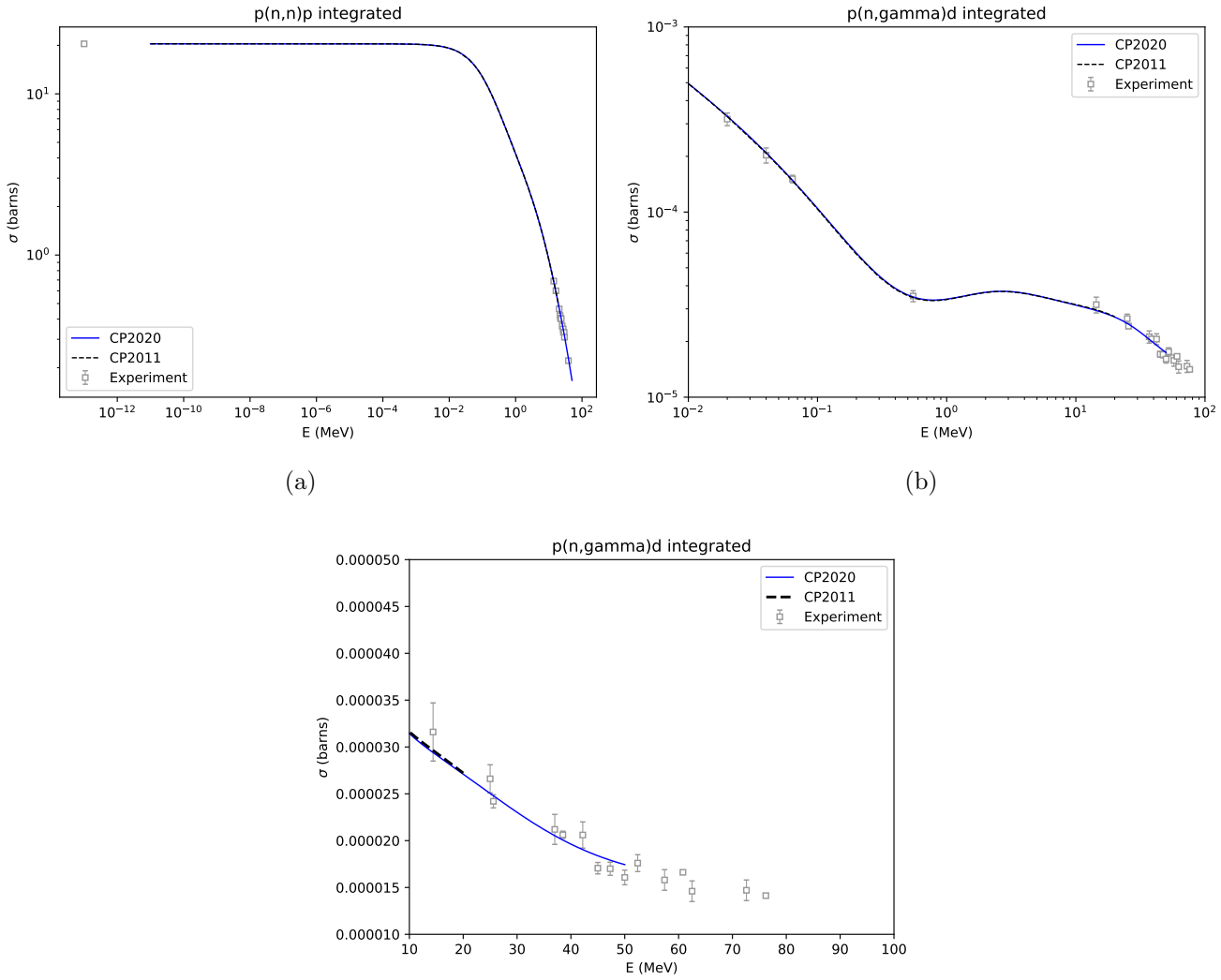

Figure 6: The CP2020 integrated cross sections (solid, blue curves) compared with those of CP2011 (dashed curves) and the experimentally observed data for: (a) $^{1}\mathrm{H}(n,n)^{1}\mathrm{H}$ reaction; (b) $^{1}\mathrm{H}(n,\gamma)^{2}\mathrm{H}$ reaction; (c) $^{1}\mathrm{H}(n,\gamma)^{2}\mathrm{H}$ reaction (focus on high-energy region). The capture process $^{1}\mathrm{H}(n,\gamma)^{2}\mathrm{H}$ has not yet been updated in an ENDF file for CP2020.

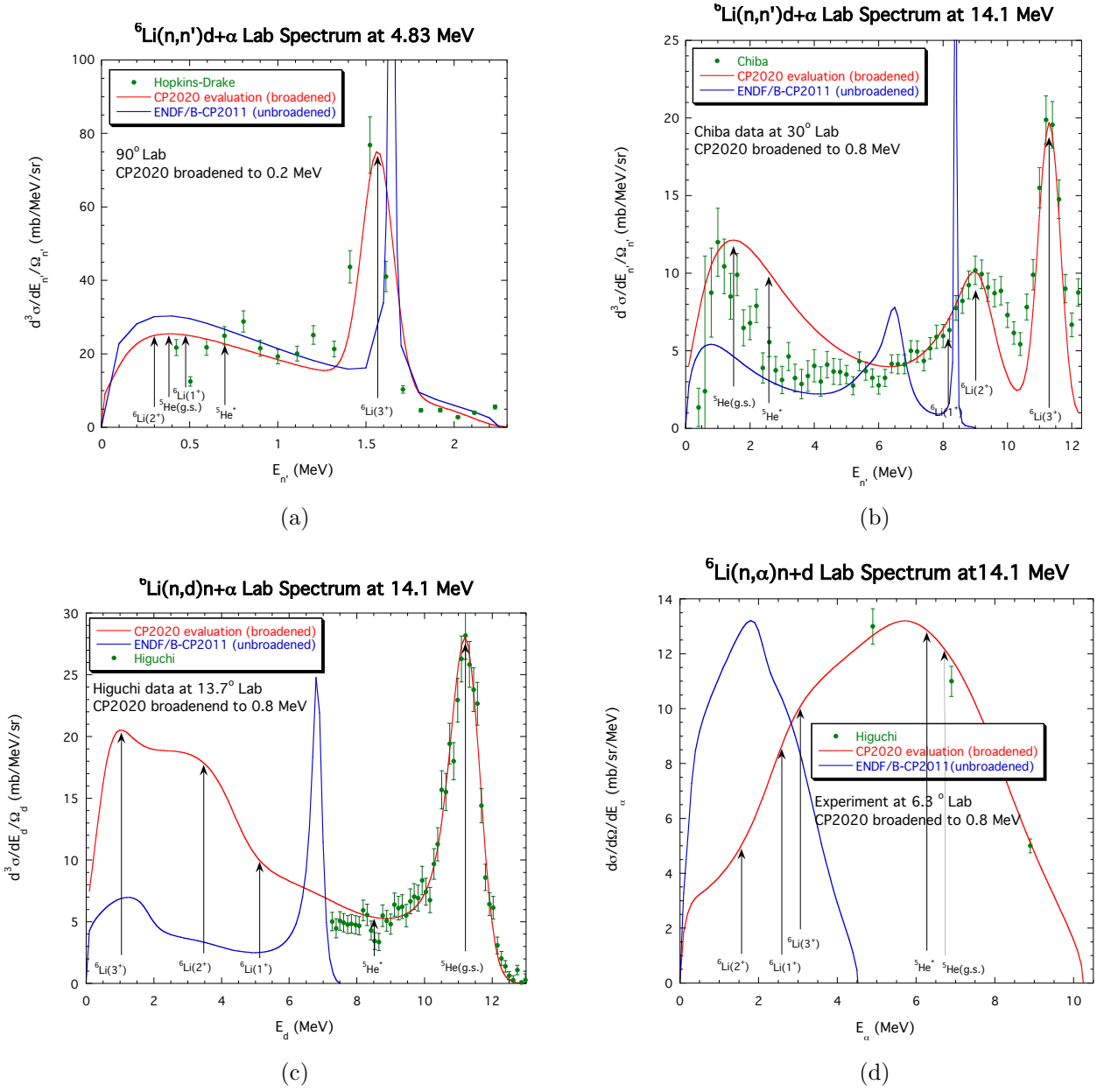

Figure 7: The CP2011 spectra (blue curves) plotted in the laboratory frame, compared with the CP2020 laboratory spectra (red curves; transformed from the center-of-mass frame) and the experimentally observed data. The CP2011 evaluation data are taken from the CP2011 ENDF file with the `LCT=1` parameter error preserved to exhibit the discrepancy between the CP2011 ENDF data and the corrected CP2020 data; (see Section 3.1.3). The CP2020 are taken directly from the post-processing, evaluation code SPECT, which have been confirmed to agree with the CP2020 ENDF file data for `n-003_Li_006.endf` for `MF` =6, `MT` =32.

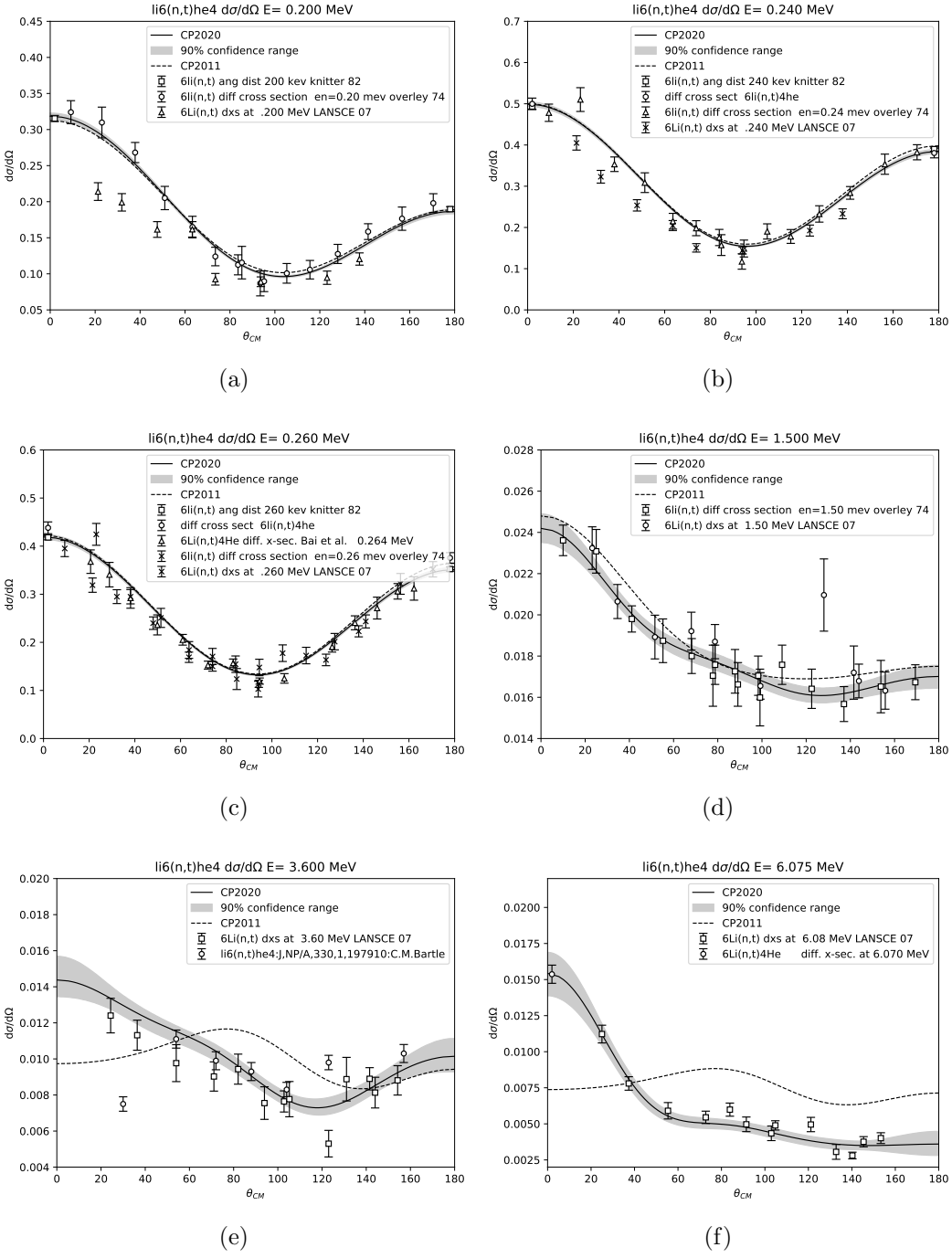

Figure 8: The CP2020 differential cross section angular distributions (solid curves), in the center-of-mass frame, compared with those of CP2011 (dashed curves; when available) and the experimentally observed data for the $^6\mathrm{Li}(n,t)^4\mathrm{He}$ reaction. The CP2011 evaluation covered neutron incident laboratory energies from $0 \leq E_n \leq 4.3$ MeV; the CP2020 fit data up to $E_n \simeq 8$ MeV. The panels (a)–(f) correspond to energies E_n (in MeV) 0.20, 0.24, 0.26, 1.50, 3.60, 6.075, respectively.

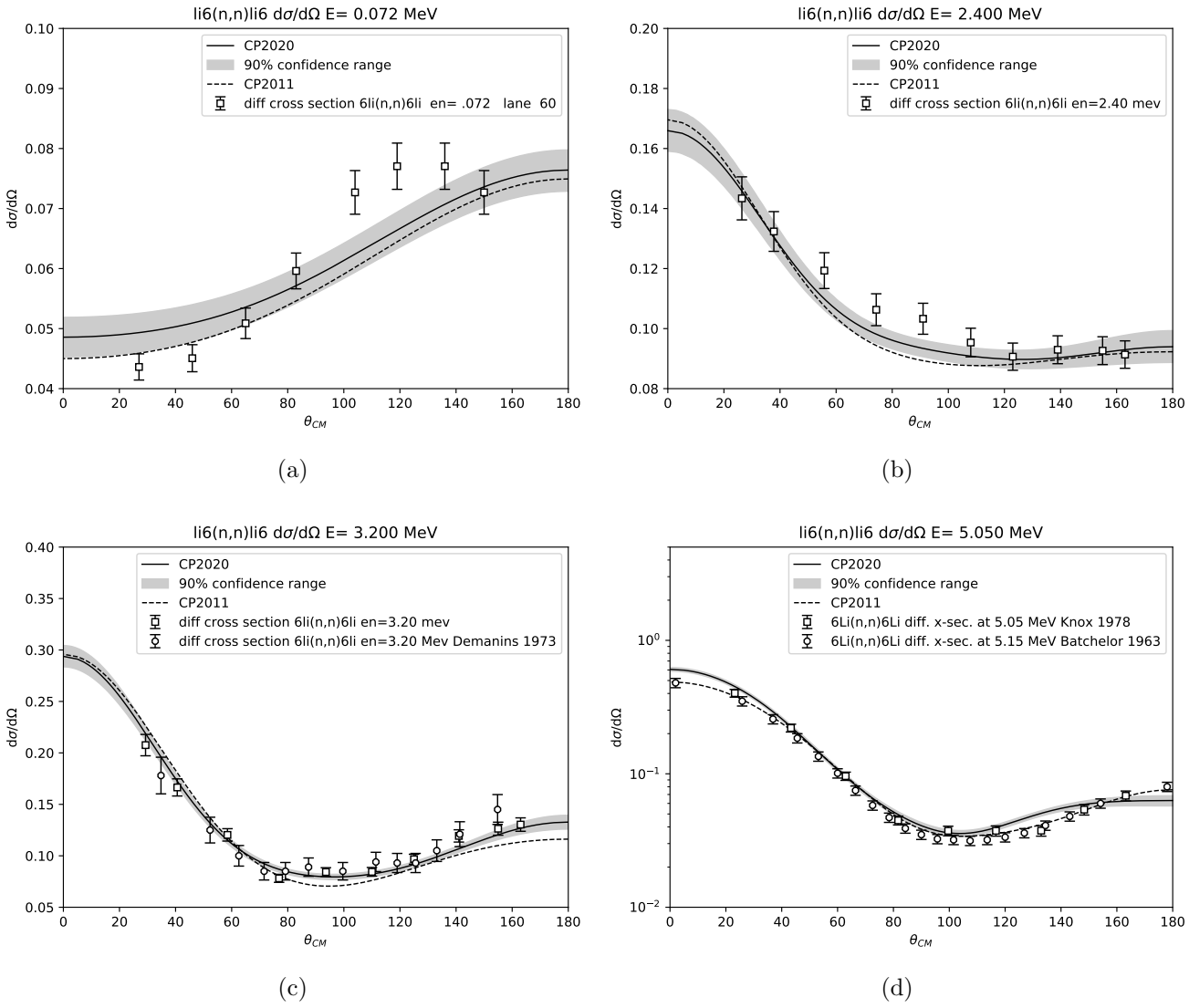

Figure 9: The CP2020 differential cross section angular distributions (solid curves), in the center-of-mass frame, compared with those of CP2011 (dashed curves) and the experimentally observed data for the ^{6}Li$(n,n)^6$Li reaction. The CP2011 evaluation covered neutron incident laboratory energies from $0 \leq E_n \leq 4.3$ MeV; the CP2020 fit data up to $E_n \simeq 8$ MeV. The panels (a)–(d) correspond to energies E_n (in MeV) 0.072, 2.4, 3.20, 5.05, respectively.

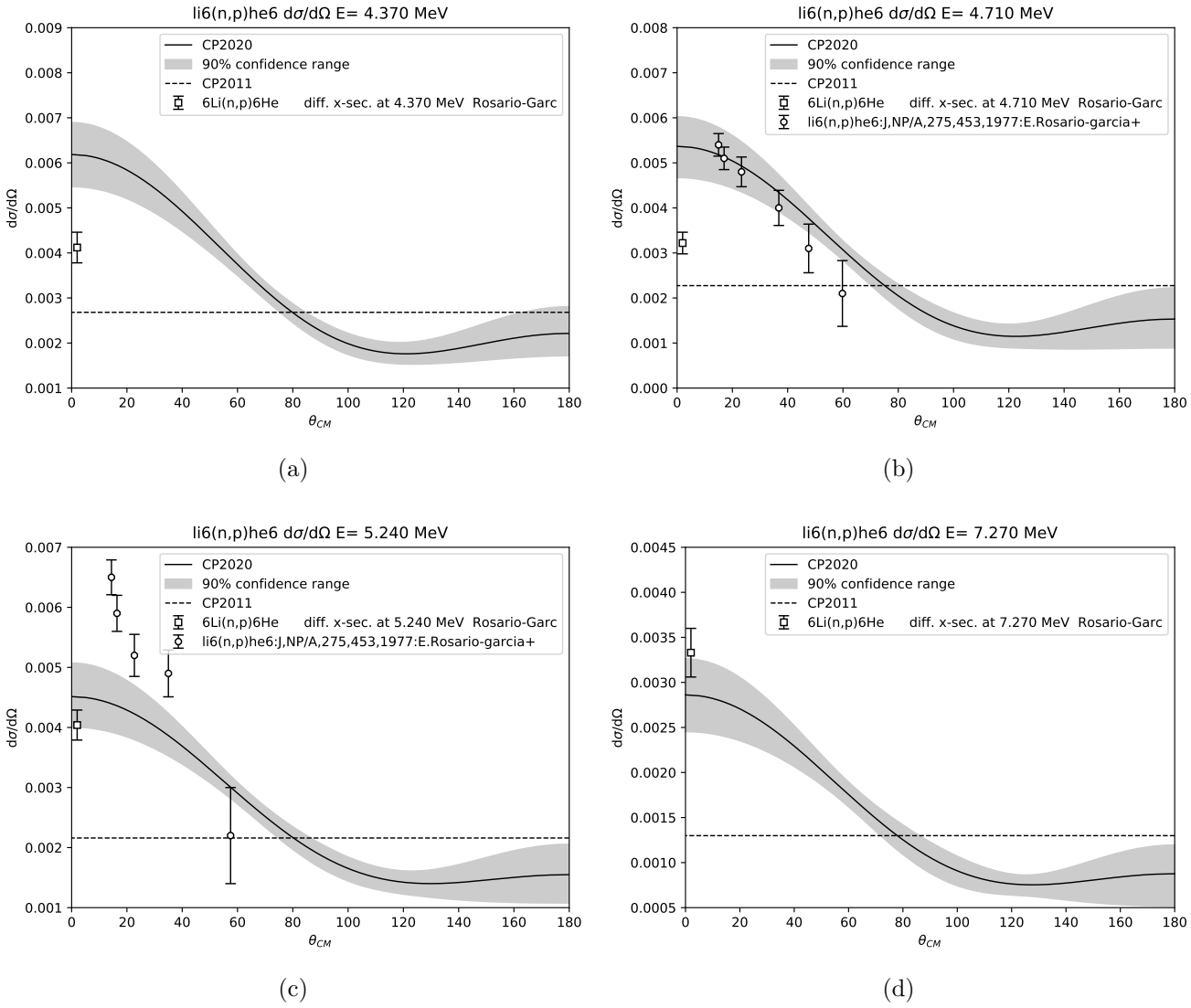

Figure 10: The CP2020 differential cross section angular distributions (solid curves), in the center-of-mass frame, compared with those of CP2011 (dashed curves) and the experimentally observed data for the $^6\mathrm{Li}(n,p)^6\mathrm{He}$ reaction. The CP2011 evaluation covered neutron incident laboratory energies from $0 \leq E_n \leq 4.3$ MeV; the CP2020 fit data up to $E_n \simeq 8$ MeV. The panels (a)–(d) covers energies E_n (in MeV) from 4.37, 4.71, 5.24, 7.27. The CP2011 data approximates the angular distributions as isotropic.

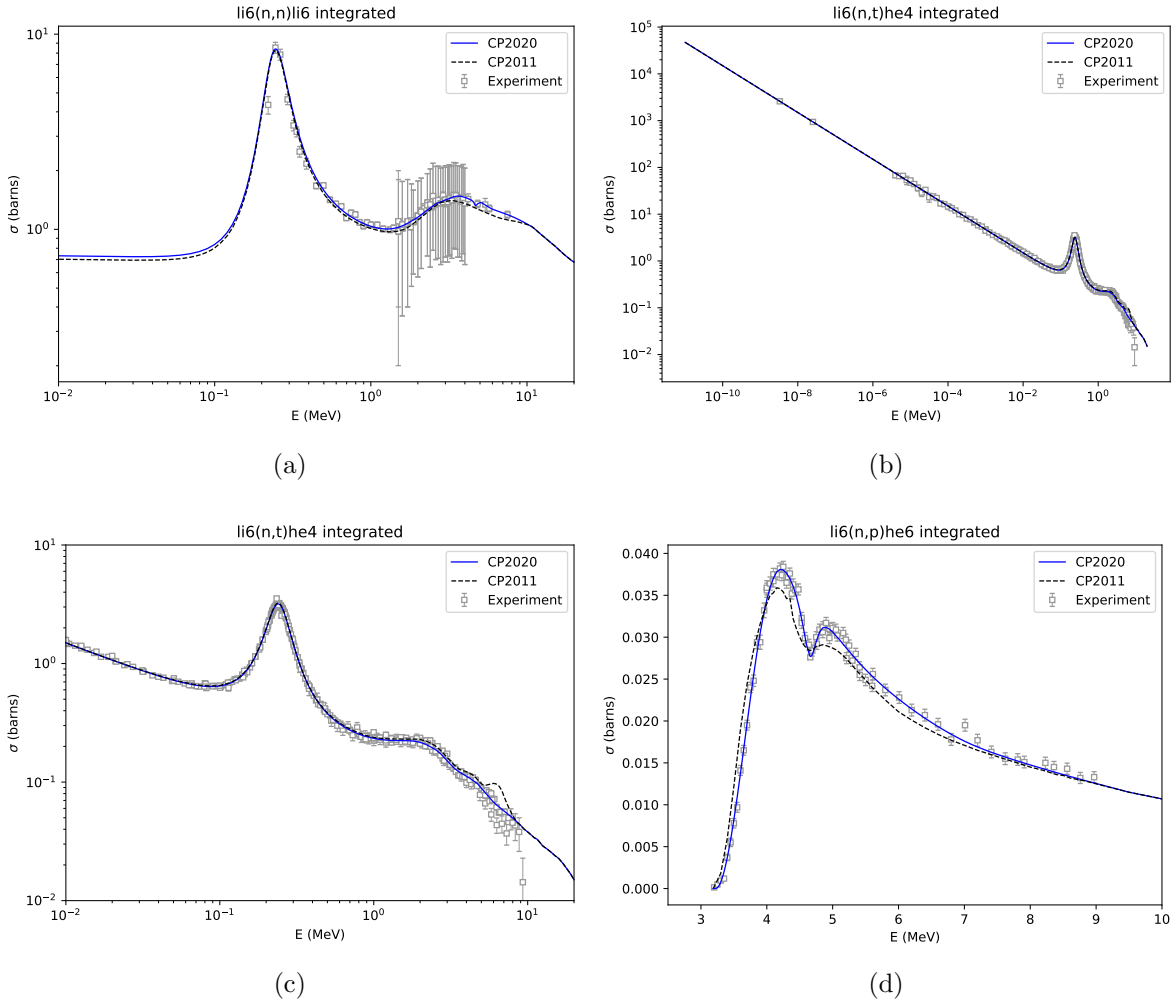

Figure 11: The CP2020 integrated cross sections (solid, blue curves) compared with those of CP2011 (dashed curves; when available) and the experimentally observed data for: (a) ^{6}Li$(n,n)^{6}$Li reaction; (b) ^{6}Li$(n,t)^{4}$He reaction; (c) ^{6}Li$(n,t)^{4}$He reaction (focus on ^{7}Li$(\frac{5}{2}^{-}$; 245 keV) resonance); (d) ^{6}Li$(n,p)^{6}$He reaction. The CP2011 evaluation covered neutron incident laboratory energies from $0 \leq E_n \leq 4.3$ MeV; the CP2020 fit data up to $E_n \simeq 8$ MeV.

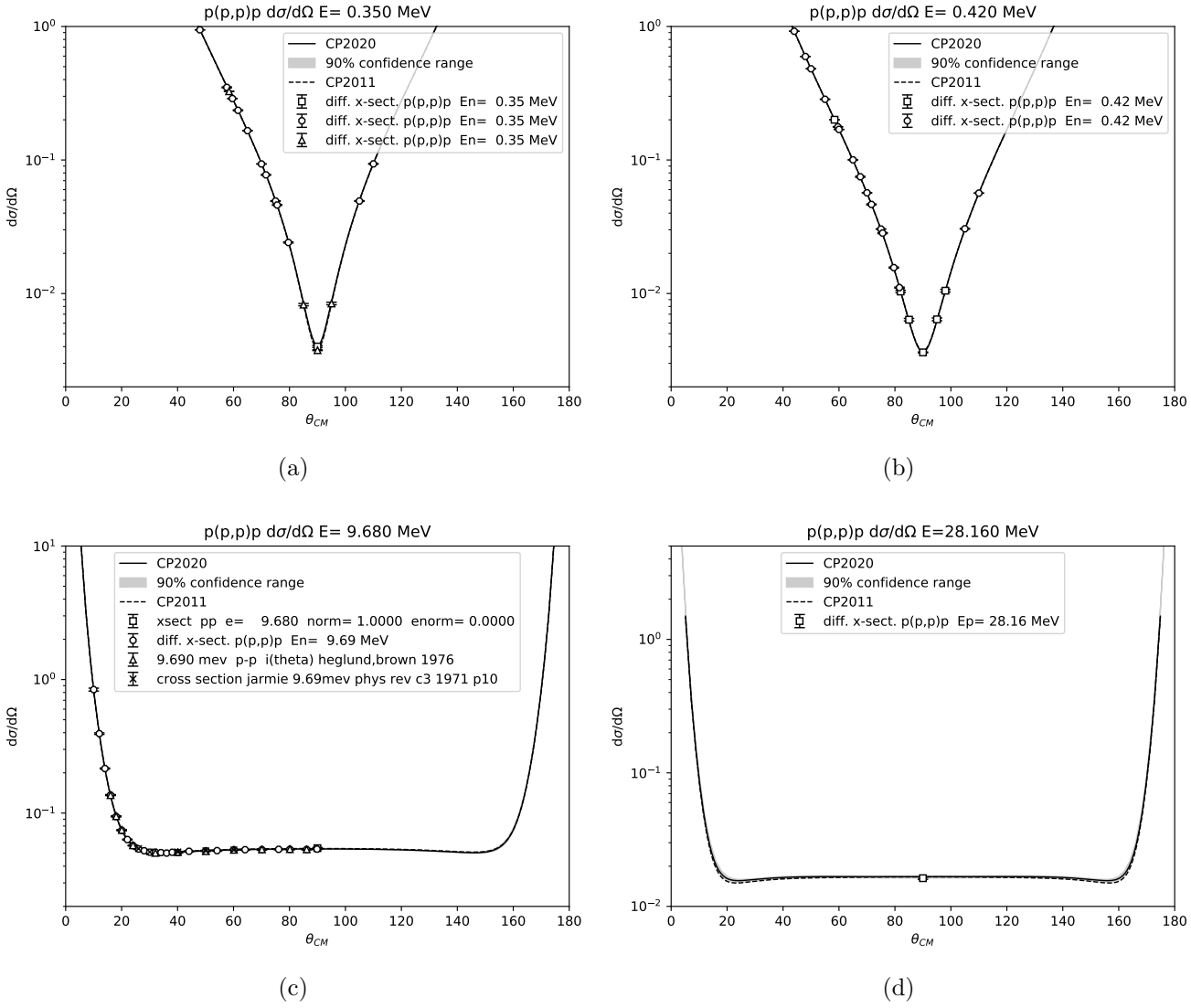

Figure 12: The CP2020 differential cross section angular distributions (solid curves), in the center-of-mass frame, compared with those of CP2011 (dashed curves) and the experimentally observed data for the $^{1}\mathrm{H}(p,p)^{1}\mathrm{H}$ reaction. The CP2011 evaluation covered neutron incident laboratory energies from $0 \leq E_p \leq 30$ MeV; the CP2020 fit data up to $E_p \simeq 50$ MeV. Panels (a)–(d) correspond to E_p (in MeV) of 0.35, 0.42, 9.68, 28.16. (Both CP2011 and CP2020 have identical high-energy extensions to $E_p \simeq 150$ MeV.)

2. ^{2}H: The CP2020 evaluated data is based upon ENDF/B-VIII.0, which contains total, elastic, nonelastic (`MT=3`), $(n, 2n)$ and capture $[(n, \gamma)]$ cross section data, as shown in Table 51. The evaluation is a hybrid of an R-matrix fit below neutron incident energy (E_n) 3.2 MeV and other methods (FKK/GNASH/GSCAN), which take the evaluation to 150 MeV. The `MF=4` data was migrated to `MF=6` to facilitate processing to the MG representation.

3. ^{3}H: The neutron-triton ($n+^{3}$H) CP2020 evaluation, taken from ENDF/B-VIII.0 (see Table 55), is part of the $A = 4$ compound system evaluation, a simultaneous analysis of $^{4}\mathrm{H} \sim n{+}^{3}\mathrm{H}$ and $^{4}\mathrm{Li} \sim p{+}^{3}\mathrm{He}$, its isospin partner, which is driven by the R-matrix analysis of the $p{+}^{3}$He data. The (Coulomb-shifted) parameters of the ^{4}Li fit have been used to predict total and elastic cross sections and angular distributions of $^{3}\mathrm{H}(n, n)^{3}\mathrm{H}$ from E_n sub-thermal to 20 MeV. The $(n, 2n)$ threshold, $E_n \approx 8.4$ MeV has been taken into account approximately in the R-matrix fit through quasi-two-body coupling to the $nn + d$ and $nn + d_0$ channels.

4. $^{3}\mathrm{He}^{\dagger}$: The $n{+}^{3}$He $\sim^{4}$ He evaluation, last updated in 2011 April, taken from ENDF/B-VIII.0 (see the summary in Table 67), includes total (up to 20 MeV), elastic (to 200 keV), capture, and charged-particle production reaction data, ((n, p) to $\sim$ 10 MeV and (n, d), integrated cross section to $\sim$ 10 MeV). The IAEA-Standards reaction $^{3}\mathrm{He}(n, p)^{3}\mathrm{H}$, in the energy range 0.0025 eV $< E_n <$ 50 keV, with few cross section measurements, is an infrequently used reference cross section. Significant amounts of data in the Coulomb dominated $p +^{3}$ H channel does not tightly constrain the evaluation. Future work should propose measurements to account for this deficiency.

5. ^{4}He: The $n{+}^{4}$He evaluation in ENDF/B-VIII.0 (Table 75), being a component of the ^{5}He compound system, which includes the important $^{3}\mathrm{H}(d, n)^{4}\mathrm{He}$ fusion reaction, has received much attention over decades and is well constrained by the data. It contains neutron total and elastic cross section and covariance information and currently goes to 20 MeV. The CP2020 library is based upon the ENDF/B-VIII.0 evaluated data file with `MF=4, MT=2` angular data migrated to `MF=6` format .

6. $^{6}\mathrm{Li}^{\dagger}$: New evaluation for CP2020. As previously mentioned, the $n{+}^{6}\mathrm{Li}{\sim}^{7}\mathrm{Li}$ system R-matrix evaluation was fairly well-developed at energies $E_n \lesssim 4.3$ MeV for the ENDF/B-VIII.0 evaluated library. The evaluation work from CP2011 for $^{6}\mathrm{Li}(n, n'd)^{4}\mathrm{He}$ (spectra shown in Fig. 7) is included in the CP2020 ENDF file, unchanged; and recent refinements to the CP2020 ENDF file are included to account for ^{6}Li * excited state contributions have been included in the CP2020 library. The neutron energy range of the analysis was doubled from 4 MeV to 8 MeV, and many new measurements were added for the neutron-induced reactions in the previous range below 4 MeV. The energy range of the triton-induced reactions was also increased, as described in the next section (3.1.4). The ^{7}Li system R-matrix analysis contains the following n-induced data: *i*) integrated and differential unpolarized $^{6}\mathrm{Li}(n, t)^{4}\mathrm{He}$, Fig. 8 reaction cross section data for E_n ranging from subthermal energies to above 8 MeV; *ii*) $^{6}\mathrm{Li}(n, n)^{6}\mathrm{Li}$, Fig. 9 elastic unpolarized differential cross sections for 49 keV $\leq E_n \leq$ 8.17 MeV and angular distributions of analyzing power (A_y) for $0.2 \leq E_n \leq 4.0$ MeV; *iii*) inelastic $^{6}\mathrm{Li}(n, n_1)^{6}\mathrm{Li}(3^{+};0)$ for $3.35 \leq E_n \leq 8.17$ MeV; *iv*) integrated cross sections for the $^{6}\mathrm{Li}(n, p)^{6}\mathrm{He}$ [Fig. 10] reac-

tion at $3.2 \leq E_n \leq 8.97$ MeV, which were highly instrumental in determining the nature of interfering $3/2^-$ resonances in the 4-6 MeV energy range [see Fig. 11(d)]; *v*) integrated cross sections for the ^{6}Li$(n,n_2)^6$Li$(0^+;1)$ reaction in the energy range $4.2 \leq E_n \leq 7.0$ MeV; and *vi*) quasi-two-body break-up data, ^{6}Li$(n,d)^5$He $(\frac{3}{2}^-;\frac{1}{2})$ for $3.35 \leq E_n \leq 7.54$ MeV with secondary neutron and CP production. We will improve the description of the ^{6}Li$(n,n'd)^4$He spectra by fitting more data [46], which were not included in the CP2011 work. An error in the CP2011 ENDF file that sets the frame-of-reference (laboratory vs. center-of-mass) was detected in the course of the CP2020 work; see Section 3.1.3 and Fig. 7.

7. ^{7}Li: The evaluated data for n+^{7}Li, which furnishes the ^{8}Li compound system is currently receiving attention to improve the description of the $E_n = 14.1$ MeV spectra with new data from inertial confinement fusion (ICF) work at the Omega laser facility[47]. (This work will be completed after the CP2020 Milestone concludes.) The current ENDF/B-VIII.0 file contains cross section and covariance information for total, elastic, inelastic, $(n,2n)$ and charged-particle spectra. The CP spectra was evaluated via a *pseudo-level* description, which current work aims to replace with a description appropriate to the continuum nature of the process.

3.1.3 Correction of CP2011 ENDF file for n+^{6}Li

The data section `MF=6, MT=32` of the CP2011 file `n-003_Li_006.endf`, which specifies the angle- and energy-coupled probability distribution function (`MF=6`) for n', d and ^{4}He from the reaction (`MT=32`) ^{6}Li$(n,n'd)^4$He particle outgoing spectra suffers from a formatting error. The parameter ENDF-6 format standard parameter `LCT=1`, as given in the CP2011, indicates that the spectra provided in the file is in the laboratory frame. The spectra provided there, according to the evaluator[48], is actually provided in the center-of-mass frame for which the parameter `LCT=2`. The figures in Fig. 7 reveal the effect of correcting this error for the CP2020 file.

3.1.4 Incident CP sublibrary

An important issue for CP transport, which is beyond the scope of this Milestone, is the determination of the upper-energy limit for evaluations and their contribution to various application-code metrics. By extending the upper energy limits of the existing evaluations, such determinations can be made on the basis of a comparison of the CP2011 and CP2020 libraries in various relevant applications codes.

The charged-particle induced scattering and reaction cross section information is largely consistent with the ENDF/B-VIII.0 files. However, CP2011 work for charged-particle projectiles p, d, α on ^{4}He does not appear in the ENDF/B-VIII.0 library. The status of the ENDF/B-VIII.0 evaluations and possible improvements of the present CP2020 work is detailed in this subsection.

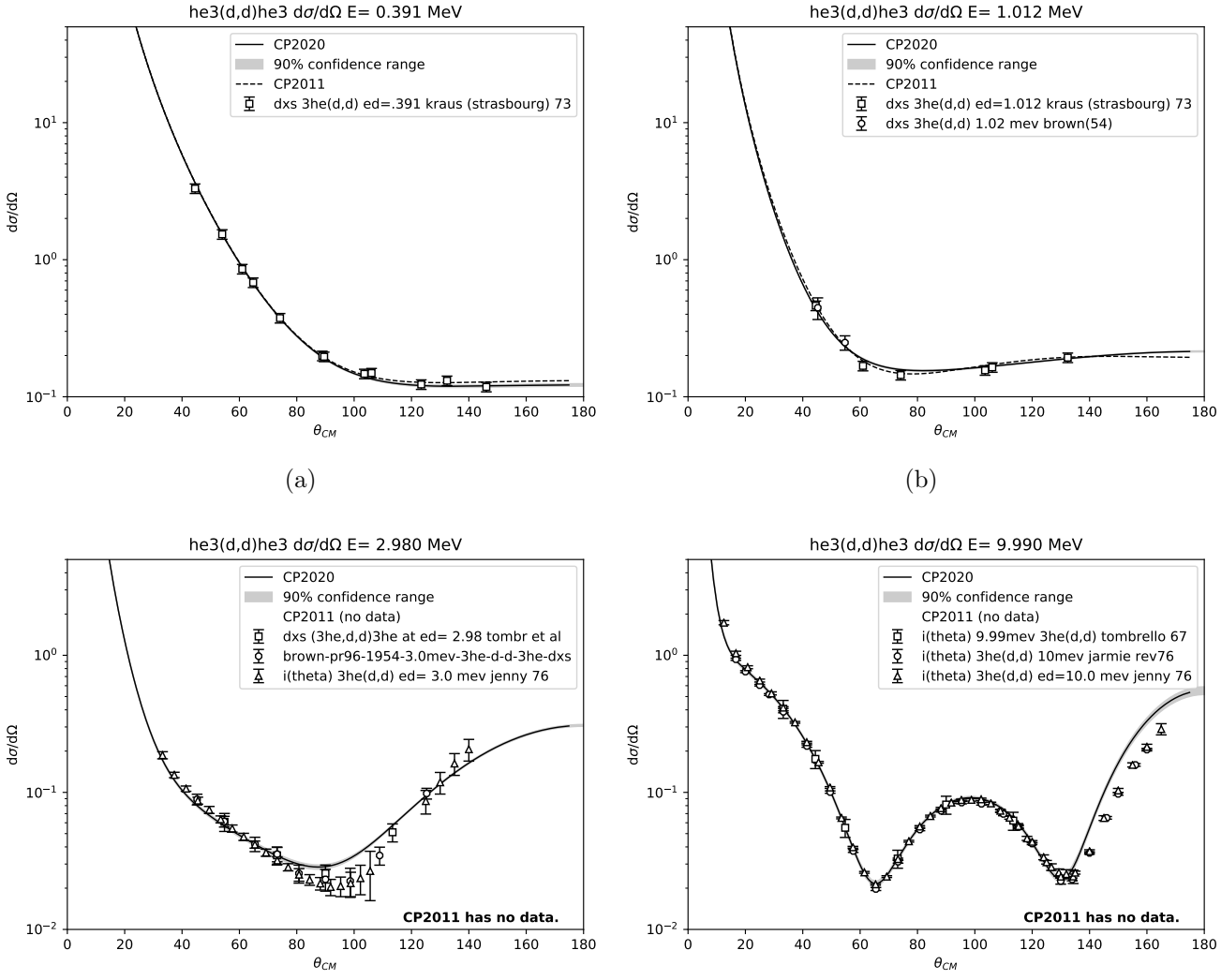

Figure 13: The CP2020 differential cross section angular distributions (solid curves), in the center-of-mass frame, compared with those of CP2011 (dashed curves; when available) and the experimentally observed data for ^{3}He$(d,d)^3$He elastic scattering. The CP2011 evaluation covered deuteron incident laboratory energies from $0 \leq E_d \leq 1.4$ MeV; the CP2020 fit data up to $E_d \simeq 10$ MeV. Panels (a) and (b) correspond to energies E_d (in MeV) of 0.39 and 1.01, respectively. Panels (c)–(d) for E_d energies 2.98 and 9.99 MeV, have only a single evaluation curve corresponding to the CP2020 evaluated file.

1. ^{1}H: This section details the current status of the charged-particle projectiles on the ^{1}H target material for CP2020.

   - New evaluation for CP2020. Incident protons on the proton ^{1}H target has been updated by incorporating more data in the region $E_p > 20$ MeV, resulting in a finer energy spacing in the ENDF file. A (very small) fraction of the data fit in the NN evaluation is shown in Fig. 12.

2. ^{3}He: This section details the current status of the charged-particle projectiles on the ^{3}He target material for the new d+^{3}He evaluation for CP2020.

   - d: New evaluation for CP2020. The previous CP2011 evaluation for d+^{3}He was covered on the domain $0 \leq E_d \leq 1.4$ MeV by the R-matrix analysis performed by Hale for ENDF/B-VII.1. The present evaluation for CP2020 extends the upper limit of this energy to $E_d \simeq 10$ MeV. New data has been added to both the existing region from Refs.[49–53].

     The overall quality of the fit, a small fraction of the experimentally observed data of which are displayed in Fig. 13 (elastic angular distributions) and Fig. 14 (reaction angular distributions) is fair with a weighted variance (or χ^2/datum) of 2.66. The full observed experimental data set is composed of 7,114 data points in energy and energy-angle. We have applied the condition that if any single data point contributes more than $\chi^2_{\max} = 40$ at the beginning of a fit-run, it is excluded from the fit. Typical fit-runs are allowed to explore for 2,000 iterations or until a solution[12] is reached. When a solution is obtained a new fit-run is initiated to ensure that the included data-points result in a stable solution.

3. ^{4}He: This section details the current status of the charged-particle projectiles on the ^{4}He target material for CP2020.

   - p: New evaluation for CP2020. The p+^{4}He evaluation for CP2011 is based on a LANL EDA R-matrix analysis including elastic, unpolarized angular distributions (shown in Fig. 15) and polarized data (not shown) for ^{4}He$(p,p)^{4}$He (for $0.95 < E_p < 23.7$ MeV) and ^{3}He$(d,d)^{3}$He. Reaction data (^{3}He$(d,p)^{4}$He) is limited to $E_d < 1.0$ MeV. The ENDF/B-VIII.0 data is from LLNL (see caption, Table 4), which is simply a fit to the nuclear-plus-Coulomb-interference cross section and excludes the more detailed angular and polarization data in the LANL R-matrix analysis.

     The CP2020 evaluation effort includes reaction data up to $E_d < 10$ MeV, to just above the three-body break-up threshold at $E_d \simeq 8.9$ MeV. The resulting extension of the elastic p induced data on ^{4}He, part of the same ^{5}Li compound system, to $E_p \lesssim 34.3$ MeV permits application codes testing between the CP2011 and CP2020 libraries to determine requirements on upper energy limits for CP.

[12] The solution is determined by the condition that the gradient of χ^2 with respect to the fit parameters p_j, $|\nabla_p \chi^2 / N_{\rm par}| < 2 \times 10^{-3}$.

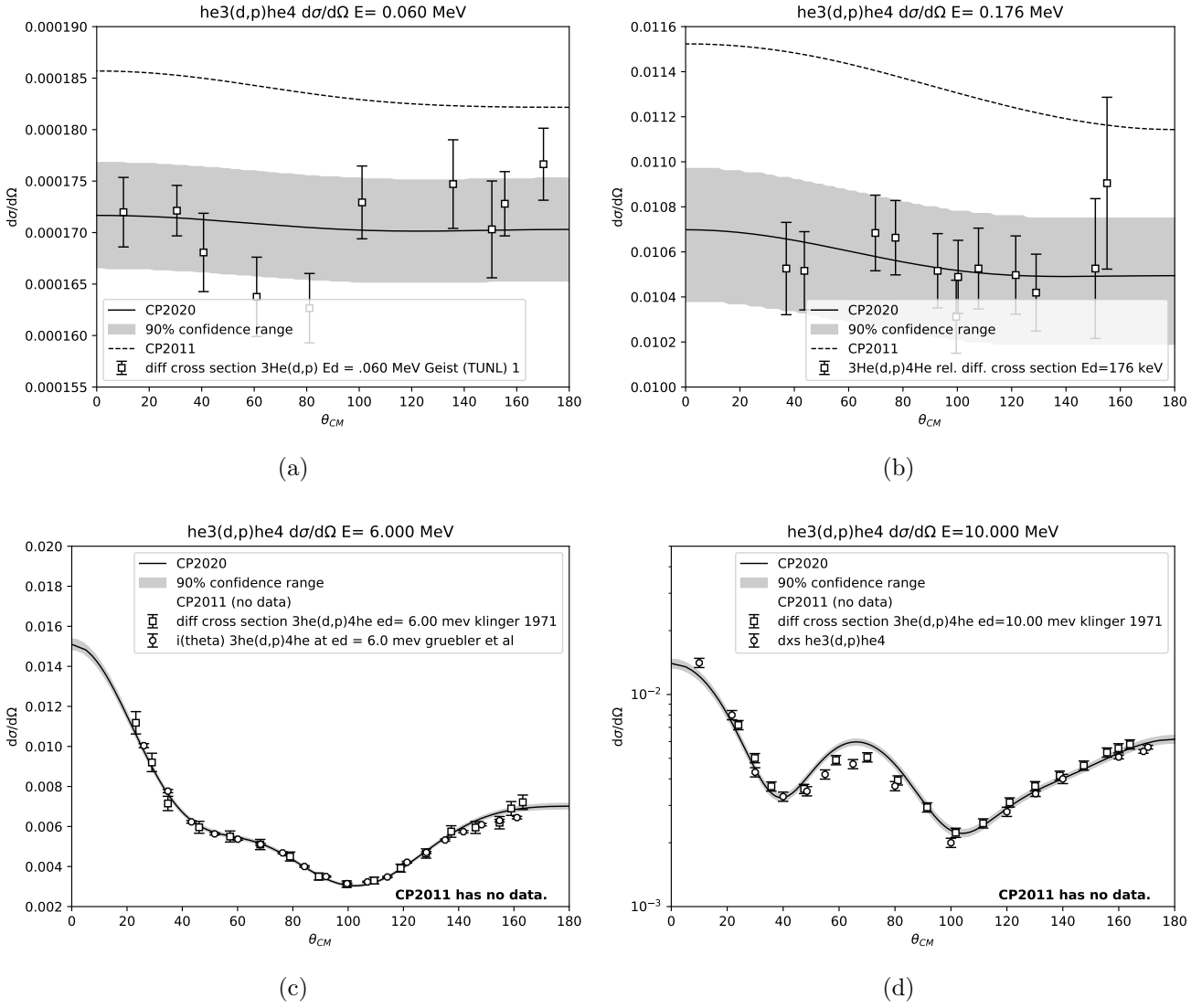

Figure 14: The CP2020 differential cross section angular distributions (solid curves), in the center-of-mass frame, compared with those of CP2011 (dashed curves; when available) and the experimentally observed data for the $^3\mathrm{He}(d,p)^4\mathrm{He}$ reaction. The CP2011 evaluation covered deuteron incident laboratory energies from $0 \leq E_d \leq 1.4$ MeV; the CP2020 fit data up to $E_d \simeq 10$ MeV. The panels (a) and (b) correspond to E_d (in MeV) of 0.060 and 0.18; note panels (c) and (d), with $E_d = 6.00$ and 10.00 MeV, respectively, have only a single evaluation curve corresponding to the CP2020 evaluated file.

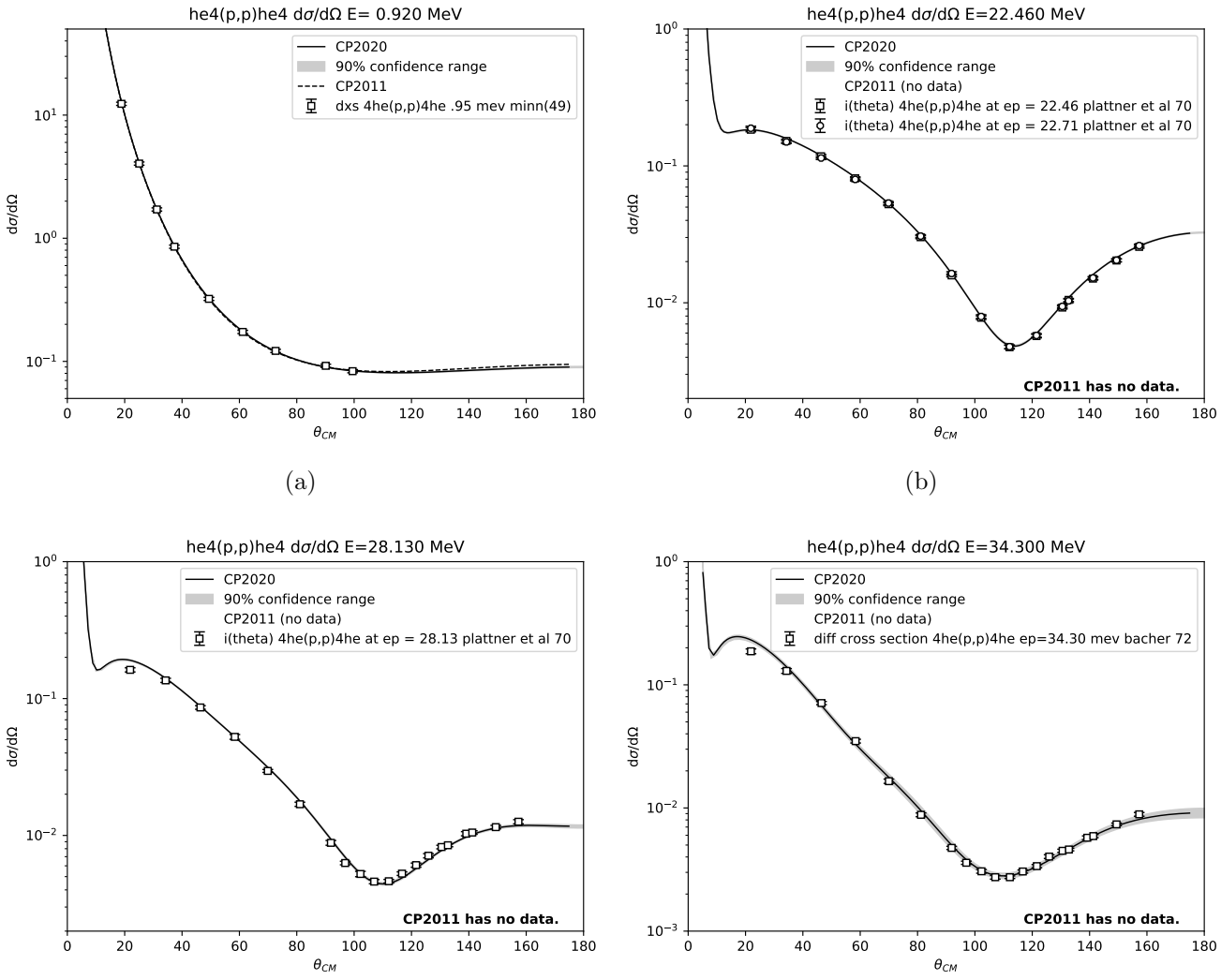

Figure 15: The CP2020 differential cross section angular distributions (solid curves), in the center-of-mass frame, compared with those of CP2011 (dashed curves; when available) and the experimentally observed data for $^4\mathrm{He}(p,p)^4\mathrm{He}$ elastic scattering. The CP2011 evaluation covered proton incident laboratory energies from $0 \leq E_p \leq 20$ MeV; the CP2020 fit data up to $E_p \simeq 34.3$ MeV; note panels (c)–(d) have only a single evaluation curve corresponding to the CP2020 evaluated file. Panel energies E_p (in MeV) are 0.92, 22.46, 28.13, 34.30.

A small portion (only a few percent, in fact) of the experimentally observed data that has been fitted for the CP2020 evaluation effort is shown in Fig. 15.

- d: The ENDF/B-VIII.0 library does not feature a d+^{4}He evaluation. The existing, CP2011 evaluation is based on an R-matrix evaluation[54] of the ^{6}Li compound system that includes elastic unpolarized and polarization differential angular distributions data for ^{4}He$(d,d)^4$He, integrated cross sections for ^{4}He$(d,pn)^4$He for E_d at 10.0, 10.25, and 11.0 MeV. The presence of the three-body np^4He break-up threshold at $E_d \approx 2.2$ MeV challenges higher-energy R-matrix analysis. We have commenced ^{6}Li compound-system evaluation work that incorporates data for ^{3}He$(t,d)^4$He and ^{3}He$(t,\gamma)^6$Li that can provide additional constraints for future, higher-energy E_d work. For CP2020, we will incorporate phase space spectra (ignores interactions between the secondary p,n and ^{4}He) to the evaluated data file.

- t: New evaluation for CP2020. The t+^{4}He entrance channel for the ^{7}Li compound system has been significantly updated since the GMH-1993 work for CP2011. The R-matrix analysis, described in detail in the ^{6}Li-target section of the previous subsection [Sec.3.1.2], includes elastic ^{4}He$(t,t)^4$He [Fig. 16] differential scattering cross sections and analyzing powers (A_y) for $E_t \leq 17$ MeV. These data extend beyond the three-body break-up threshold at $E_t \approx 11$ MeV; the ^{4}He$(t,n)^6$Li reaction data shown in Fig. 17, for 8.5 MeV $< E_t <$ 14.4MeV and ^{4}He$(t,n_1)^6$Li$(3^+;0)$ for $E_t = 12.9$ MeV.

- ^{3}He: The h+^{4}He $\sim$ ^{7}Be evaluation is fairly well characterized by the data, like its isospin-$\frac{1}{2}$ partnered compound system ^{7}Li. The R-matrix analysis, based on the three configurations h+^{4}He, p+^{6}Li, and γ+^{7}Be, takes into account elastic ^{4}He$(h,^3$He$)^4$He angular distributions for unpolarized differential cross section and polarized (A_y) data for 1.72 MeV $< E_{^3\mathrm{He}} <$ 10.8 MeV. Reaction [^{4}He$(^3$He$,p)^6$Li] data is strictly unpolarized differential cross section angular distributions for 8.2 MeV $< E_{^3\mathrm{He}} <$ 10.8 MeV and angle-integrated cross section capture data to the ^{7}Be ground-state, a reaction of significance in astrophysical and cosmological settings, among others. Recent work on the ^{7}Be compound system analysis, including previously unanalyzed reaction data, will be released in this CP2020 work, as indicated in Table 4, along with submission to CSEWG/NNDC for the next ENDF/B evaluated cross section library release.

- ^{4}He: For the ^{4}He+^{4}He $\sim$ ^{8}Be, which is fairly well developed for $E_\alpha \lesssim 10$ MeV, no new material for CP2020 is available; significant effort is required to go to higher E_α above the n^4He^{3}He threshold.

3.2 Processing of CP2020 evaluated NCS to CE & MG

This subsection details the processing of the CP2020 evaluations described in the previous section, Sec.3.1 to CE (ACE format) and MG (NDI format) libraries.

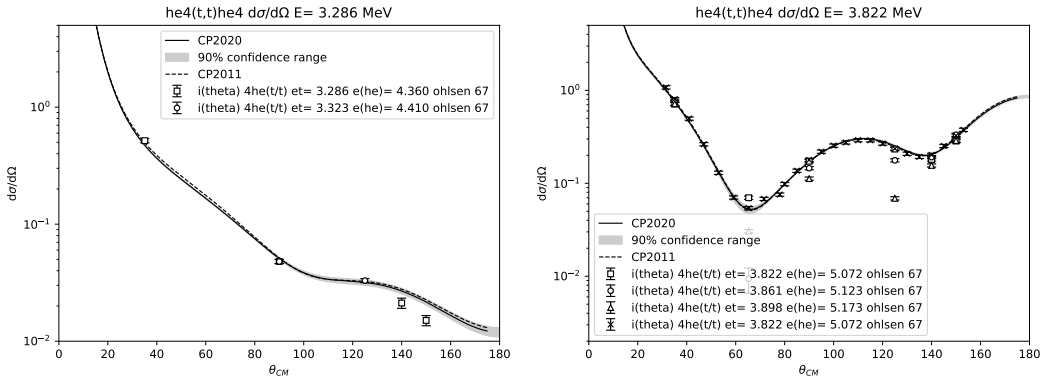

(a)

(b)

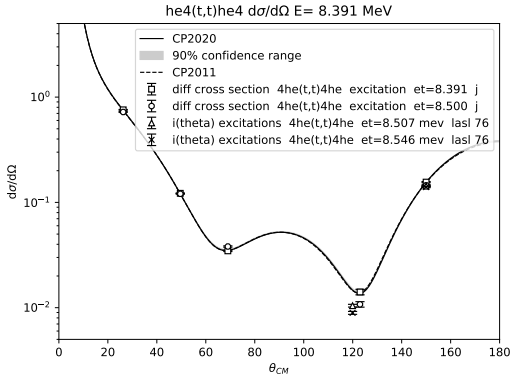

(c)

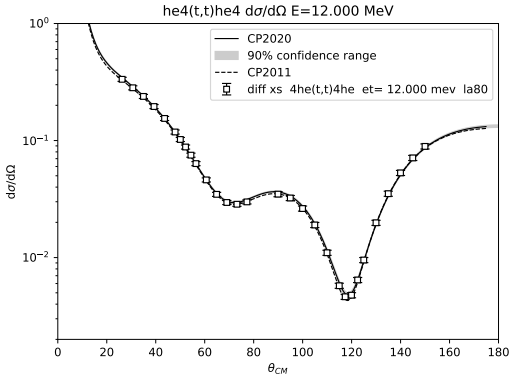

(d)

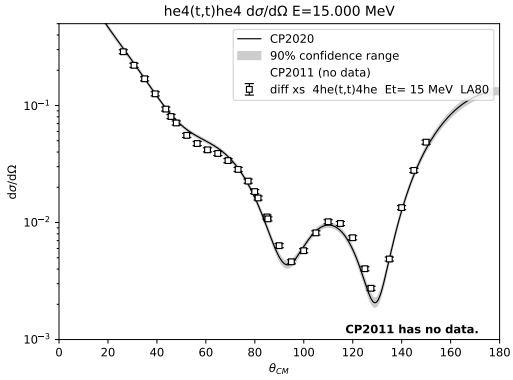

(e)

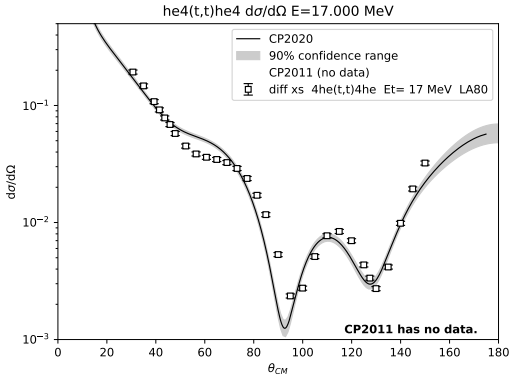

(f)

Figure 16: The CP2020 differential cross section angular distributions (solid curves), in the center-of-mass frame, compared with those of CP2011 (dashed curves, where available) and the experimentally observed data for the $^4\mathrm{He}(t,t)^4\mathrm{He}$ reaction. The CP2011 evaluation covered incident triton laboratory energies from $0 \leq E_t \leq 14$ MeV; the CP2020 fit data up to $E_t \simeq 20$ MeV. Panels (a)–(f) correspond to E_t of 3.29, 3.82, 8.39, 12.0, 15.0 and 17.0 MeV, respectively.

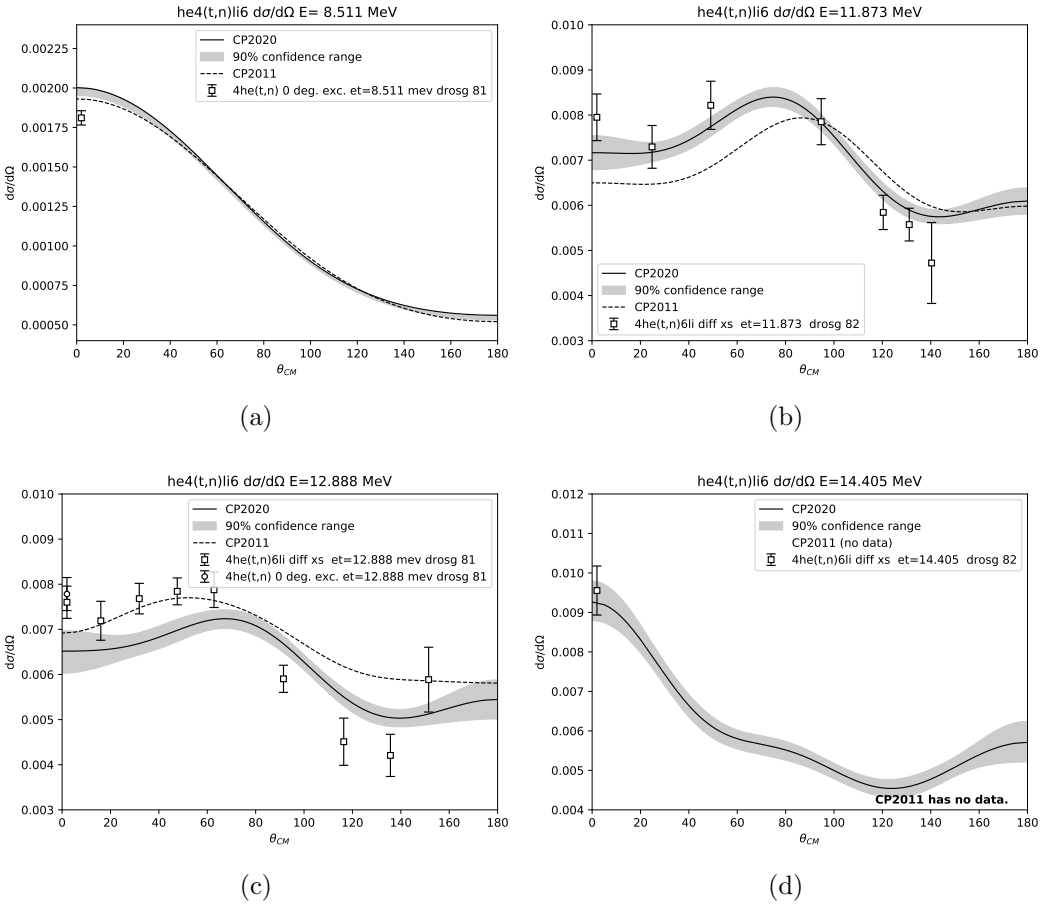

Figure 17: The CP2020 differential cross section angular distributions (solid curves), in the center-of-mass frame, compared with those of CP2011 (dashed curves) and the experimentally observed data for the $^4\mathrm{He}(t,n)^6\mathrm{Li}$ reaction. The CP2011 evaluation covered incident triton laboratory energies from $0 \leq E_t \leq 14$ MeV; the CP2020 fit data up to $E_t \simeq 20$ MeV. Panels (a)–(d) correspond to E_t of 8.51, 11.87, 12.88 and 14.41 MeV, respectively.

3.2.1 Continuous energy (CE) formatted CP cross section data

Processing ENDF files via NJOY 2016.57 to CE, ACE formatted files for incident charged particles, is essentially the same procedure as that followed for incident neutrons. The ENDF evaluation file is processed by the ACER module of NJOY and the resultant ACE file can also be checked by the ACER module. The same ACE formatting conventions are used for both neutron and charged particle data.

A sample ACER input file is given as:

```
acer
 20 30 0 50 51
 1 0 1 .011 /
 acer tape for H -  2 at       293.6  K
    128      293.6 /
 /
 /
acer
 0 50 0 54 55
 7 1 1 -1 /
 acer tape for H -  2 at       293.6  K
```

The first ACER run generates the ACE file for evaluation material ^{2}H (`MAT=128`) at room temperature, while the second ACER run checks the file. The material ID, provided on the third line (or "card") of the above ACER input file, specifies the ACE formatted file suffix, "`0.11`". The original evaluation file is contained in `tape20` (and repeated in `tape30`. The ACE library will be output on `tape50` and the `xsdir` entry will be generated on `tape51`. The checked library will be on `tape54` and its `xsdir` entry will be on `tape55`. Positive values of the tape numbers denotes files that contain ASCII data; negative numbers indicate binary data content.

3.2.2 Multigroup (MG) formatted CP-Production cross section data

The CP2020 library was processed using the same set of tools that were used to process the CP2011 library. The steps to do this processing are as follows:

1. Run NJOY 2016.53 or NJOY 21(1.0.5), invoking, in the following order, the modules:
   (a) MODER,
   (b) BROADR,
   (c) HEATR, and
   (d) GROUPR.

2. Execute the python script, `ndir.py`, which is a component of the NDVV suite that converts from a GENDF file (NJOY's "groupwise-ENDF" format) to an NDI file representation of the mutligroup data.

This set of steps is repeated for every evaluation that is to be processed.

As mentioned earlier in this report, we have used NJOY 2016.53 and NJOY 21 (v1.0.5) instead of NJOY 99.336. We have also made a small number of changes to the input decks as well as to the scripts to account for changes to the evaluation files between 2011 and 2020. The NJOY input decks were modified in order to ensure the correct `MF/MT` pairs were processed. The `ndir.py` script was modified to update the informational messages written to the NDI file indicating "CP2020" instead of "CP2011".

Improvements in multigroup processing since CP2011 The CP2011 library was processed virtually by-hand instead of the automated process with NDVV that we have used for CP2020; many of the steps that were performed for the CP2011 library have been integrated into NDVV. CP2011 was originally processed with NJOY 99.336. While there have been very few changes in the inputs between NJOY 21 and NJOY 99, there have been *many* improvements in the underlying code[12].

3.3 NJOY2016 developments and corrections

3.3.1 NJOY 2016.52 fix for charged particles with `LAW=5`

This section details a coding error in NJOY 2016 (source versions NJOY 2016.51 and before), early in the course of the CP2020 CP processing work[55].

A problem was detected when running ACER to produce an incident charged particle ace file: `NaN` values were appearing in the ACE file for a specific case where the incident charged particle and the target where the same type, with a spin $s = 0$. It has been fixed in NJOY 2016.52 (in November 2019).

For charged particle elastic scattering in the ENDF file, we can use `MF=6 LAW=5`. When this is done for identical particles (`LIDP=1`) such as proton on proton, deuteron on deuteron, triton on triton, etc., we calculate the differential cross section for structureless charged-particle scattering via the Coulomb potential using Eq.(6.10) from the ENDF manual[11]. In the NJOY module ACER, this equation was implemented incorrectly in `acefc.f90`.Adding missing parentheses solves the issue. A similar correction was made in the NJOY (all versions) module GROUPR, since the same error appears there, as well.

Identical particles with half integer spins do not have the issue. For integer spins different from 0 ($s = 1$, 2, etc.) there still is the same issue, but it will did lead to `NaN` values.

A total of 5 non-regression tests were added to the NJOY2016 code base following this issue. These 5 tests cover most of the different possibilities we may encounter in ENDF `MF6 LAW=5` (these tests only cover ACER and do not include `GROUPR`):

- test 50: `LAW=5 LTP=12` for identical particles with a spin $s = 0$ (this file produced `NaN` values)
- test 51: `LAW=5 LTP=12` for different particles (as expected, this remains the same before and after the fix)
- test 52: `LAW=5 LTP=1` for identical particles with a spin $s = 1/2$ (as expected, this remains the same before and after the fix)
- test 53: `LAW=5 LTP=1` for identical particles with a spin $s = 1$ (this changes due to the fix but the original file does not have NaN values, as expected)
- test 54: `LAW=5 LTP=1` for different particles (as expected, this remains the same before and after the fix)

3.3.2 NJOY manual error for n-body phase-space distribution

In 2016, Hale[56] discovered an error in the ENDF formats manual[11] [specifically, Eq. (6.24)] that describes LAW=6 N-body phase space distributions in the laboratory system. This error was reported at the CSEWG meeting that November, and the manual was corrected. We investigated the effect of this error on processed data for CP2011, and found that there was none.[13]

3.3.3 ACER module bug-fix/update: ACER array index overflow

For the CP2020 d+^{3}He evaluation, the ACE file produced by NJOY 2016.57 still contained (few) `NaN` values, even after the previous fixes that were made to it. This was traced back to an array index overflow in ACECPE, which treats charged particle elastic data. The function was written so that a maximum of 200 energies were accepted while the d+^{3}He evaluation had more than 200 in it. The problem was fixed by making the arrays dynamically allocated to the exact number of energy values that can be found in the ENDF file.

3.3.4 Other differences between NJOY99 and NJOY2016 for processing CP2011

This section provides additional NJOY source-change details related to the processing of CP2011 ENDF files described in Section 2.2.2.

The NJOY processing code has a function called `ptleg2` (for all versions). The purpose of this function is to convert an angular distribution given as Legendre polynomials into a tabulated

[13] This is strictly a *manual* error – not a coding error.

probability distribution. It essentially does this by linearizing the Legendre series to within the hard-coded tolerances. The NJOY code developers made a change to the NJOY source at version NJOY 2012.99 to reduce the tolerances by a factor 5 (there are two tolerances called `tol1` and `tol2`). The reduction of these tolerances leads to more angular cosine points in the resulting probability distribution.

For example, at 1e-4 MeV, the NJOY 99.336 file had 3 cosine values while the NJOY 2016.53 file had 5. (In other places, the number of angular points appear to have been roughly doubled.) By resetting the tolerances in `ptleg2`, NJOY 2016.53 only produces 3 angular points for that 1e-4 MeV energy.

3.4 NDI format & API development

The Nuclear Data Interface (NDI) has been modified to handle dE/dx ("stopping power") data. Currently, all work exists on a branch (feature/dedx) and will be part of a future release of NDI 2. The data format is similar to the neutron cross section data for NDI. Each data file consists of keywords followed by data. For example, `zaid`, `num_grps`, and `num_targets`.

Two types of dE/dx data can be read in: free electron (`free_e_dedx`) and ion (`target_ion_dedx`). This data is stored as a function of energy, density, and temperature. Standard NDI user commands retrieve this data (e.g., `ndi2_get_float_vec` for a list of energies).

3.4.1 GENDIR

The `gendir` (GENeral DIRectory) file contains a list of all isotopes and reactions of interest. The ones maintained by the Nuclear Data Team contain multigroup neutron, multigroup photon, TN, TN reactions, neutron depletion, radiochemistry chains, and neutron dosimetry sections.

The new charged particle section is 'dedx.' The location of all charged particle data should be referenced in this section. NDI currently assumes that the charged particle data available in a `gendir` entry is the same as the multigroup neutron `gendir` data (e.g., zaid is "z", library is "l", and atomic weight is "aw").

3.4.2 NDI API

The following presents keyword-function call pairs that are valid with the dedx library. The term "points" refers to a point on the energy-density-temperature grid that corresponds to the dE/dx data.

- `ndi2_get_int_val`
  - NDI_NUM_GRPS – returns the number of energy points.

  - NDI_NUM_DENSITIES – returns the number of density points.
  - NDI_NUM_TEMPS – returns the number of temperature points.
  - NDI_NUM_TARGET – returns the number of target ions.
- `ndi2_get_int_val_n`
  - NDI_TARGET_ZAID – returns the ZAID of target n = [0,num_targets].
- `ndi2_get_int_vec`
  - NDI_TARGET_ZAID – returns an array of target ZAIDs (as integers).
- `ndi2_get_float_val`
  - NDI_AT_WGT – returns the atomic weight of the *incident* charged particle.
  - NDI_AWR – returns the atomic weight ratio for the incident charged particle.
- `ndi2_get_float_vec`
  - NDI_ENERGIES – returns the energy grid for the dE/dx data.
  - NDI_DENSITIES – returns the density grid for the dE/dx data.
  - NDI_TEMPS – returns the temperature grid for the dE/dx data.
  - NDI_DEDX – returns the free-electron dE/dx data.
- `ndi2_get_float_vec_x`
  - NDI_TARGET_DEDX – returns the dE/dx data for target x, where x is a ZAID.
- `ndi2_get_string_val`
  - NDI_ZAID – returns incident particle's ZAID.
  - NDI_INFO – returns information on the data file.
  - NDI_DATE_PROCESSED – returns the date the data was processed.
  - NDI_DATE_SOURCE – returns the date the data was sourced.
  - NDI_LIB_NAME – returns the library name.
- `ndi2_get_size`
  - NDI_ZAID – returns the size of the ZAID string.
  - NDI_INFO – returns size of the information string.
  - NDI_DATE_PROCESSED – returns the size of the string containing the data was processed.

  - NDI_DATE_SOURCE – returns the size of the string containing the data was sourced.
  - NDI_LIB_NAME – returns the size of the library name string.
  - NDI_NUM_TEMPS; NDI_NUM_GRPS; NDI_NUM_DENSITIES; NDI_NUM_TARGETS – all return 1.
  - NDI_ENERGIES – returns the number of energies.
  - NDI_DENSITIES – returns the number of densities.
  - NDI_TEMPS – returns the number of temperatures.
  - NDI_TARGET – returns the number of targets.
  - NDI_DEDX; NDI_TARGET_DEDX – returns the number of energies times the number of densities times the number of temperatures.

- `ndi2_get_size_n`
  - NDI_TARGET_ZAID – returns 1 (because the target ZAID is stored as an integer).
  - NDI_TARGET_DEDX – returns the number of energies times the number of densities times the number of temperatures.
- `ndi2_get_size_x`
  - NDI_TARGET_ZAID – returns 1 (because the target ZAID is stored as an integer).
  - NDI_TARGET_DEDX – returns the number of energies times the number of densities times the number of temperatures.

3.4.3 dE/dx Data

The original dE/dx (stopping power) data is found at

`/usr/projects/data/nuclear/mc/dedx/all/`

This folder contains tabulated data produced by the FermiASCnew code.

The equivalent NDI data is at

`/usr/projects/data/nuclear/ndi/special/dedx/`

with bps, nocut, and standard libraries. Each library has a unique ZAID extension: `.000dx` for standard, `.001dx` for nocut, and `.002dx` for bps.

Two python scripts have been written to convert ACE-format dE/dx data to the NDI format. `convert.py` is the main script, and it uses the function `write_data` function from `write_data.py`.

3.4.4 Format

dE/dx data is given in a new NDI format. It contains a series of keywords followed by data pertaining to that keyword. The data is given in log-form (like the original ACE data). To get the true energy, density, temperature, etc., one must take the exponential of the data (i.e., e^{data}). A sample is presented below:

```
\dedx information translated from ACE to NDI
zaid
    1001.000dx
info
    This data has been converted from ACE to NDI
library_name
    standard
date_source
    unknown
date_processed
    2020-04-16
awr
    0.998626981306
at_wgt
    1.007280E+00
num_grps
    91
num_dens
    28
num_temps
    28
energies
    -8.517193e+00 -8.363688e+00 -8.210182e+00 -8.056676e+00 ... (91 total entries)
densities
    4.835429e+01 4.903653e+01 4.971878e+01 5.040103e+01 ... (28 total entries)
temperatures
    -1.151293e+01 -1.083068e+01 -1.014843e+01 -9.466183e+00 ... (28 total entries)
free_e_dedx
    -4.002136e+01 -4.012272e+01 -4.022826e+01 ... (91*28*28 total entries)
num_targets
    15
target_ion_dedx
    1001
    -4.861460e+01 -4.864614e+01 -4.869095e+01 ... (91*28*28 total entries)
    1002
    -4.908976e+01 -4.914400e+01 -4.920720e+01 ... (91*28*28 total entries)
    ... (15 total target ion \dedx sets of data,
         each 91*28*28 total entries of data)
```

```
end
```

Here the ZAID of the incident particle is `1001.000dx` (H-1). The library is "standard," based on the library_name keyword and the ZAID extension `.000dx`. It has 91 energy points, 28 temperatures, 28 densities, and 15 target ions. For each target ion, there is a ZAID and 91x28x28 dE/dx values.

The data is given in this order (showing energy/density/temperature points), where G is the total number of energies, N is the total number of densities, and M is the total number of temperatures:

```
ZAID
(E1, D1, T1) (E2, D1, T1) (E3, D1, T1) ... (EG, D1, T1)
(E1, D2, T1) (E2, D2, T1) (E3, D2, T1) ... (EG, D2, T1)
...
(E1, DN, T1) (E2, DN, T1) (E3, DN, T1) ... (EG, DN, T1)
(E1, D1, T2) (E2, D1, T2) (E3, D1, T2) ... (EG, D1, T2)
(E1, D2, T2) (E2, D2, T2) (E3, D2, T2) ... (EG, D2, T2)
...
(E1, DN, TM) (E2, DN, TM) (E3, DN, TM) ... (EG, DN, TM)
```

4 CP2020 library data testing, validation, and comparison to ECPL-2018 (LLNL)

In this section we describe testing of the CP2020 libraries; comparisons in some cases are made the the CP2011 files. Checks are performed at each level of the ND pipeline: *i)* the ENDF files are subjected to various *sum-rule* checks and other verification procedures by NJOY and a suite of codes maintained by the IAEA[57]. The new evaluations (NN, ^{5}Li, and ^{7}Li systems) have been subject to these checking codes. We report on these checks in this section and detail only the cases where the checking codes have resulted in errors or warnings.

4.1 ENDF validation and formatting codes

The IAEA maintains a suite of checking codes that have been employed to check the ENDF evaluation files generated for CP2020. These files have passed nearly all of the checks made with these codes. Exceptions are discussed in the following subsections. Here, we briefly describe the IAEA checking codes.

4.1.1 STANEF

This code makes basic consistency checks of the file with the ENDF-6 format standards, ensures that the `MF=1, MT=451` "directory" of `MF` files and `MT` sections is consistent with the file contents, and provides sequencing. All new evaluations have passed this code test.

4.1.2 CHECKR

The CHECKR code performs consistency checks (more deeply than STANEF) of the file with the ENDF-6 format standards. In particular it checks that ENDF-6 specification limits integral-valued control parameters (such as the number of incident, secondary and other energies for each `MF` file section). All new evaluations have passed this code test.

4.1.3 FIZCON

The evaluated data file is checked by FIZCON for valid data that conforms to recommended procedures, violations of which are noted as warnings. The validation criteria are: increasing energy-ordered data arrays; resonance parameter partial widths sum to total; Q-values are reasonable and consistent; required sections are included; secondary distributions are unit-normalized; energy is conserved by the secondary spectra. The new evaluation for n+^{6}Li is cited by FIZCON for three errors that are understood and discussed below, Section 4.3.3; all other evaluations pass FIZCON testing.

4.1.4 PSYCHE

The PSYCHE code is a physics-content ENDF file checker. From the manual[57]: "The present version checks for energy conservation for emitted particles, checks Wick's limit for elastic scattering, analyzes resonance parameter statistics, calculates thermal cross sections and resonance integrals, examines continuity across resonance region boundaries and checks Q values against mass tables. It is assumed the file being checked has passed the CHECKR program without any errors being detected." The CP2020 n+^{6}Li evaluation spectra for the process ^{6}Li$(n,n'd)^4$He (`MF` =6, `MT` =32) is shown by FIZCON results to violate energy conservation at the level of a few percent to $\lesssim 10\%$, as discussed below in Section 4.3.3.

4.1.5 INTER

Program INTER is more of a post-processing code rather than a checking code that calculates cross-sections, resonance integrals, g-factors, and fission spectrum averaged cross section, which may be used for comparisons with other post-processing codes, such as the LANL STEEP code[58].

4.1.6 DeCE

The DeCE code[36], which is an ENDF-6 formatted file manipulation and descriptive tool, has been used to ensure consistency of the `MF=2` ENDF file section with the rest of `MF` $\neq 1$ sections.

4.2 Processed file checks

As mentioned throughout this report, the ENDF evaluation files are processed via NJOY to CE and MG formatted libraries. These processed files have been subject to testing with checking codes, which are briefly described in this section.

4.2.1 checkACE

The checkACE[59, and references therein] is a series of FORTRAN subroutines which parses an ACE file and flags such conditions as the lack of cross section balance (*e.g.*, is the total given as the sum of the partial cross sections), the validity of PDF/CDF values (*e.g.*, positivity of PDF, CDF monotonically increasing), the positivity of cross sections, etc. It was written specifically for neutron cross sections, however, checkACE is applicable to charged particle cross section ACE files, since both neutron and charged particle data use the same ACE format. checkACE was used to verify all of the charged particle CP2020 files and no major issues were found.

4.2.2 checkMG

checkMG[60], coded in C, reads NDI multigroup tables and performs consistency checks on the data, similar in scope and function to checkACE. It uses the same NDI calls as the deterministic codes like PARTISN to read the NDI data. Simple checks are made for cross section balance, χ normalization, validity of Legendre scattering coefficients, neutron production balance, etc. checkMG was used to verify all of the neutron CP2020 files. After iteration and corrections to the n+^{1}H processing, no further issues were found.

4.3 Characterization of energetics in ENDF evaluated files

Energy conservation is an important check to ensure that the essential physics of time-translation invariance is enforced by the evaluation models (here, the R matrix parametrization) in two-body to two-body reactions, which trivially conserve energy in the center-of-mass frame, and two-body to n-body, where n is the number of secondary produced particles in the final state – typically $n = 3$.

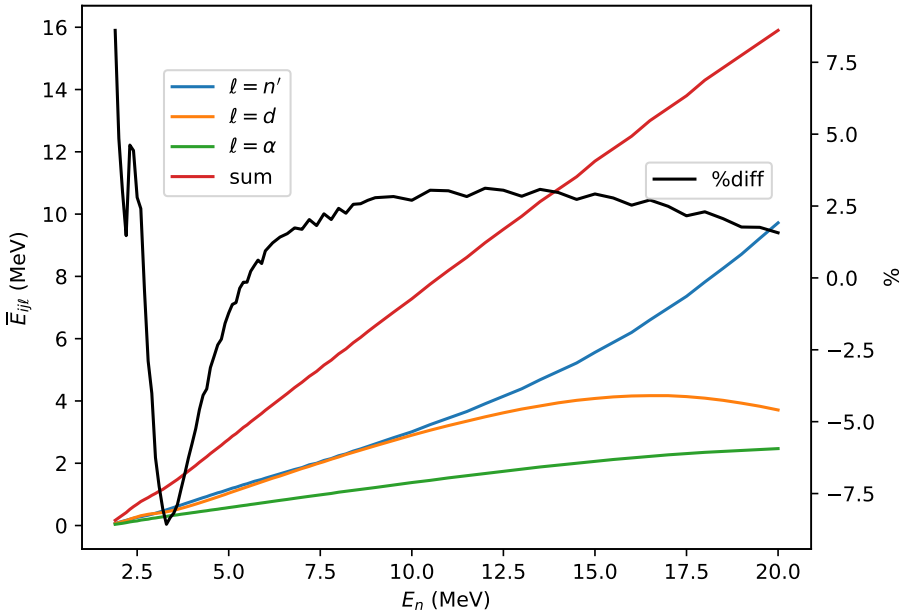

Figure 18: The CP2020 ENDF evaluation energetics of final state particles $\ell = n', d, \alpha$ for the process $i = {}^6\mathrm{Li}$ and $j = {}^6\mathrm{Li}(n, n'd){}^4\mathrm{He}$. The curve labeled 'sum' denotes the $\sum_{\ell=n',d,\alpha} \overline{E}_{ij\ell}$; '%diff' is the defect of this sum with respect to the available energy $E + Q_{ij}$. (Numerical noise is an artifact of `psyche` code interpolation.)

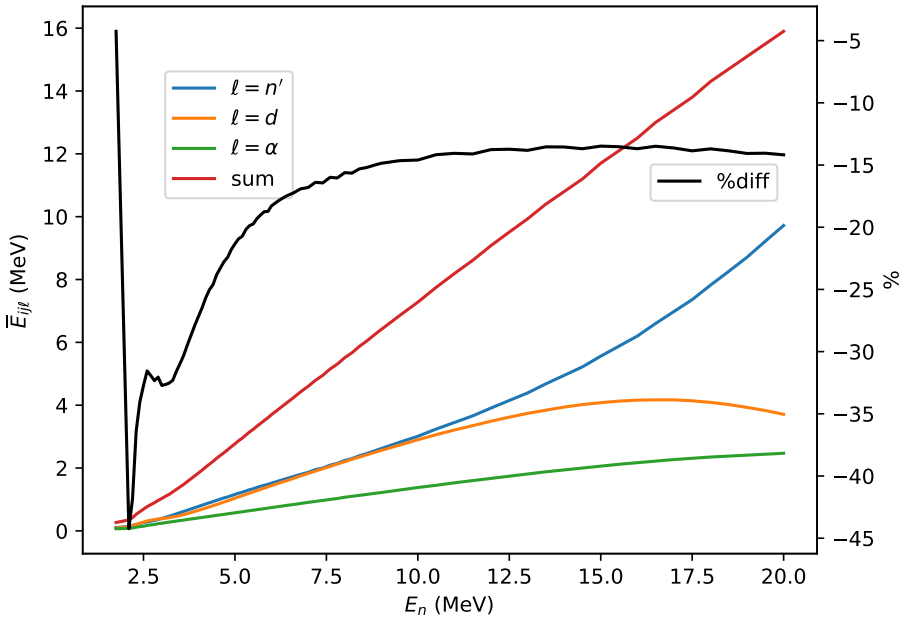

Figure 19: The CP2011 ENDF evaluation energetics, similar to Fig. 18. Note the large error relative to the available energy $E + Q_{ij}$ due to the `LCT=1`→`LCT=2` issue, discussed in Section 3.1.3, which was corrected.

Energy conservation, in $2 \rightarrow n-$body processes, follows immediately from the form of the differential cross section $d\sigma_{fi}$, expressed in the center-of-mass frame as:

$$v d\sigma_{fi}(E) = |T_{fi}|^2 (2\pi)^4 \prod_{j=3}^{n_f+2} d^3k_j \, \delta^{(3)} \left(\sum_{k=3}^{n_f+2} \mathbf{k}_k \right) \delta(E + Q - \sum_j E_j), \tag{2}$$

where v is the relative velocity of the reactants, E is the sum of the reactants incoming energy, T_{fi} is the quantum mechanical transition matrix element for the transition from the initial, two-body state i to the $n-$body final state f; the final δ function ensure that the energy available from the reactants, $E + Q$ (where Q is the difference of the total mass of the reactants and the products) is conserved in its distribution among the final state (secondary) particles with energy E_k.

The definition for the differential cross section $d\sigma_{ij}(E)$ for reaction j on material i, with a slight change in notation from the expression above [Eq. (2)], describing the process $M_i(n, z_j)X_j$, where M_i is the material nuclide, z_j is any single final state particle and X_j is the residual. Imposing energy conservation gives

$$(E + Q_{ij}) d\sigma_{ij}(E) = \sum_k E_k d\sigma_{ij}(E), \tag{3}$$

where $Q_{ij} = m_n + m_{M_i} - \sum_k m_k$ and the $\sum_k$ is over all final-state particles z_k for reaction j. Integrating over the phase space (all accessible energies and angles) for all final-state particles gives

$$E + Q_{ij} = \frac{1}{\sigma_{ij}(E)} \sum_k \int d^3k_k \frac{d\sigma_{ij}(E)}{dE_k d\hat{\mathbf{k}}_k} E_k. \tag{4}$$

Here, $\sigma_{ij}(E)$ is the integrated cross section, the $\sum_k$ is over all final-state particles, and $\frac{d\sigma_{ij}(E)}{dE_k d\hat{\mathbf{k}}_\ell}$ are the single-particle final-state energy E_k and angle $\hat{\mathbf{k}}_k$ dependent spectra; these quantities, modulo the integrated cross section $\sigma_{ij}(E)$, are stored in the ENDF-6 format in `MF=6`, the coupled energy-angle probability distribution functions. Equation (4) states that the total available energy, $E + Q_{ij}$ on material i is equal to the sum of the first moments of the single particle final state distributions.

4.3.1 Accuracy of energy conservation in breakup reactions: ^{6}Li$(n, n'd)^4$He

The IAEA code PSYCHE has been used to check the energy conservation of the process ^{6}Li$(n, n'\mathrm{d})^4$He, which is included in both the CP2011 and CP2020 `n-003_Li_006.endf` evaluation files. The data in the `MF` =6, `MT` =32 section of the CP2011 and CP2020 files is the same data (except for the error on the `LCT=1`→`LCT=2`, described in this report in Section 3.1.3). The data in Figs. 18 and 19 reflects this error in ENDF-6 format encoding of the CP2011 ENDF file for $n +^6$ Li. Figure 18 shows an expected deviation from energy conservation at the level of $\lesssim 10\%$ due to limitations in the resonance model used to describe the breakup spectra[61].

4.3.2 Kinetic Energy Released to Material (KERMA)

A recurring and long-standing issue in the generation of evaluated nuclear data and its CE and MG processed forms is that of the calculation of KERMA coefficients[62–67].

KERMA is a measure of the amount of energy deposited in the material upon which a projectile impinges. Local neutron heating of a material is proportional to the neutron flux ϕ at that position. It arises due to kinetic energy of charged-particle secondary products of the neutron-induced reaction. (Heating due to photon-induced reactions are not considered here.)

As a function of the incident neutron energy E, heating is defined[12] in terms of the KERMA coefficients $k_{ij}(E)$ for material i and reaction j as

$$H(E) = \phi(E) \sum_{i,j} \rho_i k_{ij}(E), \tag{5}$$

where ρ_i is the number density of the material; units of heating are taken to be eV/s/cm^3 so, $[k_{ij}] = \text{eV} \cdot \text{barn}$.

KERMA coefficients are related to the differential cross-section weighted sum of final-state charged-particle (indexed by ℓ) energies E_ℓ as follows. We start with the definition for the differential cross section $d\sigma_{ij}(E)$ for reaction j on material i, describing the process $M_i(n, z_j)X_j$, where M_i is the material nuclide, z_j is any single final state particle and X_j is the residual.

Then, given the discussion at the start of this section, the KERMA coefficient is proportional to the sum of the charged particle components of the averages:

$$k_{ij}(E) \equiv \sigma_{ij}(E) \sum_{\ell} \overline{E}_{ij\ell}, \tag{6}$$

where

$$\sigma_{ij}(E)\overline{E}_{ij\ell} \equiv \int d^3k_\ell \frac{d\sigma_{ij}(E)}{dE_\ell d\hat{\mathbf{k}}_\ell} E_\ell, \tag{7}$$

the quantity

$$\frac{d\sigma_{ij}(E)}{dE_\ell d\hat{\mathbf{k}}_\ell}, \tag{8}$$

is the differential-energy spectra for charged-particle ℓ in the final state, and the $\sum_\ell$ is over only charged secondaries. Conservation of energy holds on average:

$$E + Q_{ij} = \sum_k \overline{E}_{ijk}, \tag{9}$$

where the $\sum_k$ is over *all* secondaries including charged-particles, neutrons, and photons. This implies that the KERMA coefficients can be computed as

$$k_{ij}(E) = \sigma_{ij}(E)\left(E + Q_{ij} - \overline{E}_{ijn} - \overline{E}_{ij\gamma}\right). \tag{10}$$

The calculation of KERMA is performed within the NJOY processing code through the NJOY module HEATR.

4.3.3 Testing of ^{6}Li$(n,n'd)^4$He from CP2011; sources of error in KERMA

In this section, we discuss recent studies by Solomon *et al.*[66, 67] that exhibit differences in KERMA between MG library representations based on ENDF/B-VII.1, `mtmg01ex` and the CP2011 ENDF evaluations, discussed in Ref.[67]. Further, discrepancies between KERMA values tabulated in the NDI representation of the charged-particle production data and those calculated from isotropic transfer matrices derived from the differential-energy spectra, shown in Eq. (8) have been demonstrated in Ref.[66].

There are several sources of error that contribute to the discrepancies noted in [66]. The first is due to evaluation model approximations for breakup spectra made by the SPECT code, discussed in Section 4.3.1 and displayed in Fig. 18. (Recall that Fig. 19 display erroneous data that has been corrected.) These systematic, model uncertainties are estimated theoretically at the $\lesssim 10\%$ level and this is confirmed by these figures.

Another source of error, relevant for the MG (NDI format) representations of the charged-particle production data. These uncertainties, explored in a series of memoranda by Gray[62, 64, 65], indicates that multigroup averaging itself, which does not preserve multiplicative relations between continuous-energy functions, can introduce errors in KERMA at the $\lesssim 10\%$ level[65].

We further characterize the error of the CP2020 ENDF evaluated data by computing, for n+^{6}Li (`n-003_Li_006.endf`) , the heating [Eq. (5)] via the NJOY 2016.53 HEATR module and displayed in Fig. 20, panel (a) and for CP2020, Fig. 20, panel (b). In Fig. 20(a) the calculated heating (solid curve) is coincident with the upper limit, calculated at kinematic limits. (See Sec.(6.5) of Ref.[12].). The CP2020 heating curve shown in Fig. 20(b) falls in the region between the kinematic curves and is considered a more accurate representation since improvements in the ^{6}Li$(n,n'd)^4$He process have removed the pseduo-level description, which has been replaced by an R-matrix description based on the SPECT code[2].

4.4 NDI API stopping power: user testing

Tests of the NDI formatted dE/dx data and new NDI API keyword-function pairs discussed in Section 3.4 have been performed by Norris (XCP-1), described in this section.

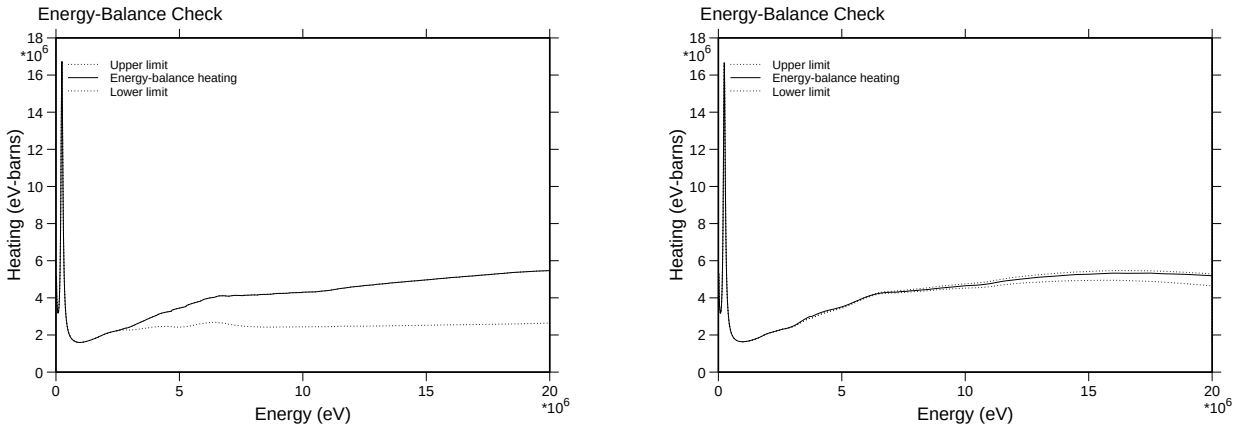

(a) (b)

Figure 20: Heating calculated for the n+^{6}Li files for (a) CP2011 and (b) CP2020 using the HEATR module of the NJOY 2016.53 code. Note that the abscissa is given in units of 10^6 eV.

4.4.1 Comparisons

The following plots compare dE/dx data from NDI to the original tabular data from the FERMI-ASCNEW code. Each run tracks a single, fully ionized 3.5 MeV alpha particle through an infinite medium of 10 g/cc 50-50 DT gas at 8 keV (Ti = Te = Tr = 8 keV). In this particular problem, hydrodynamics and coupling between the particles and background plasma were both disabled. This allows the particle to be tracked as it slows down without heating the plasma, so the plasma stays at a constant density and temperature for the entire duration of the run.

Graphs of these comparisons are shown in Fig. 21. The top two panels of the figure show dE/dx as a function of time and as a function of space, while the lower two panels display energy as a function of time and of space. The dE/dx plots show similar characteristics – a leading, sloped region which gives way to a sharp increase just before particle thermalization. This is the expected trend: the region where the stopping power slowly decreases is electron-dominated and the sharp increase is due to particle-ion interaction. Most importantly, in each case the relative difference between NDI and the reference was $< 10^{-10}$; similar agreement between the code-tabulated and NDI API is obtained for the energy.

4.5 The LLNL 2018 evaluated charged-particle data library

The Computational Nuclear Physics group at LLNL has released the evaluated charged-particle data library for 2018 (ECPL-2018). As a 'stretch' objective of the CP2020 work, we have been able to commence an assessment and preliminary processing of their ENDF-formatted evaluation data. (The library is available as part of the Milestones repository of the Nuclear Data Team; see Section 1.3.2.) We document here differences, in some places large and significant, between

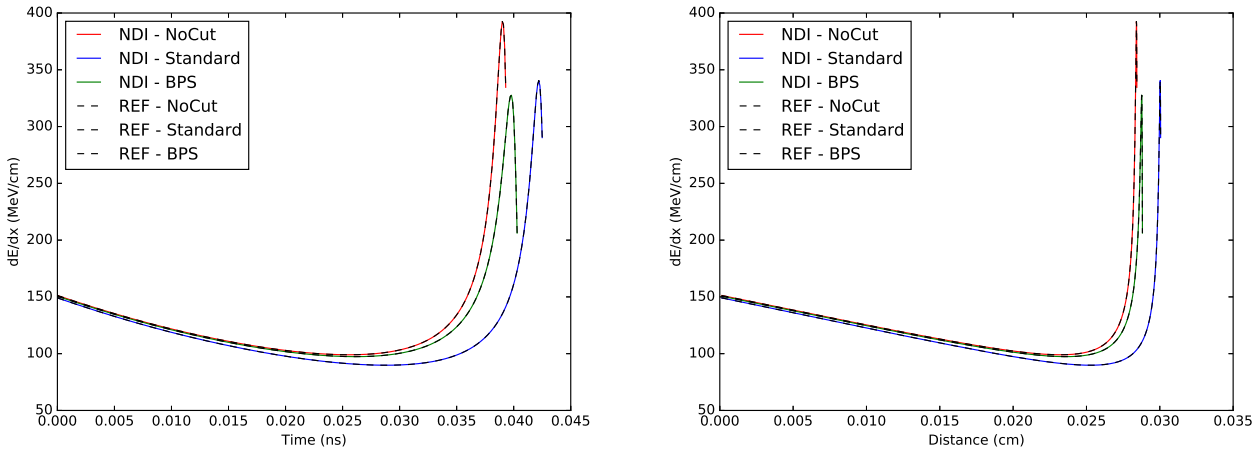

(a) (b)

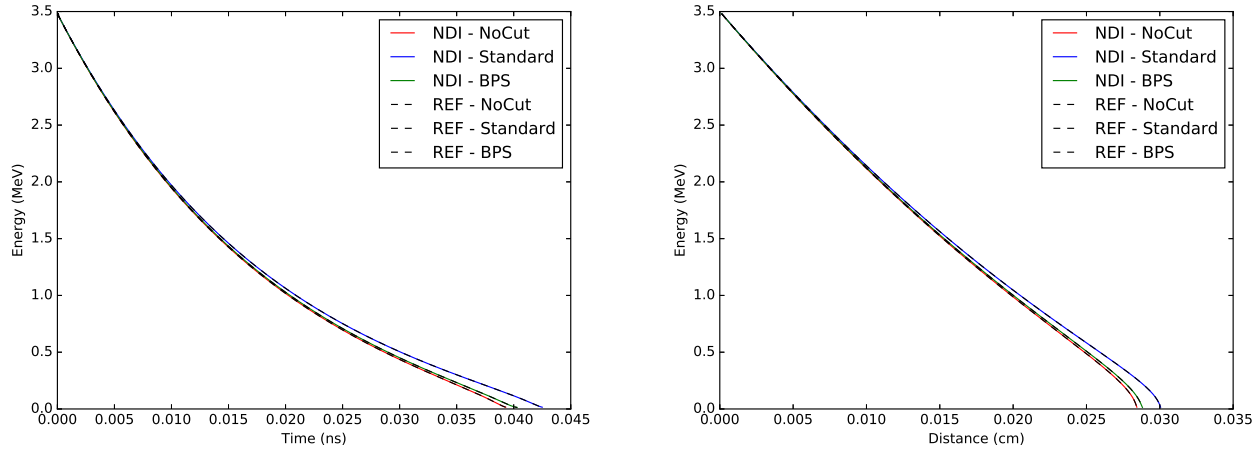

(c) (d)

Figure 21: Stopping power (dE/dx) tabular data comparison between that obtained directly from the FERMIASCNEW code and from NDI API interface, described in the text. The panels show dE/dx as a function of (a) time, (b) spatial coordinate; and energy as a function of (c) time and (d) spatial coordinate.

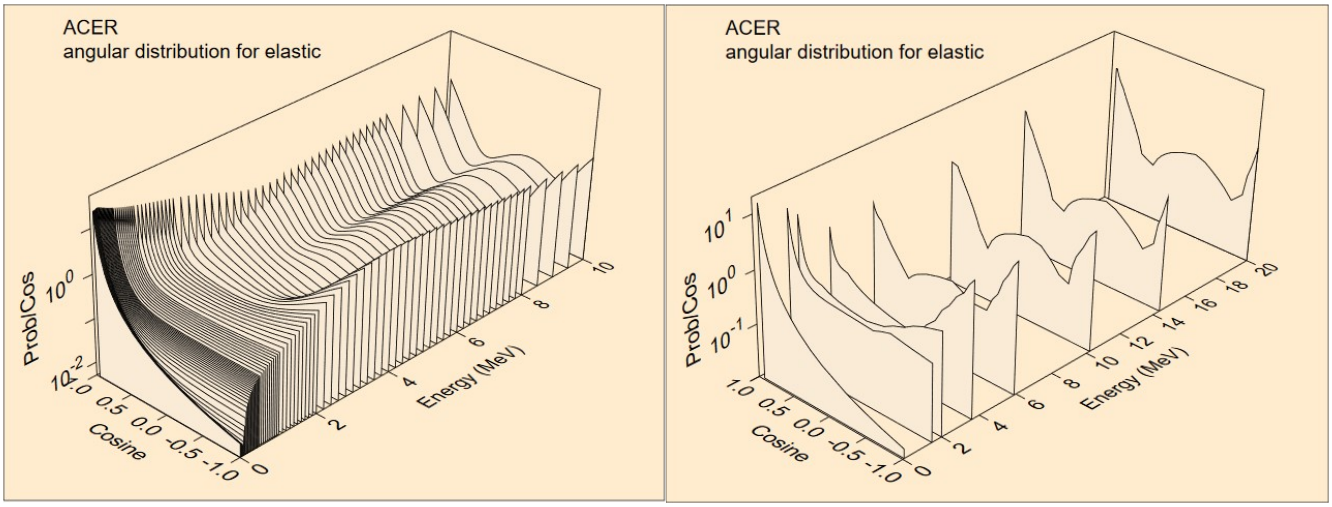

(a) (b)

Figure 22: The ^{3}H$(d,n)^4$He angular distributions as a function of outgoing neutron angle cosine and incident deuteron energy from ENDF formatted data files for (a) CP2020 and (b) ECPL-2018 as generated by the NJOY 2016.53 ACER module.

the LANL libraries of CP evaluated data and the ECPL-2018; the effect of these differences on applications has not been assessed in this work.

Comparisons of the observed experimental angular distribution data, CP2011, CP2020, and the ECPL-2018 evaluated data carried out for CP2020 should be considered preliminary. (Post-CP2020 work will be required to ensure the accuracy of our characterization of the ECPL-2018 data.)

4.5.1 Comparisons of ECPL-2018 with LANL CP evaluations

The ENDF-formatted ECPL-2018 data we received[68] included data formatting that was not ENDF-6[11] compliant. Sections in the ENDL format[69], designated by "reaction identifier" `C=0,...,98`, had been recorded in the file for `C=20` and `C=30`, for reaction processes corresponding to $(n,n'\gamma)$ and $(n,\gamma n\alpha)$, respectively , with 'placeholder' sections `MT=-C`. Consultations between LLNL and LANL personnel determined the appropriate ENDF-6 format convention (*e.g.*, `MF` =6, `MT` =102, `LR=1` for `C=20`).

Though we are unable to process the complete ECPL-2018 library pending further revisions to the d+^{4}He and h+^{3}H files, we've made graphical comparisons for some of the other files that correspond to elastic scattering and reaction data from the NN and ^{5}Li compound systems. The ^{1}H$(p,p)^1$H evaluation comparisons are shown in Fig. 23. Data from the ^{5}Licompound system are shown in Figs. 24 to 26.

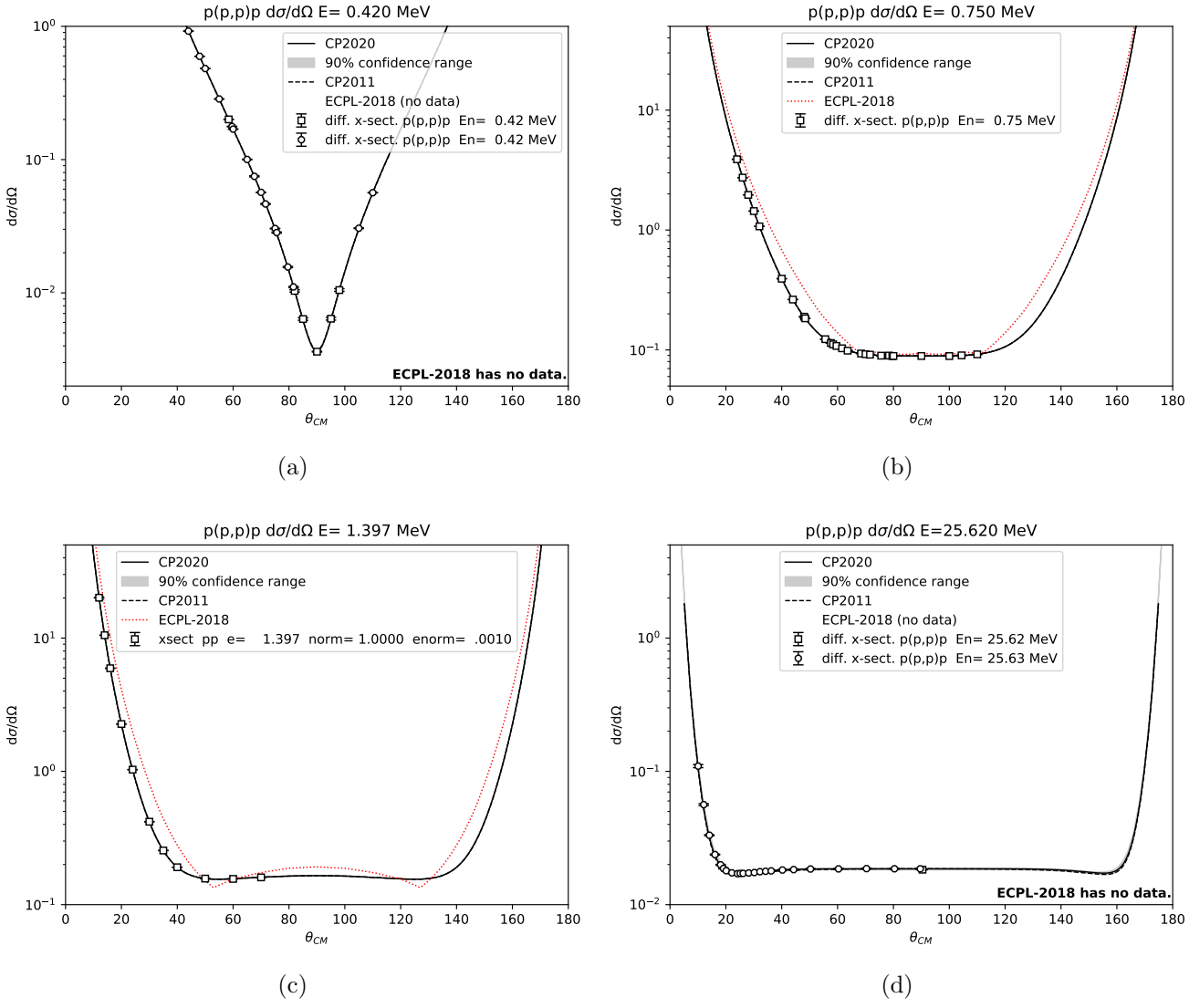

Figure 23: The differential cross section angular distributions in the center-of-mass frame for CP2020 (solid curves) compared with those of CP2011 (dashed curves, when available), the ECPL-2018 ENDF evaluated data, and the experimentally observed data for $^1\mathrm{H}(p,p)^1\mathrm{H}$ scattering. Panels correspond to values of the deuteron laboratory energy E_d (in MeV): 0.42, 0.75, 1.40, 25.62.

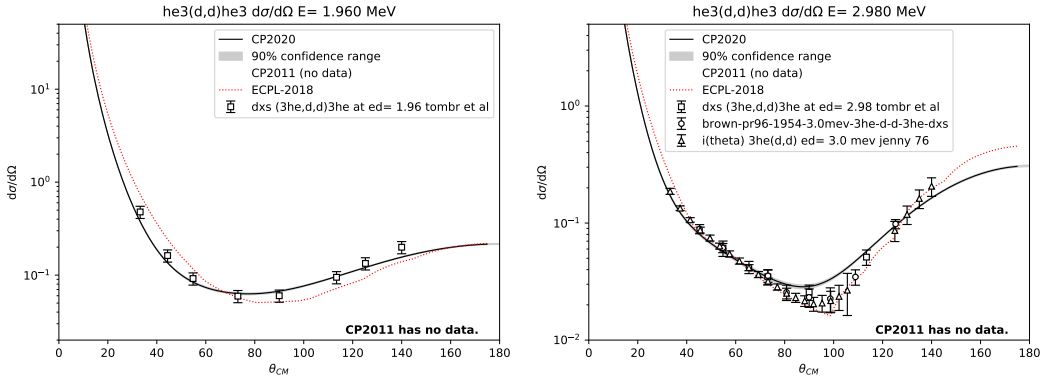

(a)

(b)

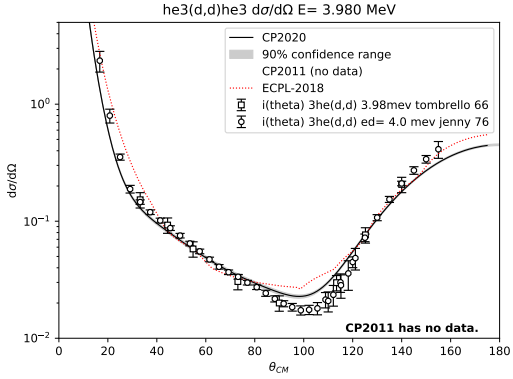

(c)

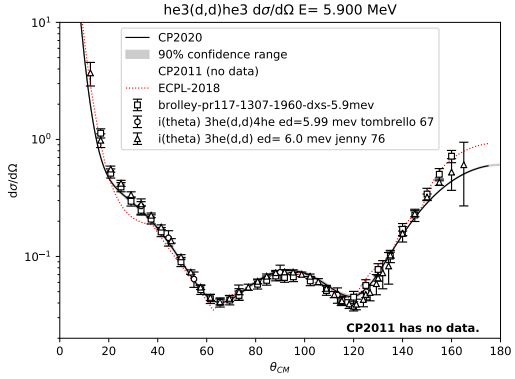

(d)

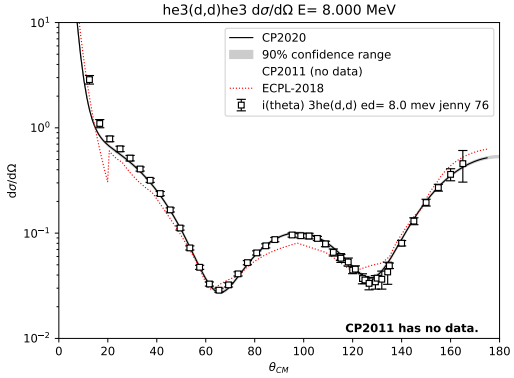

(e)

Figure 24: The differential cross section angular distributions in the center-of-mass frame for CP2020 (solid curves) compared with those of CP2011 (dashed curves, when available), the ECPL-2018 ENDF evaluated data, and the experimentally observed data for the ^{3}He$(d,d)^3$He reaction. Panels correspond to values of the deuteron laboratory energy E_d (in MeV): 1.96, 2.98, 3.98, 5.90, and 8.00.

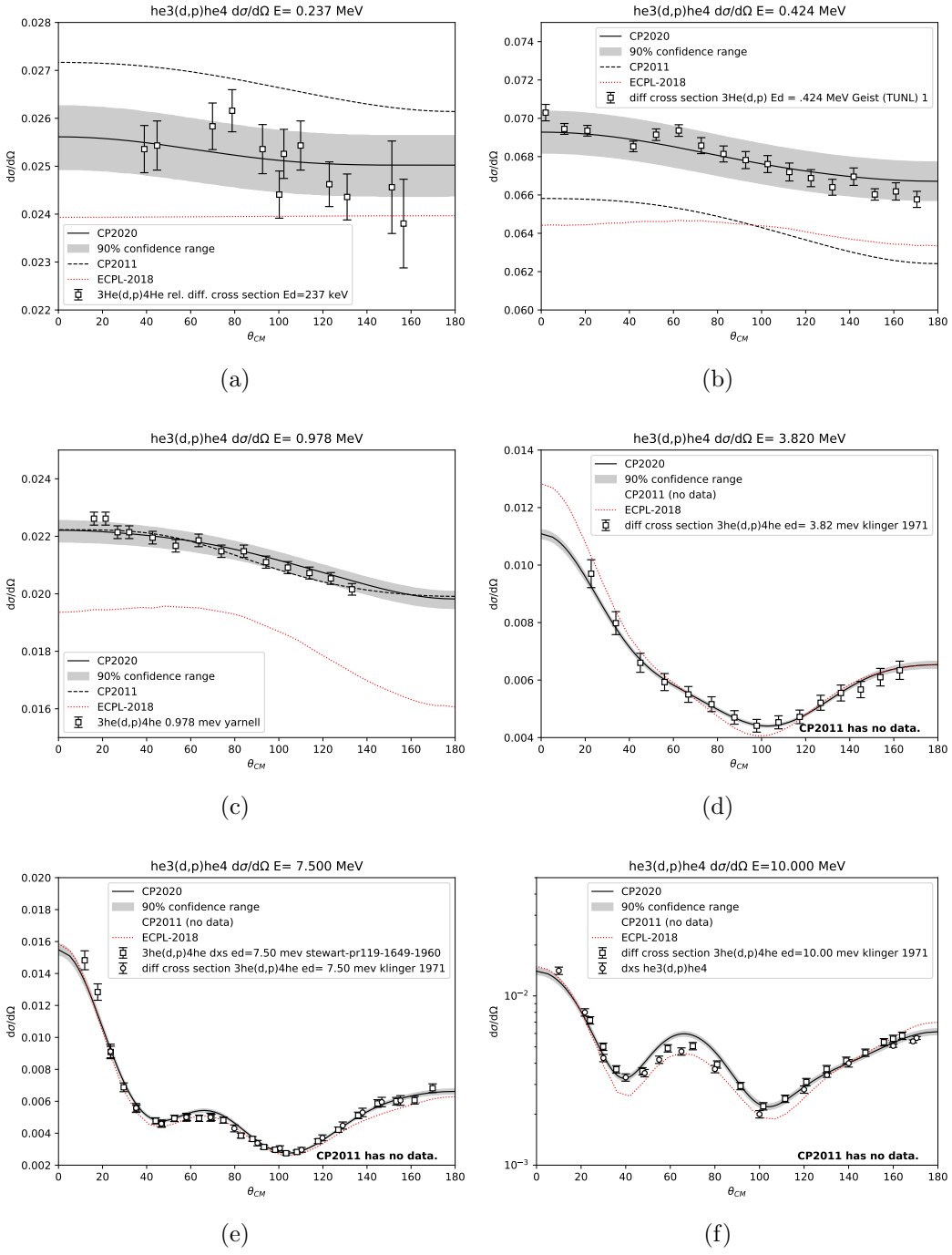

Figure 25: The differential cross section angular distributions in the center-of-mass frame for CP2020 (solid curves) compared with those of CP2011 (dashed curves, when available), the ECPL-2018 ENDF evaluated data (dotted curves), and the experimentally observed data for the ^{3}He$(d,p)^4$He reaction. Panels correspond to values of the deuteron laboratory energy E_d (in MeV): 0.24, 0.42, 0.98, 3.82, 7.50, 10.0.

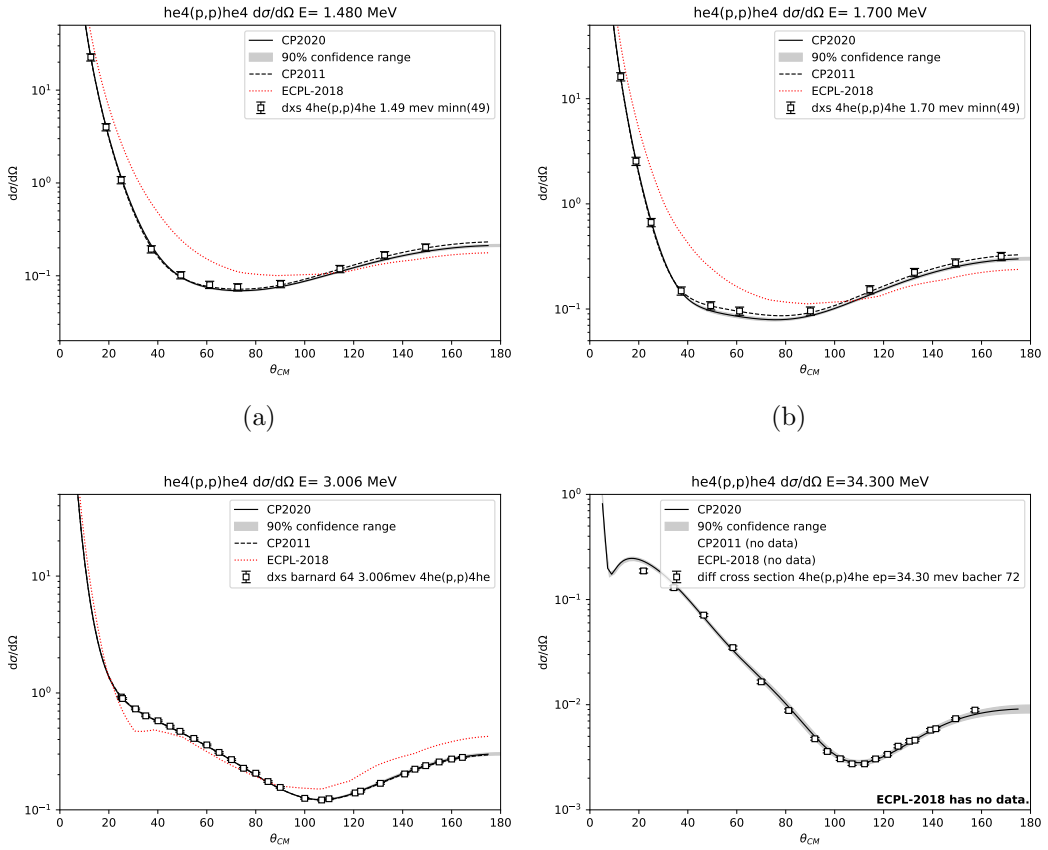

Figure 26: The differential cross section angular distributions in the center-of-mass frame for CP2020 (solid curves) compared with those of CP2011 (dashed curves, when available), the ECPL-2018 ENDF evaluated data (dotted curves), and the experimentally observed data for the ^{4}He$(p,p)^4$He reaction. Panels correspond to values of the deuteron laboratory energy E_p (in MeV): 1.48, 1.70, 3.01 and 34.30.

Figure 24 shows a comparison of the CP2020, CP2011 and ECPL-2018 evaluated data compared to the observed experimental data a five deuteron laboratory energies E_d. This graphical representation of the ECPL-2018 data (here and in the other figures showing this data) is interpolated from an energy grid that is more coarse than that for CP2011 and CP2020; the level of error introduced by this interpolation, if any, has not been studied. The comparison of the reaction ^{3}He(d,p)^{4}He angular distributions are also shown in Fig. 25.

The ECPL-2018 d+^{3}H file has been processed via NJOY 2016.53 to the CE representation. The angular distributions as a function of deuteron laboratory energy are compared in Fig. 22.

4.6 Verification of the CP2020 CE & MG libraries

In response to recommendations from the CP2020 final review committee[70] we have undertaken sample testing of the CE (ACE formatted) nuclear cross section data libraries. "Pencil beam" (aka "broomstick") problems for deuterons impinging on tritons (d+^{3}H) have been performed[71]. These studies used extensively in Monte Carlo neutronic code verification studies[72]. At Los Alamos, they were used to verify the changes associated with the upgrade of NJOY[12]/ MCNP[37] to allow continuous angular distributions[73] (instead of discrete angular distributions) from $S(\alpha, \beta)$ scattering. Recently, "pencil beam" problems have been applied to the verification of charged particle data for MCNP.

In addition to the pencil-beam studies discussed below, another verification test for CP2020 was performed to compare the continuous energy reaction cross sections generated by ACER with multigroup reaction cross sections generated by GROUPR from the same evaluation file. This method was also used in the verification of the most recent $S(\alpha, \beta)$ neutron libraries at Los Alamos[71].

4.6.1 "Pencil beam" problem description

A pencil beam (also known as a "broomstick") problem in Monte Carlo is a fixed source problem in which mono-energetic source particles are directed along a thin cylinder (pencil beam or broomstick) of target material. The source particles will collide once with a target nucleus and then either be scattered out of the cylinder or absorbed in a nuclear reaction.

The cylinder is surrounded by void that has zero importance. Using the `frv` option of the `ft` tally card in MCNP, the angular distribution of the scattered particles relative to their starting direction can be tallied on the surface of the pencil beam. Tallies are also kept of the energy distribution of the scattered particles as they leave the pencil beam; cell-based tallies can also be recorded as desired. At present, MCNP does not tally reactions from deuterons, tritons, helium3s, and alphas; reactions tallies from protons are, however, tracked.

4.6.2 MCNP sample input deck

A sample MCNP input deck is given below for 5 MeV deuterons impinging on tritons. Deuteron transport is specified by the `d` identifiers on the `imp`, `mode`, `phys`, `cut`, and `f` tally cards. Triton target nuclei are specified by the `m1` card entry of `1003.00o`. The `o` suffix of the `zaid` identifies deuteron transport (see Table 5 below). An arbitrary density of 1.0 g/cc for the triton material is set in the card for cell 1.

```
test deck for ENDF/B VIII cp in MCNP
1 1 -1.00 -1 2 -3 imp:d=1
2 0 1:-2:3 imp:d=0
1 cx 1.0e-8
2 px -100
3 px 100
mode d
cut:d j 0
phys:d 150 J J J 0 J J J J J 1 1 0
nps 100000000
sdef pos= 0 0 0 erg=5.0 vec=1 0 0 nrm=1 dir=1
tmp 2.53e-08 2.53e-08
lca 7j -2
m1 1003.00o 1.0
f1:d 1
e1 0.01 498I 5.0 10.0 T
f4:d 1
fm4 (1 1 50) (1 1 51)
f14:d 1
f31:d 1
c31 -0.995 198I 0.0 199I 1.0
ft31 frv 1 0 0
print
```

The pencil beam material is inside of cylindrical surface 1 in between planar surfaces 2 and 3. Note that for MCNP6, the angular cosine bins on the tallies (the `c` cards) assume an initial value of -1.0 – as opposed to MCNP5, where the user has to supply the -1.0.

The `lca 7J -2` card activates a special option in MCNP 6.2 where "source particles immediately collide; and all progeny escape. In other words, all secondary particles produced are transported with no interactions and no decay. This option is used to compute and tally double-differential cross sections." Without a `lca` card, the statistics for the scattered charged particle angular and energy distributions are very noisy (since most particles propagate within the cut-off angle window and don't need the scattering distributions) and also smeared in energy. They are smeared in energy since charged particles lose energy continuously along their flight path and thus their

Source Particle	`mode`, `phys`, `imp`, `cut`, and `F` (tally) cards	Target `zaid` index ID (`M` card)
proton	`h`	`h`
deuteron	`d`	`o`
triton	`t`	`r`
helium3	`s`	`s`
alpha	`a`	`a`

Table 5: MCNP particle identifier conventions used in the CP2020 verification efforts.

energies differ from the original source energy at the first real collision. This is why the special `lca` option immediately collides the particles.

The `lca` option does not include particles which scatter within the center of mass (COM) cut-off angle of 0.96 to 1.0. For same particle scattering, the symmetric angles between -1.0 and -0.96 are also excluded. Since all of the particle histories are used, the tallies are well converged for the scattering angle distribution and the scattered energy distribution.

The `cut:d J 0` card is required to override MCNP's default lower energy limits for charged particles. The hard-wired lower limit for these charged particles transported by MCNP is 1 keV, but the code default limits are 1,2,3,3, and 4 MeV for protons, deuterons, tritons, helium3s, and alphas, respectively.

For this sample problem, 100 million particle histories were run and the whole calculation ran in 5 to 15 minutes on 1 CPU on the `snow` mainframe platform. Unfortunately, MCNP does not allow threading for CP transport like it does for neutron transport.

4.6.3 Comparison of MCNP tallies to ACE cross section

Two plots of results from the DT sample problem are given below. The first shows the angular scattering distribution and the second shows the energy distribution of the scattered deuterons. Experimentally measured angular points from the data used in the evaluation were converted to the centered of mass and approximately normalized to show the similar shapes.

The MCNP tallies are shown as a fine histogram (corresponding to a fine angular grid). The center of mass ACER probability distribution function (pdf) points of the 5 MeV angular scattering distribution calculated by NJOY from the evaluation file were converted to the lab frame for comparison. The `lca` option only samples points from the bounded scattering data. There is, therefore, no tally response in the lab angles (0.998506 to 1.0) corresponding to the 0.96 to 1.0 com cut-off angles for this particular reaction.

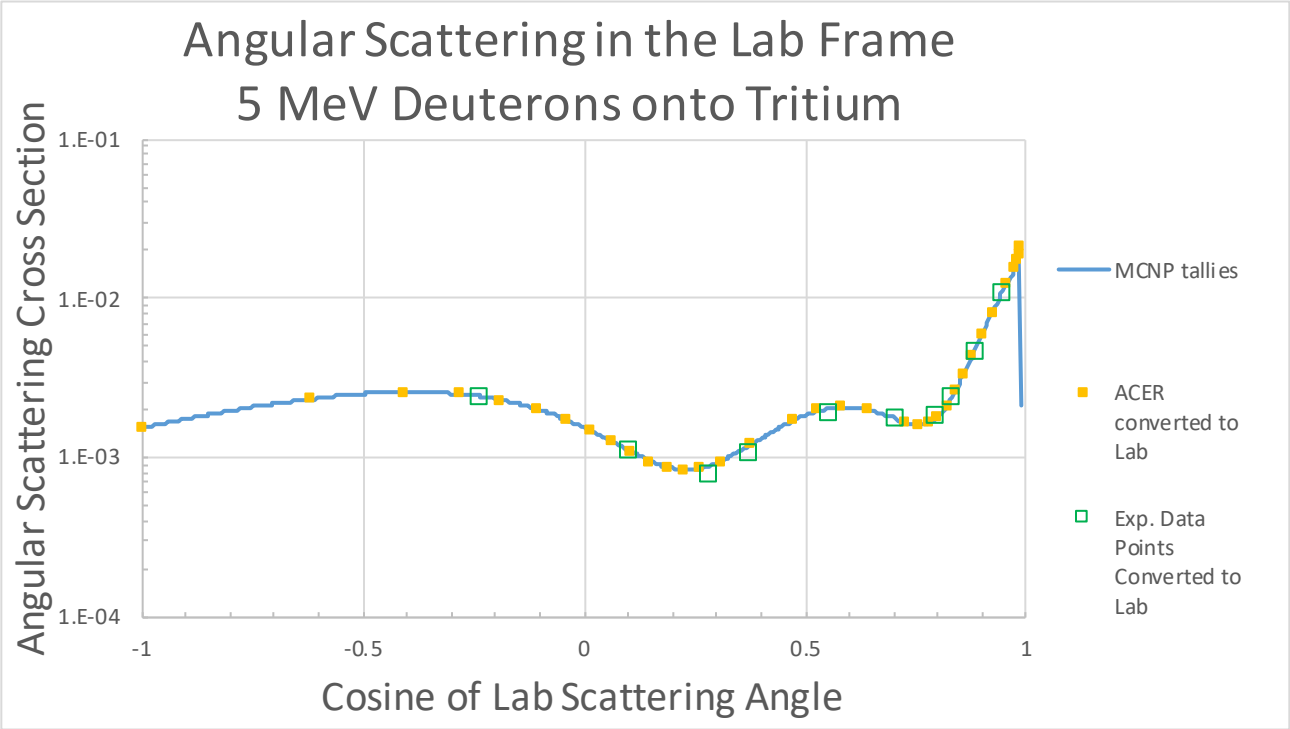

Figure 27: Laboratory angular scattering distribution for 5 MeV deuterons on tritons. (Note that the normalization of the 2 curves is arbitrary.)

Angles in the lab $\mu_l = \cos\theta_l$ may be calculated from the COM angles μ_c as:

$$\mu_l = \frac{(1 + A\mu_c)}{\sqrt{A^2 + 2A\mu_c + 1}}, \tag{11}$$

where A is the mass of the target in unit of the mass of the projectile. Angular cross sections σ_l at lab angles are related to COM cross sections σ_c as:

$$\sigma_l(\mu_l) = \sigma_c(\mu_c)\frac{d\mu_c}{d\mu_l}, \tag{12}$$

where

$$\frac{d\mu_l}{d\mu_c} = \frac{-A(1 + A\mu_c)}{(A^2 + 2A\mu_c + 1)^{3/2}} + \frac{A}{\sqrt{A^2 + 2A\mu_c + 1}}. \tag{13}$$

The energy distribution for the scattered deuterons is shown in Fig. 28. Here, the very fine MCNP tallies are shown at their midpoint values. The depressions at the low and high energy ends of the curve are a result of the tally bin boundaries not exactly lining up with the true minimum and maximum scattered energies.

The ACER results in Fig. 28 were calculated from the 5 MeV incident deuteron angular elastic scattering distribution as follows. The scattered deuteron energy E_{scat} is given in terms of the incident lab energy E_{inc} and the COM angle μ_c as:

$$E_{\text{scat}} = E_{\text{inc}}\frac{A^2 + 2A\mu_c + 1}{(A + 1)^2} \tag{14}$$

The values that are plotted are the pdf values of the distribution associated with the center of mass angle versus the energies of the scattered deuterons at the same angle.

4.6.4 Impact of "pencil beam" results

The process of setting up and running a pencil beam problem exercises both the Monte Carlo code and the nuclear data. Particle histories are followed in the calculation requiring that the code can read and use the data without error and produce the requested tallies. This gives a format-consistency test of code and data. It exercises the code and data in the essential actions of a complete modeling simulation.

This kind of verification test is not a code (or data) validation – since no real physical data measurements are modelled. Nevertheless, it is a useful verification exercise and often exposes consistency problems in the data, the xsdir directory entries, or in the Monte Carlo code itself. For the CP2020 project, this exercise uncovered some incorrect dictionary entries in the deuteron onto Li7 evaluation.

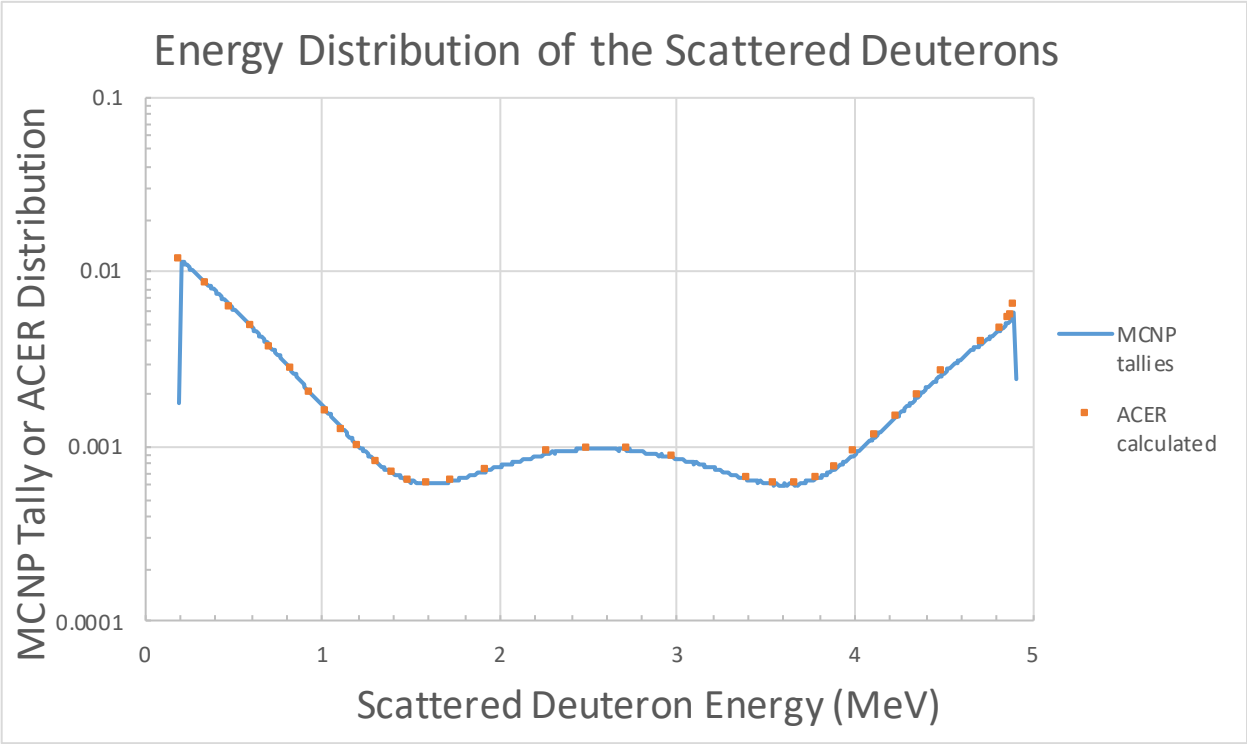

Figure 28: Energy distribution of scattered deuterons leaving the pencil beam (arbitrary normalization).

4.6.5 Complete testing for charged-particle transport in MCNP

Complete testing of the 25 charged particle ACE files from CP2020 requires 5 different kinds of charged particle transport in MCNP, which depend on the ACE file and MCNP problem setup; protons, deuterons, tritons, helium3s, or alphas may be transported. The target nuclei may be any of these 5 particles or ^{6}Li or ^{7}Li nuclei.

The following table lists the particle identifier to be used on the `mode`, `phys`, `imp`, `f` (tally), `cut`, and `m` (material) cards for each of the 5 source particles. Notice that the `zaid` index ID is different for deuterons and tritons than it is for the other source particles. This is because `d` and `t` were already used for discrete and thermal $S(\alpha, \beta)$ neutron data, respectively, before the charged particle transport data capability was added to MCNP.

The following table summarizes the CP2020 data and gives the energy range for the data. Note that NJOY establishes the energy range used in the ACER files from the limits of the elastic scattering data in the evaluation. The MCNP defaults for the lower energy bound can be changed by a cut card. However, in no case can the lower energy in NJOY or MCNP go below 1 keV.

4.6.6 ACER–GROUPR Comparisons

The second verification method used for CP2020 is to compare the integrated reaction cross sections from ACER with the multi-group reaction cross sections from GROUPR based on the same evaluation file. Assuming the same evaluation file was used for both, this comparison provides some verification assurance because independent code modules (ACER and GROUPR) are used to calculate the same integrated cross section.

A sample GROUPR input is given below for deuterons impinging on tritons. Note that the RECONR module must also be used to convert the evaluation file into the pointwise format required by GROUPR.

With the very low values of the reaction cross sections in the DT evaluation file, RECONR produces some underflow NaN's in the pointwise file used by GROUPR. These NaN's must be manually set to zero before the GROUPR module can be called. (Otherwise, GROUPR crashes on the NaN values.) Since, the NaN's do not appear for other evaluations, they may be the result of the extra low energy reaction cross sections present in the DT evaluation.

	Incident particle	Particle id	Target	`zaid`	MCNP min E (MeV)	low E (MeV)	high E (MeV)	Source
1	proton	h	proton	1001.00h	1	0.001	150	lanl
2	proton	h	deuteron	1002.00h	1	0.1	150	lanl
3	proton	h	triton	1003.00h	1	0.0001	12	lanl
4	proton	h	helium3	2003.00h	1	0.001	20	lanl
5	proton	h	alpha	2004.00h	1	0.02	34.3	lanl
6	proton	h	Li-6	3006.00h	1	0.001	2.5	lanl
7	proton	h	Li-7	3007.00h	1	0.0001	3	lanl
8	deuteron	d	deuteron	1002.00o	2	0.0001	10	lanl
9	deuteron	d	triton	1003.00o	2	0.01	10	lanl
10	deuteron	d	helium3	2003.00o	2	0.1	20	lanl
11	deuteron	d	alpha	2004.00o	2	0.01	10	lanl
12	deuteron	d	Li-6	3006.00o	2	0.001	1	lanl
13	deuteron	d	Li-7	3007.00o	2	0.02	20	lanl
14	triton	t	triton	1003.00r	3	0.0005	2	lanl
15	triton	t	helium3	2003.00r	3	0.0001	3	lanl
16	triton	t	alpha	2004.00r	3	0.1	20	lanl
17	triton	t	Li-6	3006.00r	3	0.02	20	lanl
18	triton	t	Li-7	3007.00r	3	1	200	tendl
19	helium3	s	helium3	2003.00s	3	0.004	2	lanl
20	helium3	s	alpha	2004.00s	3	0.02	11	lanl
21	helium3	s	Li-6	3006.00s	3	0.02	20	lanl
22	helium3	s	Li-7	3007.00s	3	1	200	tendl
23	alpha	a	alpha	2004.00a	4	0.1	20	lanl
24	alpha	a	Li-6	3006.00a	4	1	200	tendl
25	alpha	a	Li-7	3007.00a	4	1	200	tendl

Table 6: Summary of CP2020 charged particle data.

```
reconr
21 22 /
'automated processing using ndvv.njoy.process see *.log files' /
131 0 0 /
100.0 0.0 0.01 5.0000000000000004e-08 /
0 /
groupr
20 22 0 0 /
131 2 0 2 4 1 1 1 /
'groupr run for CP data' /
0.0 /
1e10 /
3 50 /
3 51 /
6 50 /
6 51 /
0 /
0 /
stop
```

In this example, a built-in GROUPR library group structure called "CSEWG" with 239 groups was used to give a relatively fine energy grid. The fine energy grid reduces the effect of the weighting function on the final cross sections. The weighting function for this example is "constant" – i.e., use the energy group widths.

In the following figure, the multi-group GROUPR cross sections are shown by histograms, while the continuous energy ACER cross sections are shown as a smooth curve.

5 Conclusion and future work priorities

The CP2020 Level-2 Milestone work documented in this report, is a collaborative effort between personnel in three divisions (Computer, Computational and Statistical Sciences Division, Theoretical Division, & X-Computational Physics) housed in two Associate Laboratory Directorates (Science, Technology and Engineering & Weapons). The completion criteria was, as detailed as complete on the first page of this report, broadly to deliver modern charged-particle transport tabular data libraries, a revised version of NDI, and documentation[74].

We gave an overview of the four classes of nuclear data, as prescribed and defined in the CP2011 Level-2 effort, encompassing *i)* evaluated nuclear cross section data, *ii)* continuous-energy NCS data, *iii)* multigroup NCS data, and *iv)* CP stopping power (dE/dx) data. We outlined at progressively finer levels of detail, the *Nuclear Data pipeline*, as shown in Fig. 1, that begins with evaluation of experimentally observed data by adjusting fit parameters of nuclear data models in

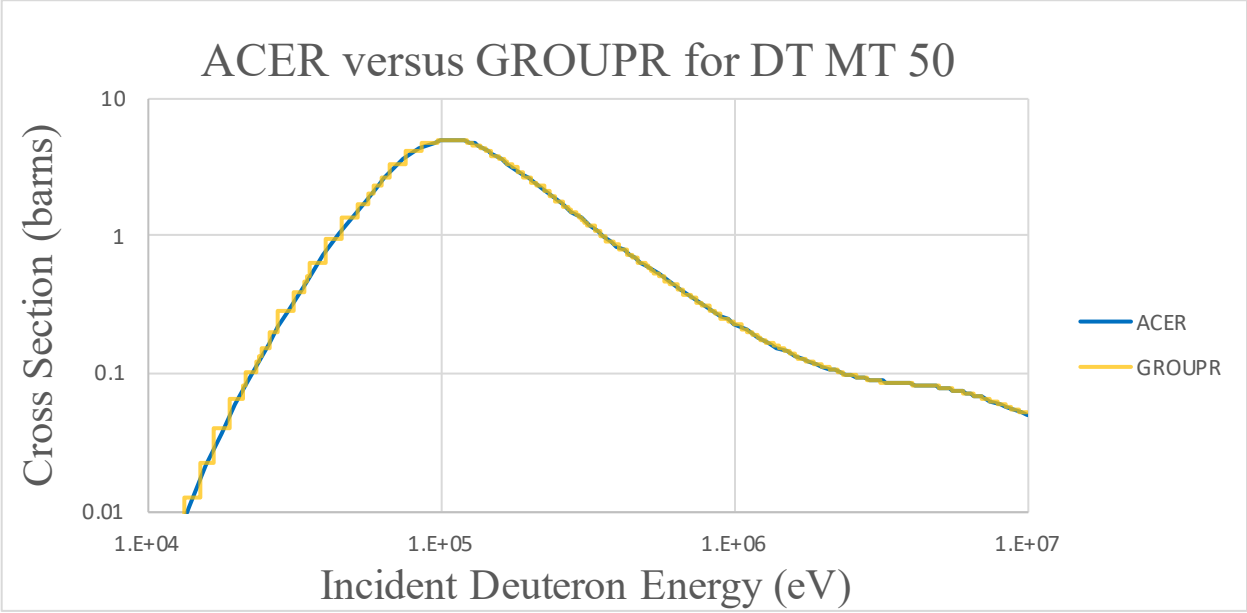

Figure 29: Comparison of ACER and GROUPR cross sections for $^{3}\mathrm{H}(d,n)^{4}\mathrm{He}$ (`MT=50`).

an optimization procedure, goes through a processing code (here NJOY) to generate cross section libraries from the underlying ENDF formatted evaluated data to formats (ACE and NDI) that allow users and applications codes to employ the nuclear reaction and scattering cross sections for applications of interest in nuclear security, energy and safety.

Further, the CPT L2 teams collected information on the sources of the evaluations and their processing as used to deliver the CPT data for CP2011 effort. This was done in the interest of providing continuity of the current CP2020 effort to the past CP2011 work. Evaluation work that was new for CP2011 was described in terms of the experimental data included in the evaluations. Efforts to *re*-process these evaluations in the CP2020 project using both old code tools (NJOY 99) and new processing tools (NJOY 2016 and NJOY 21) were described, with particular focus on the reproducibility of the CE and MG libraries with the new processing capabilities. New evaluation work for CP2020 was described in some detail, including new experimentally observed data that was included in the existing evaluations; tabular data (in the appendices) and graphical plots comparing the old CP2011 evaluations (where available), the new evaluated data, and the experimentally observed data, were developed to allow users to better understand the underlying physics and evaluation models used to develop the evaluated data represented by the ENDF formatted data files.

During the course of this CP2020 work, we have discovered and corrected several errors, involving documentation, codes, and ENDF-encoded data that affected the content of the CE and MG library data that is consumed by user applications codes. These have been described in detail in this report.

We have provided some testing of the ENDF data files that allow quality assurance and some uncertainty quantification to users. The work has been organized in an online repository that stores the evaluated data, documentation, and code.

5.1 Priorities for future work

The CP2020 project for charged-particle transport applications has made several advances in the areas of CP-relevant evaluations – extending to higher energies previous evaluations, processing to CE and MG formatted cross-section libraries, and in the development of user-application interfaces to improve nuclear data usability. While systematic verification and validation were not undertaken as a Milestone objective, some testing of the evaluation files was performed to address recent and long-standing issues of energy-conservation related to the role of charged-particle secondaries and recoil nuclei.

The main objectives of this CP2020 L2 effort were the documentation and clarification of previous ENDF evaluation data, the production of new ENDF evaluations, and the processing of both new and old ENDF evaluations with new NJOY code versions to ACE and NDI formats. Through this work, we have identified a list of prioritized future research objectives that will permit the development of high-fidelity cross section libraries for use in obtaining accurate simulations in a variety of applications where the characteristics of nuclear cross sections and the energy-transport mechanisms are important.

The priorities for future work fall into three main categories and address each the four main types of ND discussed in Section 1.1.

5.1.1 Priorities in future evaluation work

At the base of the ND pipeline [Fig. 1] is the evaluation work of going from experimentally observed data to resonance-parameter and/or continuous energy and angle representations of the data (constrained by known, essential principles of physics like conservation rules, symmetries, and causality). The three phases of the evaluation effort – data handling, modeling and model fitting, and post-processing require modernization of existing code tools. Modeling of the complex physical processes of direct and resonant nuclear reactions – particularly those resulting in breakup of the target nucleus and/or the projectile – in an accurate and economical manner require new model developments. This will allow the evaluations to go to higher energies. Going to higher energies also ensures that existing, lower-energy evaluations are robust with respect to the data and that model dependencies and inaccuracies are under control.

The following priorities address each of the three parts of the evaluation process.

1. Data-handling/uncertainty quantification priority: refactor existing data-handling codes to use the latest innovations of the NNDC (likely `json`-based) *experimental templates* being

developed by Neudecker and collaborators[75];

2. Evaluation priority: extend energy range of precision (R matrix theoretical) cross section models to the full, 'official' laboratory-energy range of 0 to 20 MeV for all projectiles;

3. Post-processing priority: improve the communication, interoperability and usability of evaluated nuclear data by making available pointwise, continuous energy and angle representations of this data as well as resonance-parameter (R matrix parameters) descriptions of the data.

5.1.2 Priorities in future processing codes

Inclusion of processing for the neutron-induced, charged-particle production data into NDVV, which is currently not in-place, should be effected; the amount of extra data this would introduce in the MG NDI library is relatively small, but CP is becoming more valued. A relatively small tasking effort would be required to automate the steps outlined in Section 3.2.2. However, testing and implementation to generalization to automation so that it works for all materials could require considerable additional effort.

The NDI format is becoming an increasingly important deliverable to our customers. However, the Nuclear Data Team has been relying on a script to generate this format that is neither well developed nor robust. A formal NJOY 2016/NJOY 21 module for creating NDI representations of the data – called NDIR – would ameliorate this deficiency. A significant effort for module development, testing, and production roll-out for long-term use is required.

The following priorities address developments required for the improvements just discussed.

1. Development of modern, robust NDIR NJOY module to efficiently produce NDI-formatted data from neutron induced multigroup energy (*e.g.*, GENDF or GNDS) data.

2. The preferred tool for automating processing, NDVV, is not currently capable of processing charged particle evaluations. Development of this capability would improve quality control of the processing effort and reduce the effort associated with preparing input files and running code. Develop practice of including charged-particle production data along with the other data that is regularly produced.

3. Current light element and charged particle evaluations based on EDA R-matrix analysis have always required the resulting cross sections and angular-energy distributions to be linearized due to the incompatibility between EDA's general R-matrix formalism (and associated relativistic kinematics) and the formalisms available in the ENDF format. Within the code modernization process for NJOY, a new R-matrix kernel has been developed that can be extended to EDA specifications. Consistency between evaluation and processing can be improved if the new kernel can be used by both EDA and NJOY.

4. The comparisons between CP2011 and CP2020 in this report were generated using the start of a new effort for visualizing ENDF data. Legacy NJOY visualization capabilities, while

still able to create professional-looking plots, are limited to certain types of data and lacks a modern interface. Expanding the modernized capability would help future evaluation efforts and enable direct comparisons between evaluated and application data.

5. A modern tool to convert ENDF-based energy and angular distributions into proper double differential cross section data would be useful for multiple applications, including the visualization capabilities mentioned in the previous point. Visualization of double differential data allows more readily for comparisons between distributions with differing representations. Such a tool would feed into modernization efforts for several NJOY components, including ACER, HEATR, GROUPR, and ERRORR.

5.1.3 Priorities in future user-interface work

The addition of stopping power data to NDI has confirmed the difficulty of adding new data types to NDI. This reaffirms the need for a new, updated version of NDI (NDI 3). NDI 3 will make implementing new data types more straightforward. It might also be useful to have additional charged-particle production data files. Producing charged-particles requires only reaction data, and not scattering or fission data. NDI 2 suffers from being too slow because it typically reads in 618 group scattering data, which is O(618x618). Having separate data, much like the radiochemistry dosimetry files, could speed up data reading for charged-particle production.

Additionally, there needs to be an independent reader of CPT ACE data, possibly combined with a standardized generic ACE reader. Currently, codes that use CPT ACE data have their own internal readers, which makes updating data formats difficult. Any changes to the CPT ACE data require changes to the host codes readers. It would be preferable to have a reader developed by the nuclear data team that other codes could interface with, much like NDI with multigroup data.

Appendices

A ENDF/B version comparisons in digest form

The ENDF format is not easily legible. A sample of the ENDF data for the file `n-003_Li_006.endf` for the process $^6\mathrm{Li}(n,n'd)^4\mathrm{He}$ is shown in the next table.

```
 3.006000+3 5.963450+0          0          2          3          0 325 6 32
 1.000000+0 1.000000+0          0          1          1          2 325 6 32
          2          2                                              325 6 32
 1.721184+6 1.000000+0 2.000000+7 1.000000+0                        325 6 32
 0.000000+0 0.000000+0          1          2          1         81 325 6 32
         81          2                                              325 6 32
 0.000000+0 1.721184+6          0          0          6          3 325 6 32
 0.000000+0 0.000000+0 5.000000+4 3.442222-5 5.810200+4 0.000000+0 325 6 32
```

```
 0.000000+0 1.800000+6          0          0          6          3 325 6 32
 0.000000+0 0.000000+0 5.000000+4 3.442222-5 5.810200+4 0.000000+0 325 6 32
 0.000000+0 1.900000+6          0          0          8          4 325 6 32
 0.000000+0 0.000000+0 5.000000+4 1.203195-5 1.000000+5 9.783956-6 325 6 32
 1.314400+5 0.000000+0                                             325 6 32
 0.000000+0 2.000000+6          0          0         12          6 325 6 32
 0.000000+0 0.000000+0 5.000000+4 6.419084-6 1.000000+5 6.917682-6 325 6 32
 1.500000+5 5.678785-6 2.000000+5 1.797095-6 2.047800+5 0.000000+0 325 6 32
 0.000000+0 2.100000+6          0          0         14          7 325 6 32
 0.000000+0 0.000000+0 5.000000+4 4.287791-6 1.000000+5 4.966690-6 325 6 32
 1.500000+5 4.785990-6 2.000000+5 4.007392-6 2.500000+5 2.498895-6 325 6 32
```

This table contains `MF=6, MT=32` data, which corresponds to the energy and angular distribution of the neutron, deuteron and alpha-particle secondary charged-particle production. There is no textual information.

The tables in this appendix are intended to allow the determination of the content of the files, in a form that is readable. It also should permit the reader to distinguish differences and extensions of the four different sets of ENDF libraries that are referenced in this report: ENDF/B-VII.1, CP2011, ENDF/B-VIII.0, and CP2020.

MF	MT	Description	Energy range [MeV]
3		Reaction cross sections	
	2	(z,z0)	(1.00, 200.00)
	3	(z,nonelas.)	(1.00, 200.00)
	4	(z,n)	(9.29, 200.00)
	5	(z,anything)	(0.00, 200.00)
	16	(z,2n)	(37.56, 200.00)
	17	(z,3n)	(59.24, 200.00)
	22	(z,nα)	(9.43, 200.00)
	28	(z,np)	(6.31, 200.00)
	102	(z,γ)	(0.00, 200.00)
	103	(z,p)	(3.54, 200.00)
	104	(z,d)	(2.61, 200.00)
	105	(z,t)	(23.66, 200.00)
	106	(z,^{3}He)	(22.20, 200.00)
	107	(z,α)	(3.64, 200.00)
6		Energy-angle distributions for emitted particles	
	2	(z,z0)	
	4	(z,n)	
	5	(z,anything)	
	16	(z,2n)	
	17	(z,3n)	
	22	(z,nα)	
	28	(z,np)	
	102	(z,γ)	
	103	(z,p)	
	104	(z,d)	
	105	(z,t)	
	106	(z,^{3}He)	
	107	(z,α)	

Table 7: CP2011 library, file: a-003_Li_006.endf

MF	MT	Description	Energy range [MeV]
3		Reaction cross sections	
	2	(z,z0)	(1.00, 200.00)
	3	(z,nonelas.)	(1.00, 200.00)
	4	(z,n)	(9.29, 200.00)
	5	(z,anything)	(0.00, 200.00)
	16	(z,2n)	(37.56, 200.00)
	17	(z,3n)	(59.24, 200.00)
	22	(z,nα)	(9.43, 200.00)
	28	(z,np)	(6.31, 200.00)
	102	(z,γ)	(0.00, 200.00)
	103	(z,p)	(3.54, 200.00)
	104	(z,d)	(2.61, 200.00)
	105	(z,t)	(23.66, 200.00)
	106	(z,^{3}He)	(22.20, 200.00)
	107	(z,α)	(3.64, 200.00)
6		Energy-angle distributions for emitted particles	
	2	(z,z0)	
	4	(z,n)	
	5	(z,anything)	
	16	(z,2n)	
	17	(z,3n)	
	22	(z,nα)	
	28	(z,np)	
	102	(z,γ)	
	103	(z,p)	
	104	(z,d)	
	105	(z,t)	
	106	(z,^{3}He)	
	107	(z,α)	

Table 8: CP2020 library, file: a-003_Li_006.endf

MF	MT	Description	Energy range [MeV]
3		Reaction cross sections	
	2	(z,z0)	(1.00, 200.00)
	3	(z,nonelas.)	(1.00, 200.00)
	4	(z,n)	(5.51, 200.00)
	5	(z,anything)	(0.00, 200.00)
	16	(z,2n)	(17.63, 200.00)
	17	(z,3n)	(46.80, 200.00)
	22	(z,nα)	(11.39, 200.00)
	28	(z,np)	(14.72, 200.00)
	37	(z,4n)	(67.25, 200.00)
	102	(z,γ)	(0.00, 200.00)
	103	(z,p)	(4.02, 200.00)
	104	(z,d)	(11.23, 200.00)
	105	(z,t)	(4.02, 200.00)
	106	(z,^{3}He)	(29.12, 200.00)
	107	(z,α)	(0.75, 200.00)
6		Energy-angle distributions for emitted particles	
	2	(z,z0)	
	4	(z,n)	
	5	(z,anything)	
	16	(z,2n)	
	17	(z,3n)	
	22	(z,nα)	
	28	(z,np)	
	37	(z,4n)	
	102	(z,γ)	
	103	(z,p)	
	104	(z,d)	
	105	(z,t)	
	106	(z,^{3}He)	
	107	(z,α)	

Table 9: CP2011 library, file: `a-003_Li_007.endf`

MF	MT	Description	Energy range [MeV]
3		Reaction cross sections	
	2	(z,z0)	(1.00, 200.00)
	3	(z,nonelas.)	(1.00, 200.00)
	4	(z,n)	(5.51, 200.00)
	5	(z,anything)	(0.00, 200.00)
	16	(z,2n)	(17.63, 200.00)
	17	(z,3n)	(46.80, 200.00)
	22	(z,nα)	(11.39, 200.00)
	28	(z,np)	(14.72, 200.00)
	37	(z,4n)	(67.25, 200.00)
	102	(z,γ)	(0.00, 200.00)
	103	(z,p)	(4.02, 200.00)
	104	(z,d)	(11.23, 200.00)
	105	(z,t)	(4.02, 200.00)
	106	(z,^{3}He)	(29.12, 200.00)
	107	(z,α)	(0.75, 200.00)
6		Energy-angle distributions for emitted particles	
	2	(z,z0)	
	4	(z,n)	
	5	(z,anything)	
	16	(z,2n)	
	17	(z,3n)	
	22	(z,nα)	
	28	(z,np)	
	37	(z,4n)	
	102	(z,γ)	
	103	(z,p)	
	104	(z,d)	
	105	(z,t)	
	106	(z,^{3}He)	
	107	(z,α)	

Table 10: CP2020 library, file: `a-003_Li_007.endf`

MF	MT	Description	Energy range [MeV]
3		Reaction cross sections	
	2	(z,z0)	(0.10, 20.00)
6		Energy-angle distributions for emitted particles	
	2	(z,z0)	

Table 11: CP2011 library, file: `a-002_He_004.endf`

MF	MT	Description	Energy range [MeV]
3		Reaction cross sections	
	2	(z,z0)	(0.29, 20.00)
6		Energy-angle distributions for emitted particles	
	2	(z,z0)	

Table 12: ENDF/B-VIII.0 library, file: `a-002_He_004.endf`

MF	MT	Description	Energy range [MeV]
3		Reaction cross sections	
	2	(z,z0)	(0.10, 20.00)
6		Energy-angle distributions for emitted particles	
	2	(z,z0)	

Table 13: CP2020 library, file: `a-002_He_004.endf`

MF	MT	Description	Energy range [MeV]
3		Reaction cross sections	
	2	(z,z0)	(0.01, 10.00)
	28	(z,np)	(3.34, 10.00)
6		Energy-angle distributions for emitted particles	
	2	(z,z0)	

Table 14: CP2011 library, file: `d-002_He_004.endf`

MF	MT	Description	Energy range [MeV]
3		Reaction cross sections	
	2	(z,z0)	(0.01, 10.00)
	28	(z,np)	(3.34, 10.00)
6		Energy-angle distributions for emitted particles	
	2	(z,z0)	

Table 15: CP2020 library, file: `d-002_He_004.endf`

MF	MT	Description	Energy range [MeV]
3		Reaction cross sections	
	2	(z,z0)	(0.01, 10.00)
	50	(z,n_0)	(0.00, 30.00)
	51	(z,n_1)	(3.71, 10.00)
6		Energy-angle distributions for emitted particles	
	2	(z,z0)	
	50	(z,n_0)	
	51	(z,n_1)	

Table 16: ENDF/B-VII.1 library, file: `d-001_H_003.endf`

MF	MT	Description	Energy range [MeV]
3		Reaction cross sections	
	2	(z,z0)	(0.01, 10.00)
	50	(z,n_0)	(0.00, 30.00)
	51	(z,n_1)	(3.71, 10.00)
6		Energy-angle distributions for emitted particles	
	2	(z,z0)	
	50	(z,n_0)	
	51	(z,n_1)	

Table 17: CP2011 library, file: `d-001_H_003.endf`

MF	MT	Description	Energy range [MeV]
3		Reaction cross sections	
	2	(z,z0)	(0.01, 10.00)
	50	(z,n_0)	(0.00, 30.00)
	51	(z,n_1)	(3.71, 10.00)
6		Energy-angle distributions for emitted particles	
	2	(z,z0)	
	50	(z,n_0)	
	51	(z,n_1)	

Table 18: ENDF/B-VIII.0 library, file: `d-001_H_003.endf`

MF	MT	Description	Energy range [MeV]
3		Reaction cross sections	
	2	(z,z0)	(0.01, 10.00)
	50	(z,n_0)	(0.00, 30.00)
	51	(z,n_1)	(3.71, 10.00)
6		Energy-angle distributions for emitted particles	
	2	(z,z0)	
	50	(z,n_0)	
	51	(z,n_1)	

Table 19: CP2020 library, file: `d-001_H_003.endf`

MF	MT	Description	Energy range [MeV]
3		Reaction cross sections	
	2	(z,z0)	(0.00, 10.00)
	50	(z,n_0)	(0.00, 10.00)
	600	(z,p_0)	(0.00, 10.00)
6		Energy-angle distributions for emitted particles	
	2	(z,z0)	
	50	(z,n_0)	
	600	(z,p_0)	

Table 20: ENDF/B-VII.1 library, file: `d-001_H_002.endf`

MF	MT	Description	Energy range [MeV]
3		Reaction cross sections	
	2	(z,z0)	(0.00, 10.00)
	50	(z,n_0)	(0.00, 10.00)
	600	(z,p_0)	(0.00, 10.00)
6		Energy-angle distributions for emitted particles	
	2	(z,z0)	
	50	(z,n_0)	
	600	(z,p_0)	

Table 21: CP2011 library, file: `d-001_H_002.endf`

MF	MT	Description	Energy range [MeV]
3		Reaction cross sections	
	2	(z,z0)	(0.00, 10.00)
	50	(z,n_0)	(0.00, 10.00)
	600	(z,p_0)	(0.00, 10.00)
6		Energy-angle distributions for emitted particles	
	2	(z,z0)	
	50	(z,n_0)	
	600	(z,p_0)	

Table 22: ENDF/B-VIII.0 library, file: `d-001_H_002.endf`

MF	MT	Description	Energy range [MeV]
3		Reaction cross sections	
	2	(z,z0)	(0.00, 10.00)
	50	(z,n_0)	(0.00, 10.00)
	600	(z,p_0)	(0.00, 10.00)
6		Energy-angle distributions for emitted particles	
	2	(z,z0)	
	50	(z,n_0)	
	600	(z,p_0)	

Table 23: CP2020 library, file: `d-001_H_002.endf`

MF	MT	Description	Energy range [MeV]
3		Reaction cross sections	
	2	(z,z0)	(0.01, 1.40)
	600	(z,p_0)	(0.00, 1.40)
6		Energy-angle distributions for emitted particles	
	2	(z,z0)	
	600	(z,p_0)	

Table 24: ENDF/B-VII.1 library, file: `d-002_He_003.endf`

MF	MT	Description	Energy range [MeV]
3		Reaction cross sections	
	2	(z,z0)	(0.01, 1.40)
	600	(z,p_0)	(0.00, 1.40)
6		Energy-angle distributions for emitted particles	
	2	(z,z0)	
	600	(z,p_0)	

Table 25: CP2011 library, file: `d-002_He_003.endf`

MF	MT	Description	Energy range [MeV]
3		Reaction cross sections	
	2	(z,z0)	(0.01, 1.40)
	600	(z,p_0)	(0.00, 1.40)
6		Energy-angle distributions for emitted particles	
	2	(z,z0)	
	600	(z,p_0)	

Table 26: ENDF/B-VIII.0 library, file: `d-002_He_003.endf`

MF	MT	Description	Energy range [MeV]
3		Reaction cross sections	
	2	(z,z0)	(0.01, 20.00)
	600	(z,p_0)	(0.01, 20.00)
6		Energy-angle distributions for emitted particles	
	2	(z,z0)	
	600	(z,p_0)	

Table 27: CP2020 library new evaluation, file: `d-002_He_003.endf`

MF	MT	Description	Energy range [MeV]
3		Reaction cross sections	
	2	(z,z0)	(0.02, 20.00)
	22	(z,nα)	(0.02, 20.00)
	700	(z,t_0)	(1.28, 20.00)
6		Energy-angle distributions for emitted particles	
	2	(z,z0)	
	22	(z,nα)	
	700	(z,t_0)	

Table 28: ENDF/B-VII.1 library, file: `d-003_Li_007.endf`

MF	MT	Description	Energy range [MeV]
3		Reaction cross sections	
	2	(z,z0)	(0.02, 20.00)
	22	(z,nα)	(0.02, 20.00)
	700	(z,t_0)	(1.28, 20.00)
6		Energy-angle distributions for emitted particles	
	2	(z,z0)	
	22	(z,nα)	
	700	(z,t_0)	

Table 29: CP2011 library, file: `d-003_Li_007.endf`

MF	MT	Description	Energy range [MeV]
3		Reaction cross sections	
	2	(z,z0)	(0.02, 20.00)
	16	(z,2n)	(4.98, 20.00)
	22	(z,nα)	(0.00, 20.00)
	103	(z,p)	(0.25, 20.00)
	700	(z,t_0)	(1.28, 20.00)
6		Energy-angle distributions for emitted particles	
	2	(z,z0)	
	16	(z,2n)	
	22	(z,nα)	
	103	(z,p)	
	700	(z,t_0)	

Table 30: ENDF/B-VIII.0 library, file: `d-003_Li_007.endf`

MF	MT	Description	Energy range [MeV]
3		Reaction cross sections	
	2	(z,z0)	(0.02, 20.00)
	22	(z,nα)	(0.02, 20.00)
	700	(z,t_0)	(1.28, 20.00)
6		Energy-angle distributions for emitted particles	
	2	(z,z0)	
	22	(z,nα)	
	700	(z,t_0)	

Table 31: CP2020 library, file: `d-003_Li_007.endf`

MF	MT	Description	Energy range [MeV]
3		Reaction cross sections	
	2	(z,z0)	(0.00, 5.00)
	50	(z,n_0)	(0.00, 5.00)
	600	(z,p_0)	(0.00, 5.00)
	800	(z,α_0)	(0.00, 5.00)
6		Energy-angle distributions for emitted particles	
	2	(z,z0)	
	50	(z,n_0)	
	600	(z,p_0)	
	800	(z,α_0)	

Table 32: ENDF/B-VII.1 library, file: `d-003_Li_006.endf`

MF	MT	Description	Energy range [MeV]
3		Reaction cross sections	
	2	(z,z0)	(0.00, 1.00)
	34	(z,n^{3}He)	(0.00, 12.00)
	50	(z,n_0)	(0.00, 12.00)
	116	(z,pt)	(0.00, 12.00)
	600	(z,p_0)	(0.00, 12.00)
	800	(z,α_0)	(0.00, 8.00)
6		Energy-angle distributions for emitted particles	
	2	(z,z0)	
	34	(z,n^{3}He)	
	50	(z,n_0)	
	116	(z,pt)	
	600	(z,p_0)	
	800	(z,α_0)	

Table 33: CP2011 library, file: `d-003_Li_006.endf`

MF	MT	Description	Energy range [MeV]
3		Reaction cross sections	
	2	(z,z0)	(0.00, 5.00)
	50	(z,n_0)	(0.00, 5.00)
	600	(z,p_0)	(0.00, 5.00)
	800	(z,α_0)	(0.00, 5.00)
6		Energy-angle distributions for emitted particles	
	2	(z,z0)	
	50	(z,n_0)	
	600	(z,p_0)	
	800	(z,α_0)	

Table 34: ENDF/B-VIII.0 library, file: `d-003_Li_006.endf`

MF	MT	Description	Energy range [MeV]
3		Reaction cross sections	
	2	(z,z0)	(0.00, 1.00)
	34	(z,n^{3}He)	(0.00, 12.00)
	50	(z,n_0)	(0.00, 12.00)
	116	(z,pt)	(0.00, 12.00)
	600	(z,p_0)	(0.00, 12.00)
	800	(z,α_0)	(0.00, 8.00)
6		Energy-angle distributions for emitted particles	
	2	(z,z0)	
	34	(z,n^{3}He)	
	50	(z,n_0)	
	116	(z,pt)	
	600	(z,p_0)	
	800	(z,α_0)	

Table 35: CP2020 library, file: `d-003_Li_006.endf`

MF	MT	Description	Energy range [MeV]
3		Reaction cross sections	
	2	(z,z0)	(0.02, 20.00)
	112	(z,pα)	(0.02, 20.00)
	650	(z,d_0)	(0.02, 20.00)
6		Energy-angle distributions for emitted particles	
	2	(z,z0)	
	112	(z,pα)	
	650	(z,d_0)	

Table 36: ENDF/B-VII.1 library, file: `h-003_Li_006.endf`

MF	MT	Description	Energy range [MeV]
3		Reaction cross sections	
	2	(z,z0)	(0.02, 20.00)
	112	(z,pα)	(0.02, 20.00)
	650	(z,d_0)	(0.02, 20.00)
6		Energy-angle distributions for emitted particles	
	2	(z,z0)	
	112	(z,pα)	
	650	(z,d_0)	

Table 37: CP2011 library, file: `h-003_Li_006.endf`

MF	MT	Description	Energy range [MeV]
3		Reaction cross sections	
	2	(z,z0)	(0.02, 20.00)
	112	(z,pα)	(0.02, 20.00)
	650	(z,d_0)	(0.02, 20.00)
6		Energy-angle distributions for emitted particles	
	2	(z,z0)	
	112	(z,pα)	
	650	(z,d_0)	

Table 38: ENDF/B-VIII.0 library, file: `h-003_Li_006.endf`

MF	MT	Description	Energy range [MeV]
3		Reaction cross sections	
	2	(z,z0)	(0.02, 20.00)
	112	(z,pα)	(0.02, 20.00)
	650	(z,d_0)	(0.02, 20.00)
6		Energy-angle distributions for emitted particles	
	2	(z,z0)	
	112	(z,pα)	
	650	(z,d_0)	

Table 39: CP2020 library, file: `h-003_Li_006.endf`

MF	MT	Description	Energy range [MeV]
3		Reaction cross sections	
	2	(z,z0)	(1.00, 200.00)
	3	(z,nonelas.)	(1.00, 200.00)
	4	(z,n)	(0.00, 200.00)
	5	(z,anything)	(0.00, 200.00)
	16	(z,2n)	(13.19, 200.00)
	22	(z,nα)	(0.00, 200.00)
	28	(z,np)	(0.00, 200.00)
	102	(z,γ)	(0.00, 200.00)
	103	(z,p)	(0.00, 200.00)
	104	(z,d)	(0.00, 200.00)
	105	(z,t)	(1.26, 200.00)
	106	(z,^{3}He)	(0.68, 200.00)
	107	(z,α)	(0.00, 200.00)
6		Energy-angle distributions for emitted particles	
	2	(z,z0)	
	4	(z,n)	
	5	(z,anything)	
	16	(z,2n)	
	22	(z,nα)	
	28	(z,np)	
	102	(z,γ)	
	103	(z,p)	
	104	(z,d)	
	105	(z,t)	
	106	(z,^{3}He)	
	107	(z,α)	

Table 40: CP2011 library, file: `h-003_Li_007.endf`

MF	MT	Description	Energy range [MeV]
3		Reaction cross sections	
	2	(z,z0)	(1.00, 200.00)
	3	(z,nonelas.)	(1.00, 200.00)
	4	(z,n)	(0.00, 200.00)
	5	(z,anything)	(0.00, 200.00)
	16	(z,2n)	(13.19, 200.00)
	22	(z,nα)	(0.00, 200.00)
	28	(z,np)	(0.00, 200.00)
	102	(z,γ)	(0.00, 200.00)
	103	(z,p)	(0.00, 200.00)
	104	(z,d)	(0.00, 200.00)
	105	(z,t)	(1.26, 200.00)
	106	(z,^{3}He)	(0.68, 200.00)
	107	(z,α)	(0.00, 200.00)
6		Energy-angle distributions for emitted particles	
	2	(z,z0)	
	4	(z,n)	
	5	(z,anything)	
	16	(z,2n)	
	22	(z,nα)	
	28	(z,np)	
	102	(z,γ)	
	103	(z,p)	
	104	(z,d)	
	105	(z,t)	
	106	(z,^{3}He)	
	107	(z,α)	

Table 41: CP2020 library, file: `h-003_Li_007.endf`

MF	MT	Description	Energy range [MeV]
3		Reaction cross sections	
	2	(z,z0)	(0.02, 11.00)
	102	(z,γ)	(0.02, 11.00)
	600	(z,p_0)	(7.05, 11.00)
6		Energy-angle distributions for emitted particles	
	2	(z,z0)	
	600	(z,p_0)	

Table 42: CP2011 library, file: `h-002_He_004.endf`

MF	MT	Description	Energy range [MeV]
3		Reaction cross sections	
	2	(z,z0)	(0.27, 20.00)
6		Energy-angle distributions for emitted particles	
	2	(z,z0)	

Table 43: ENDF/B-VIII.0 library, file: `h-002_He_004.endf`

MF	MT	Description	Energy range [MeV]
3		Reaction cross sections	
	2	(z,z0)	(0.02, 11.00)
	102	(z,γ)	(0.02, 11.00)
	600	(z,p_0)	(7.05, 11.00)
6		Energy-angle distributions for emitted particles	
	2	(z,z0)	
	600	(z,p_0)	

Table 44: CP2020 library, file: `h-002_He_004.endf`

MF	MT	Description	Energy range [MeV]
3		Reaction cross sections	
	2	(z,z0)	(0.00, 2.00)
	111	(z,2p)	(0.00, 20.00)
6		Energy-angle distributions for emitted particles	
	2	(z,z0)	
	111	(z,2p)	

Table 45: ENDF/B-VII.1 library, file: `h-002_He_003.endf`

MF	MT	Description	Energy range [MeV]
3		Reaction cross sections	
	2	(z,z0)	(0.00, 2.00)
	111	(z,2p)	(0.00, 20.00)
6		Energy-angle distributions for emitted particles	
	2	(z,z0)	
	111	(z,2p)	

Table 46: CP2011 library, file: `h-002_He_003.endf`

MF	MT	Description	Energy range [MeV]
3		Reaction cross sections	
	2	(z,z0)	(0.00, 20.00)
	111	(z,2p)	(0.00, 20.00)
6		Energy-angle distributions for emitted particles	
	2	(z,z0)	
	111	(z,2p)	

Table 47: ENDF/B-VIII.0 library, file: `h-002_He_003.endf`

MF	MT	Description	Energy range [MeV]
3		Reaction cross sections	
	2	(z,z0)	(0.00, 2.00)
	111	(z,2p)	(0.00, 20.00)
6		Energy-angle distributions for emitted particles	
	2	(z,z0)	
	111	(z,2p)	

Table 48: CP2020 library, file: `h-002_He_003.endf`

MF	MT	Description	Energy range [MeV]
3		Reaction cross sections	
	1	(n,total)	(0.00, 150.00)
	2	(z,z0)	(0.00, 150.00)
	3	(z,nonelas.)	(0.00, 150.00)
	16	(z,2n)	(3.34, 150.00)
	102	(z,γ)	(0.00, 150.00)
4		Angular distributions for emitted particles	
	2	(z,z0)	
6		Energy-angle distributions for emitted particles	
	16	(z,2n)	
8		Radioactivity and fission-product yield data	
	102	(z,γ)	
9		Multiplicities for radioactive nuclide production	
	102	(z,γ)	
12		Multiplicities for photon production	
	102	(z,γ)	
14		Angular distributions for photon production	
	102	(z,γ)	
33		Data covariances for reaction cross sections	
	1	(n,total)	
	2	(z,z0)	
	16	(z,2n)	
	102	(z,γ)	

Table 49: ENDF/B-VII.1 library, file: `n-001_H_002.endf`

MF	MT	Description	Energy range [MeV]
3		Reaction cross sections	
	1	(n,total)	(0.00, 150.00)
	2	(z,z0)	(0.00, 150.00)
	16	(z,2n)	(3.34, 150.00)
	102	(z,γ)	(0.00, 150.00)
6		Energy-angle distributions for emitted particles	
	2	(z,z0)	
	16	(z,2n)	
	102	(z,γ)	

Table 50: CP2011 library, file: `n-001_H_002.endf`

MF	MT	Description	Energy range [MeV]
3		Reaction cross sections	
	1	(n,total)	(0.00, 150.00)
	2	(z,z0)	(0.00, 150.00)
	3	(z,nonelas.)	(0.00, 150.00)
	16	(z,2n)	(3.34, 150.00)
	102	(z,γ)	(0.00, 150.00)
4		Angular distributions for emitted particles	
	2	(z,z0)	
6		Energy-angle distributions for emitted particles	
	16	(z,2n)	
8		Radioactivity and fission-product yield data	
	102	(z,γ)	
9		Multiplicities for radioactive nuclide production	
	102	(z,γ)	
12		Multiplicities for photon production	
	102	(z,γ)	
14		Angular distributions for photon production	
	102	(z,γ)	
33		Data covariances for reaction cross sections	
	1	(n,total)	
	2	(z,z0)	
	16	(z,2n)	
	102	(z,γ)	

Table 51: ENDF/B-VIII.0 library, file: `n-001_H_002.endf`

MF	MT	Description	Energy range [MeV]
3		Reaction cross sections	
	1	(n,total)	(0.00, 150.00)
	2	(z,z0)	(0.00, 150.00)
	16	(z,2n)	(3.34, 150.00)
	102	(z,γ)	(0.00, 150.00)
6		Energy-angle distributions for emitted particles	
	2	(z,z0)	
	16	(z,2n)	
	102	(z,γ)	

Table 52: CP2020 library, file: `n-001_H_002.endf`

MF	MT	Description	Energy range [MeV]
3		Reaction cross sections	
	1	(n,total)	(0.00, 20.00)
	2	(z,z0)	(0.00, 20.00)
	16	(z,2n)	(8.35, 20.00)
4		Angular distributions for emitted particles	
	2	(z,z0)	
	16	(z,2n)	
5		Energy distributions for emitted particles	
	16	(z,2n)	

Table 53: ENDF/B-VII.1 library, file: `n-001_H_003.endf`

MF	MT	Description	Energy range [MeV]
3		Reaction cross sections	
	1	(n,total)	(0.00, 20.00)
	2	(z,z0)	(0.00, 20.00)
	16	(z,2n)	(8.35, 20.00)
6		Energy-angle distributions for emitted particles	
	2	(z,z0)	
	16	(z,2n)	

Table 54: CP2011 library, file: `n-001_H_003.endf`

MF	MT	Description	Energy range [MeV]
3		Reaction cross sections	
	1	(n,total)	(0.00, 20.00)
	2	(z,z0)	(0.00, 20.00)
	16	(z,2n)	(8.35, 20.00)
4		Angular distributions for emitted particles	
	2	(z,z0)	
	16	(z,2n)	
5		Energy distributions for emitted particles	
	16	(z,2n)	

Table 55: ENDF/B-VIII.0 library, file: `n-001_H_003.endf`

MF	MT	Description	Energy range [MeV]
3		Reaction cross sections	
	1	(n,total)	(0.00, 20.00)
	2	(z,z0)	(0.00, 20.00)
	16	(z,2n)	(8.35, 20.00)
6		Energy-angle distributions for emitted particles	
	2	(z,z0)	
	16	(z,2n)	

Table 56: CP2020 library, file: `n-001_H_003.endf`

MF	MT	Description	Energy range [MeV]
3		Reaction cross sections	
	1	(n,total)	(0.00, 20.00)
	2	(z,z0)	(0.00, 20.00)
	3	(z,nonelas.)	(0.00, 20.00)
	4	(z,n)	(1.75, 20.00)
	24	(z,2nα)	(4.32, 20.00)
	51	(z,n_1)	(1.75, 20.00)
	52	(z,n_2)	(2.34, 20.00)
	...	(z,n_i)	...
	81	(z,n_n)	(18.10, 20.00)
	102	(z,γ)	(0.00, 20.00)
	103	(z,p)	(3.18, 20.00)
	105	(z,t)	(0.00, 20.00)
4		Angular distributions for emitted particles	
	2	(z,z0)	
	24	(z,2nα)	
	51	(z,n_1)	
	52	(z,n_2)	
	...	(z,n_i)	
	81	(z,n_n)	
5		Energy distributions for emitted particles	
	24	(z,2nα)	
6		Energy-angle distributions for emitted particles	
	105	(z,t)	
12		Multiplicities for photon production	
	57	(z,n_n)	
	102	(z,γ)	
14		Angular distributions for photon production	
	57	(z,n_n)	
	102	(z,γ)	
33		Data covariances for reaction cross sections	
	1	(n,total)	
	2	(z,z0)	
	4	(z,n)	
	24	(z,2nα)	
	102	(z,γ)	
	103	(z,p)	
	105	(z,t)	

Table 57: ENDF/B-VII.1 library, file: `n-003_Li_006.endf`

MF	MT	Description	Energy range [MeV]
3		Reaction cross sections	
	1	(n,total)	(0.00, 20.00)
	2	(z,z0)	(0.00, 20.00)
	4	(z,n)	(4.16, 20.00)
	32	(z,nd)	(1.75, 20.00)
	41	(z,2np)	(4.32, 20.00)
	57	(z,n_n)	(4.16, 20.00)
	102	(z,γ)	(0.00, 20.00)
	103	(z,p)	(3.18, 20.00)
	105	(z,t)	(0.00, 20.00)
6		Energy-angle distributions for emitted particles	
	2	(z,z0)	
	32	(z,nd)	
	41	(z,2np)	
	57	(z,n_n)	
	102	(z,γ)	
	103	(z,p)	
	105	(z,t)	

Table 58: CP2011 library, file: `n-003_Li_006.endf`

MF	MT	Description	Energy range [MeV]
3		Reaction cross sections	
	1	(n,total)	(0.00, 20.00)
	2	(z,z0)	(0.00, 20.00)
	4	(z,n)	(1.75, 20.00)
	24	(z,2nα)	(4.32, 20.00)
	51	(z,n_1)	(1.75, 20.00)
	52	(z,n_2)	(2.34, 20.00)
	...	(z,n_i)	...
	81	(z,n_n)	(18.10, 20.00)
	102	(z,γ)	(0.00, 20.00)
	103	(z,p)	(3.18, 20.00)
	105	(z,t)	(0.00, 20.00)
4		Angular distributions for emitted particles	
	2	(z,z0)	
	24	(z,2nα)	
	51	(z,n_1)	
	52	(z,n_2)	
	...	(z,n_i)	
	81	(z,n_n)	
5		Energy distributions for emitted particles	
	24	(z,2nα)	
6		Energy-angle distributions for emitted particles	
	105	(z,t)	
12		Multiplicities for photon production	
	57	(z,n_n)	
	102	(z,γ)	
14		Angular distributions for photon production	
	57	(z,n_n)	
	102	(z,γ)	
33		Data covariances for reaction cross sections	
	2	(z,z0)	
	105	(z,t)	

Table 59: ENDF/B-VIII.0 library, file: `n-003_Li_006.endf`

MF	MT	Description	Energy range [MeV]
3		Reaction cross sections	
	1	(n,total)	(0.00, 20.00)
	2	(z,z0)	(0.00, 20.00)
	4	(z,n)	(4.16, 20.00)
	32	(z,nd)	(1.72, 20.00)
	41	(z,2np)	(4.32, 20.00)
	51	(z,n_1)	(4.16, 20.00)
	102	(z,γ)	(0.00, 20.00)
	103	(z,p)	(3.18, 20.00)
	105	(z,t)	(0.00, 20.00)
6		Energy-angle distributions for emitted particles	
	2	(z,z0)	
	32	(z,nd)	
	41	(z,2np)	
	51	(z,n_1)	
	102	(z,γ)	
	103	(z,p)	
	105	(z,t)	

Table 60: CP2020 library new evaluation, file: `n-003_Li_006.endf`

MF	MT	Description	Energy range [MeV]
3		Reaction cross sections	
	1	(n,total)	(0.00, 20.00)
	2	(z,z0)	(0.00, 20.00)
	4	(z,n)	(0.55, 20.00)
	16	(z,2n)	(8.29, 20.00)
	24	(z,2nα)	(9.98, 20.00)
	25	(z,3nα)	(12.52, 20.00)
	51	(z,n_1)	(0.55, 20.00)
	52	(z,n_2)	(3.15, 20.00)
	...	(z,n_i)	...
	82	(z,n_n)	(19.73, 20.00)
	102	(z,γ)	(0.00, 20.00)
	104	(z,d)	(8.87, 20.00)
4		Angular distributions for emitted particles	
	2	(z,z0)	
	16	(z,2n)	
	24	(z,2nα)	
	25	(z,3nα)	
	51	(z,n_1)	
	52	(z,n_2)	
	...	(z,n_i)	
	82	(z,n_n)	
5		Energy distributions for emitted particles	
	16	(z,2n)	
	24	(z,2nα)	
	25	(z,3nα)	
12		Multiplicities for photon production	
	51	(z,n_1)	
	102	(z,γ)	
14		Angular distributions for photon production	
	51	(z,n_1)	
	102	(z,γ)	

Table 61: ENDF/B-VII.1 library, file: `n-003_Li_007.endf`

MF	MT	Description	Energy range [MeV]
3		Reaction cross sections	
	1	(n,total)	(0.00, 20.00)
	2	(z,z0)	(0.00, 20.00)
	4	(z,n)	(0.55, 20.00)
	11	(z,2nd)	(9.98, 20.00)
	16	(z,2n)	(8.29, 20.00)
	42	(z,3np)	(12.52, 20.00)
	51	(z,n_1)	(0.55, 20.00)
	52	(z,n_2)	(3.15, 20.00)
	...	(z,n_i)	...
	82	(z,n_n)	(19.73, 20.00)
	102	(z,γ)	(0.00, 20.00)
	104	(z,d)	(8.87, 20.00)
6		Energy-angle distributions for emitted particles	
	2	(z,z0)	
	11	(z,2nd)	
	16	(z,2n)	
	42	(z,3np)	
	51	(z,n_1)	
	52	(z,n_2)	
	...	(z,n_i)	
	82	(z,n_n)	
	102	(z,γ)	
	104	(z,d)	

Table 62: CP2011 library, file: `n-003_Li_007.endf`

MF	MT	Description	Energy range [MeV]
3		Reaction cross sections	
	1	(n,total)	(0.00, 20.00)
	2	(z,z0)	(0.00, 20.00)
	4	(z,n)	(0.55, 20.00)
	16	(z,2n)	(8.29, 20.00)
	24	(z,2nα)	(9.98, 20.00)
	25	(z,3nα)	(12.52, 20.00)
	51	(z,n_1)	(0.55, 20.00)
	52	(z,n_2)	(3.15, 20.00)
	...	(z,n_i)	...
	82	(z,n_n)	(19.73, 20.00)
	102	(z,γ)	(0.00, 20.00)
	104	(z,d)	(8.87, 20.00)
4		Angular distributions for emitted particles	
	2	(z,z0)	
	16	(z,2n)	
	24	(z,2nα)	
	25	(z,3nα)	
	51	(z,n_1)	
	52	(z,n_2)	
	...	(z,n_i)	
	82	(z,n_n)	
5		Energy distributions for emitted particles	
	16	(z,2n)	
	24	(z,2nα)	
	25	(z,3nα)	
12		Multiplicities for photon production	
	51	(z,n_1)	
	102	(z,γ)	
14		Angular distributions for photon production	
	51	(z,n_1)	
	102	(z,γ)	

Table 63: ENDF/B-VIII.0 library, file: `n-003_Li_007.endf`

MF	MT	Description	Energy range [MeV]
3		Reaction cross sections	
	1	(n,total)	(0.00, 20.00)
	2	(z,z0)	(0.00, 20.00)
	4	(z,n)	(0.55, 20.00)
	11	(z,2nd)	(9.98, 20.00)
	16	(z,2n)	(8.29, 20.00)
	42	(z,3np)	(12.52, 20.00)
	51	(z,n_1)	(0.55, 20.00)
	52	(z,n_2)	(3.15, 20.00)
	...	(z,n_i)	...
	82	(z,n_n)	(19.73, 20.00)
	102	(z,γ)	(0.00, 20.00)
	104	(z,d)	(8.87, 20.00)
6		Energy-angle distributions for emitted particles	
	2	(z,z0)	
	11	(z,2nd)	
	16	(z,2n)	
	42	(z,3np)	
	51	(z,n_1)	
	52	(z,n_2)	
	...	(z,n_i)	
	82	(z,n_n)	
	102	(z,γ)	
	104	(z,d)	

Table 64: CP2020 library, file: `n-003_Li_007.endf`

MF	MT	Description	Energy range [MeV]
3		Reaction cross sections	
	1	(n,total)	(0.00, 20.00)
	2	(z,z0)	(0.00, 20.00)
	102	(z,γ)	(0.00, 20.00)
	103	(z,p)	(0.00, 20.00)
	104	(z,d)	(4.36, 20.00)
4		Angular distributions for emitted particles	
	2	(z,z0)	

Table 65: ENDF/B-VII.1 library, file: `n-002_He_003.endf`

MF	MT	Description	Energy range [MeV]
3		Reaction cross sections	
	1	(n,total)	(0.00, 20.00)
	2	(z,z0)	(0.00, 20.00)
	102	(z,γ)	(0.00, 20.00)
	103	(z,p)	(0.00, 20.00)
	104	(z,d)	(4.36, 20.00)
6		Energy-angle distributions for emitted particles	
	2	(z,z0)	
	102	(z,γ)	
	103	(z,p)	
	104	(z,d)	

Table 66: CP2011 library, file: `n-002_He_003.endf`

MF	MT	Description	Energy range [MeV]
3		Reaction cross sections	
	1	(n,total)	(0.00, 20.00)
	2	(z,z0)	(0.00, 20.00)
	102	(z,γ)	(0.00, 20.00)
	103	(z,p)	(0.00, 20.00)
	104	(z,d)	(4.36, 20.00)
4		Angular distributions for emitted particles	
	2	(z,z0)	

Table 67: ENDF/B-VIII.0 library, file: `n-002_He_003.endf`

MF	MT	Description	Energy range [MeV]
3		Reaction cross sections	
	1	(n,total)	(0.00, 20.00)
	2	(z,z0)	(0.00, 20.00)
	102	(z,γ)	(0.00, 20.00)
	103	(z,p)	(0.00, 20.00)
	104	(z,d)	(4.36, 20.00)
6		Energy-angle distributions for emitted particles	
	2	(z,z0)	
	102	(z,γ)	
	103	(z,p)	
	104	(z,d)	

Table 68: CP2020 library, file: `n-002_He_003.endf`

MF	MT	Description	Energy range [MeV]
3		Reaction cross sections	
	1	(n,total)	(0.00, 20.00)
	2	(z,z0)	(0.00, 20.00)
	102	(z,γ)	(0.00, 20.00)
4		Angular distributions for emitted particles	
	2	(z,z0)	
6		Energy-angle distributions for emitted particles	
	102	(z,γ)	
33		Data covariances for reaction cross sections	
	1	(n,total)	
	2	(z,z0)	
	102	(z,γ)	

Table 69: ENDF/B-VII.1 library, file: `n-001_H_001.endf`

MF	MT	Description	Energy range [MeV]
3		Reaction cross sections	
	1	(n,total)	(0.00, 20.00)
	2	(z,z0)	(0.00, 20.00)
	102	(z,γ)	(0.00, 20.00)
6		Energy-angle distributions for emitted particles	
	2	(z,z0)	
	102	(z,γ)	

Table 70: CP2011 library, file: `n-001_H_001.endf`

MF	MT	Description	Energy range [MeV]
3		Reaction cross sections	
	1	(n,total)	(0.00, 20.00)
	2	(z,z0)	(0.00, 20.00)
	102	(z,γ)	(0.00, 20.00)
4		Angular distributions for emitted particles	
	2	(z,z0)	
6		Energy-angle distributions for emitted particles	
	102	(z,γ)	
33		Data covariances for reaction cross sections	
	1	(n,total)	
	2	(z,z0)	
	102	(z,γ)	

Table 71: ENDF/B-VIII.0 library, file: `n-001_H_001.endf`

MF	MT	Description	Energy range [MeV]
3		Reaction cross sections	
	1	(n,total)	(0.00, 50.00)
	2	(z,z0)	(0.00, 50.00)
	102	(z,γ)	(0.00, 50.00)
6		Energy-angle distributions for emitted particles	
	2	(z,z0)	
	102	(z,γ)	
33		Data covariances for reaction cross sections	
	1	(n,total)	
	2	(z,z0)	
	102	(z,γ)	

Table 72: CP2020 library new evaluation, file: `n-001_H_001.endf`

MF	MT	Description	Energy range [MeV]
3		Reaction cross sections	
	1	(n,total)	(0.00, 20.00)
	2	(z,z0)	(0.00, 20.00)
4		Angular distributions for emitted particles	
	2	(z,z0)	
33		Data covariances for reaction cross sections	
	1	(n,total)	
	2	(z,z0)	

Table 73: ENDF/B-VII.1 library, file: `n-002_He_004.endf`

MF	MT	Description	Energy range [MeV]
3		Reaction cross sections	
	1	(n,total)	(0.00, 20.00)
	2	(z,z0)	(0.00, 20.00)
6		Energy-angle distributions for emitted particles	
	2	(z,z0)	

Table 74: CP2011 library, file: `n-002_He_004.endf`

MF	MT	Description	Energy range [MeV]
3		Reaction cross sections	
	1	(n,total)	(0.00, 20.00)
	2	(z,z0)	(0.00, 20.00)
4		Angular distributions for emitted particles	
	2	(z,z0)	
33		Data covariances for reaction cross sections	
	1	(n,total)	
	2	(z,z0)	

Table 75: ENDF/B-VIII.0 library, file: `n-002_He_004.endf`

MF	MT	Description	Energy range [MeV]
3		Reaction cross sections	
	1	(n,total)	(0.00, 20.00)
	2	(z,z0)	(0.00, 20.00)
6		Energy-angle distributions for emitted particles	
	2	(z,z0)	

Table 76: CP2020 library, file: `n-002_He_004.endf`

MF	MT	Description	Energy range [MeV]
3		Reaction cross sections	
	2	(z,z0)	(0.00, 20.00)
	111	(z,2p)	(7.33, 20.00)
6		Energy-angle distributions for emitted particles	
	2	(z,z0)	
	111	(z,2p)	

Table 77: ENDF/B-VII.1 library, file: `p-002_He_003.endf`

MF	MT	Description	Energy range [MeV]
3		Reaction cross sections	
	2	(z,z0)	(0.00, 20.00)
	111	(z,2p)	(7.33, 20.00)
6		Energy-angle distributions for emitted particles	
	2	(z,z0)	
	111	(z,2p)	

Table 78: CP2011 library, file: `p-002_He_003.endf`

MF	MT	Description	Energy range [MeV]
3		Reaction cross sections	
	2	(z,z0)	(0.00, 20.00)
	111	(z,2p)	(7.33, 20.00)
6		Energy-angle distributions for emitted particles	
	2	(z,z0)	
	111	(z,2p)	

Table 79: ENDF/B-VIII.0 library, file: `p-002_He_003.endf`

MF	MT	Description	Energy range [MeV]
3		Reaction cross sections	
	2	(z,z0)	(0.00, 20.00)
	111	(z,2p)	(7.33, 20.00)
6		Energy-angle distributions for emitted particles	
	2	(z,z0)	
	111	(z,2p)	

Table 80: CP2020 library, file: `p-002_He_003.endf`

MF	MT	Description	Energy range [MeV]
3		Reaction cross sections	
	2	(z,z0)	(0.00, 150.00)
6		Energy-angle distributions for emitted particles	
	2	(z,z0)	

Table 81: ENDF/B-VII.1 library, file: `p-001_H_001.endf`

MF	MT	Description	Energy range [MeV]
3		Reaction cross sections	
	2	(z,z0)	(0.00, 150.00)
6		Energy-angle distributions for emitted particles	
	2	(z,z0)	

Table 82: CP2011 library, file: `p-001_H_001.endf`

MF	MT	Description	Energy range [MeV]
3		Reaction cross sections	
	2	(z,z0)	(0.00, 150.00)
6		Energy-angle distributions for emitted particles	
	2	(z,z0)	

Table 83: ENDF/B-VIII.0 library, file: `p-001_H_001.endf`

MF	MT	Description	Energy range [MeV]
3		Reaction cross sections	
	2	(z,z0)	(0.00, 150.00)
6		Energy-angle distributions for emitted particles	
	2	(z,z0)	

Table 84: CP2020 library new evaluation, file: `p-001_H_001.endf`

MF	MT	Description	Energy range [MeV]
3		Reaction cross sections	
	2	(z,z0)	(0.02, 20.00)
6		Energy-angle distributions for emitted particles	
	2	(z,z0)	

Table 85: CP2011 library, file: `p-002_He_004.endf`

MF	MT	Description	Energy range [MeV]
3		Reaction cross sections	
	2	(z,z0)	(0.11, 20.00)
6		Energy-angle distributions for emitted particles	
	2	(z,z0)	

Table 86: ENDF/B-VIII.0 library, file: `p-002_He_004.endf`

MF	MT	Description	Energy range [MeV]
3		Reaction cross sections	
	2	(z,z0)	(0.02, 34.30)
	650	(z,d_0)	(23.02, 34.30)
6		Energy-angle distributions for emitted particles	
	2	(z,z0)	
	650	(z,d_0)	

Table 87: CP2020 library new evaluation, file: `p-002_He_004.endf`

MF	MT	Description	Energy range [MeV]
3		Reaction cross sections	
	2	(z,z0)	(0.10, 150.00)
	28	(z,np)	(3.34, 150.00)
	102	(z,γ)	(0.10, 150.00)
6		Energy-angle distributions for emitted particles	
	2	(z,z0)	
	28	(z,np)	
	102	(z,γ)	

Table 88: ENDF/B-VII.1 library, file: `p-001_H_002.endf`

MF	MT	Description	Energy range [MeV]
3		Reaction cross sections	
	2	(z,z0)	(0.10, 150.00)
	28	(z,np)	(3.34, 150.00)
	102	(z,γ)	(0.10, 150.00)
6		Energy-angle distributions for emitted particles	
	2	(z,z0)	
	28	(z,np)	
	102	(z,γ)	

Table 89: CP2011 library, file: `p-001_H_002.endf`

MF	MT	Description	Energy range [MeV]
3		Reaction cross sections	
	2	(z,z0)	(0.10, 150.00)
	28	(z,np)	(3.34, 150.00)
	102	(z,γ)	(0.10, 150.00)
6		Energy-angle distributions for emitted particles	
	2	(z,z0)	
	28	(z,np)	
	102	(z,γ)	

Table 90: ENDF/B-VIII.0 library, file: `p-001_H_002.endf`

MF	MT	Description	Energy range [MeV]
3		Reaction cross sections	
	2	(z,z0)	(0.10, 150.00)
	28	(z,np)	(3.34, 150.00)
	102	(z,γ)	(0.10, 150.00)
6		Energy-angle distributions for emitted particles	
	2	(z,z0)	
	28	(z,np)	
	102	(z,γ)	

Table 91: CP2020 library, file: `p-001_H_002.endf`

MF	MT	Description	Energy range [MeV]
3		Reaction cross sections	
	2	(z,z0)	(0.00, 12.00)
	50	(z,n_0)	(1.02, 20.00)
	650	(z,d_0)	(5.38, 12.00)
6		Energy-angle distributions for emitted particles	
	2	(z,z0)	
	50	(z,n_0)	
	650	(z,d_0)	

Table 92: ENDF/B-VII.1 library, file: `p-001_H_003.endf`

MF	MT	Description	Energy range [MeV]
3		Reaction cross sections	
	2	(z,z0)	(0.00, 12.00)
	50	(z,n_0)	(1.02, 20.00)
	650	(z,d_0)	(5.38, 12.00)
6		Energy-angle distributions for emitted particles	
	2	(z,z0)	
	50	(z,n_0)	
	650	(z,d_0)	

Table 93: CP2011 library, file: `p-001_H_003.endf`

MF	MT	Description	Energy range [MeV]
3		Reaction cross sections	
	2	(z,z0)	(0.00, 12.00)
	50	(z,n_0)	(1.02, 20.00)
	650	(z,d_0)	(5.38, 12.00)
6		Energy-angle distributions for emitted particles	
	2	(z,z0)	
	50	(z,n_0)	
	650	(z,d_0)	

Table 94: ENDF/B-VIII.0 library, file: `p-001_H_003.endf`

MF	MT	Description	Energy range [MeV]
3		Reaction cross sections	
	2	(z,z0)	(0.00, 12.00)
	50	(z,n_0)	(1.02, 20.00)
	650	(z,d_0)	(5.38, 12.00)
6		Energy-angle distributions for emitted particles	
	2	(z,z0)	
	50	(z,n_0)	
	650	(z,d_0)	

Table 95: CP2020 library, file: `p-001_H_003.endf`

MF	MT	Description	Energy range [MeV]
3		Reaction cross sections	
	2	(z,z0)	(0.00, 2.50)
	750	(n,^{3}He$_0$)	(0.00, 2.50)
6		Energy-angle distributions for emitted particles	
	2	(z,z0)	
	750	(n,^{3}He$_0$)	

Table 96: ENDF/B-VII.1 library, file: `p-003_Li_006.endf`

MF	MT	Description	Energy range [MeV]
3		Reaction cross sections	
	2	(z,z0)	(0.00, 2.50)
	750	(n,^{3}He$_0$)	(0.00, 2.50)
6		Energy-angle distributions for emitted particles	
	2	(z,z0)	
	750	(n,^{3}He$_0$)	

Table 97: CP2011 library, file: `p-003_Li_006.endf`

MF	MT	Description	Energy range [MeV]
3		Reaction cross sections	
	2	(z,z0)	(0.00, 2.50)
	750	(n,^{3}He$_0$)	(0.00, 2.50)
6		Energy-angle distributions for emitted particles	
	2	(z,z0)	
	750	(n,^{3}He$_0$)	

Table 98: ENDF/B-VIII.0 library, file: `p-003_Li_006.endf`

MF	MT	Description	Energy range [MeV]
3		Reaction cross sections	
	2	(z,z0)	(0.00, 2.50)
	750	(n,^{3}He$_0$)	(0.00, 2.50)
6		Energy-angle distributions for emitted particles	
	2	(z,z0)	
	750	(n,^{3}He$_0$)	

Table 99: CP2020 library, file: `p-003_Li_006.endf`

MF	MT	Description	Energy range [MeV]
3		Reaction cross sections	
	2	(z,z0)	(0.00, 10.00)
	50	(z,n_0)	(1.88, 10.00)
	650	(z,d_0)	(5.75, 10.00)
	800	(z,α_0)	(0.00, 10.00)
6		Energy-angle distributions for emitted particles	
	2	(z,z0)	
	50	(z,n_0)	
	650	(z,d_0)	
	800	(z,α_0)	

Table 100: ENDF/B-VII.1 library, file: `p-003_Li_007.endf`

MF	MT	Description	Energy range [MeV]
3		Reaction cross sections	
	2	(z,z0)	(0.00, 3.00)
	50	(z,n_0)	(1.88, 3.00)
	800	(z,α_0)	(0.00, 12.01)
6		Energy-angle distributions for emitted particles	
	2	(z,z0)	
	50	(z,n_0)	
	800	(z,α_0)	

Table 101: CP2011 library, file: `p-003_Li_007.endf`

MF	MT	Description	Energy range [MeV]
3		Reaction cross sections	
	2	(z,z0)	(0.00, 20.00)
	50	(z,n_0)	(1.88, 20.00)
	51	(z,n_1)	(2.37, 20.00)
	650	(z,d_0)	(5.75, 20.00)
	800	(z,α_0)	(0.00, 20.00)
6		Energy-angle distributions for emitted particles	
	2	(z,z0)	
	50	(z,n_0)	
	51	(z,n_1)	
	650	(z,d_0)	
	800	(z,α_0)	

Table 102: ENDF/B-VIII.0 library, file: `p-003_Li_007.endf`

MF	MT	Description	Energy range [MeV]
3		Reaction cross sections	
	2	(z,z0)	(0.00, 3.00)
	50	(z,n_0)	(1.88, 3.00)
	800	(z,α_0)	(0.00, 12.01)
6		Energy-angle distributions for emitted particles	
	2	(z,z0)	
	50	(z,n_0)	
	800	(z,α_0)	

Table 103: CP2020 library, file: `p-003_Li_007.endf`

MF	MT	Description	Energy range [MeV]
3		Reaction cross sections	
	2	(z,z0)	(0.02, 20.00)
	22	(z,nα)	(0.02, 20.00)
	650	(z,d_0)	(0.02, 20.00)
6		Energy-angle distributions for emitted particles	
	2	(z,z0)	
	22	(z,nα)	
	650	(z,d_0)	

Table 104: ENDF/B-VII.1 library, file: `t-003_Li_006.endf`

MF	MT	Description	Energy range [MeV]
3		Reaction cross sections	
	2	(z,z0)	(0.02, 20.00)
	22	(z,nα)	(0.02, 20.00)
	650	(z,d_0)	(0.02, 20.00)
6		Energy-angle distributions for emitted particles	
	2	(z,z0)	
	22	(z,nα)	
	650	(z,d_0)	

Table 105: CP2011 library, file: `t-003_Li_006.endf`

MF	MT	Description	Energy range [MeV]
3		Reaction cross sections	
	2	(z,z0)	(0.02, 20.00)
	22	(z,nα)	(0.02, 20.00)
	650	(z,d_0)	(0.02, 20.00)
6		Energy-angle distributions for emitted particles	
	2	(z,z0)	
	22	(z,nα)	
	650	(z,d_0)	

Table 106: ENDF/B-VIII.0 library, file: `t-003_Li_006.endf`

MF	MT	Description	Energy range [MeV]
3		Reaction cross sections	
	2	(z,z0)	(0.02, 20.00)
	22	(z,nα)	(0.02, 20.00)
	650	(z,d_0)	(0.02, 20.00)
6		Energy-angle distributions for emitted particles	
	2	(z,z0)	
	22	(z,nα)	
	650	(z,d_0)	

Table 107: CP2020 library, file: `t-003_Li_006.endf`

MF	MT	Description	Energy range [MeV]
3		Reaction cross sections	
	2	(z,z0)	(1.00, 200.00)
	3	(z,nonelas.)	(1.00, 200.00)
	4	(z,n)	(0.00, 200.00)
	5	(z,anything)	(0.00, 200.00)
	16	(z,2n)	(0.00, 200.00)
	17	(z,3n)	(14.48, 200.00)
	22	(z,nα)	(0.00, 200.00)
	28	(z,np)	(9.22, 200.00)
	102	(z,γ)	(0.00, 200.00)
	103	(z,p)	(3.41, 200.00)
	104	(z,d)	(6.04, 200.00)
	105	(z,t)	(0.68, 200.00)
	106	(z,^{3}He)	(15.98, 200.00)
	107	(z,α)	(0.00, 200.00)
6		Energy-angle distributions for emitted particles	
	2	(z,z0)	
	4	(z,n)	
	5	(z,anything)	
	16	(z,2n)	
	17	(z,3n)	
	22	(z,nα)	
	28	(z,np)	
	102	(z,γ)	
	103	(z,p)	
	104	(z,d)	
	105	(z,t)	
	106	(z,^{3}He)	
	107	(z,α)	

Table 108: CP2011 library, file: `t-003_Li_007.endf`

MF	MT	Description	Energy range [MeV]
3		Reaction cross sections	
	2	(z,z0)	(0.00, 20.00)
	17	(z,3n)	(14.48, 20.00)
	24	(z,2nα)	(0.00, 20.00)
	50	(z,n$_0$)	(0.00, 20.00)
6		Energy-angle distributions for emitted particles	
	2	(z,z0)	
	17	(z,3n)	
	24	(z,2nα)	
	50	(z,n$_0$)	

Table 109: ENDF/B-VIII.0 library, file: `t-003_Li_007.endf`

MF	MT	Description	Energy range [MeV]
3		Reaction cross sections	
	2	(z,z0)	(1.00, 200.00)
	3	(z,nonelas.)	(1.00, 200.00)
	4	(z,n)	(0.00, 200.00)
	5	(z,anything)	(0.00, 200.00)
	16	(z,2n)	(0.00, 200.00)
	17	(z,3n)	(14.48, 200.00)
	22	(z,nα)	(0.00, 200.00)
	28	(z,np)	(9.22, 200.00)
	102	(z,γ)	(0.00, 200.00)
	103	(z,p)	(3.41, 200.00)
	104	(z,d)	(6.04, 200.00)
	105	(z,t)	(0.68, 200.00)
	106	(z,^{3}He)	(15.98, 200.00)
	107	(z,α)	(0.00, 200.00)
6		Energy-angle distributions for emitted particles	
	2	(z,z0)	
	4	(z,n)	
	5	(z,anything)	
	16	(z,2n)	
	17	(z,3n)	
	22	(z,nα)	
	28	(z,np)	
	102	(z,γ)	
	103	(z,p)	
	104	(z,d)	
	105	(z,t)	
	106	(z,^{3}He)	
	107	(z,α)	

Table 110: CP2020 library, file: `t-003_Li_007.endf`

MF	MT	Description	Energy range [MeV]
3		Reaction cross sections	
	2	(z,z0)	(0.00, 3.00)
	28	(z,np)	(0.00, 20.00)
	650	(z,d_0)	(0.00, 20.00)
6		Energy-angle distributions for emitted particles	
	2	(z,z0)	
	28	(z,np)	
	650	(z,d_0)	

Table 111: ENDF/B-VII.1 library, file: `t-002_He_003.endf`

MF	MT	Description	Energy range [MeV]
3		Reaction cross sections	
	2	(z,z0)	(0.00, 3.00)
	28	(z,np)	(0.00, 20.00)
	650	(z,d_0)	(0.00, 20.00)
6		Energy-angle distributions for emitted particles	
	2	(z,z0)	
	28	(z,np)	
	650	(z,d_0)	

Table 112: CP2011 library, file: `t-002_He_003.endf`

MF	MT	Description	Energy range [MeV]
3		Reaction cross sections	
	2	(z,z0)	(0.00, 3.00)
	28	(z,np)	(0.00, 20.00)
	650	(z,d_0)	(0.00, 20.00)
6		Energy-angle distributions for emitted particles	
	2	(z,z0)	
	28	(z,np)	
	650	(z,d_0)	

Table 113: ENDF/B-VIII.0 library, file: `t-002_He_003.endf`

MF	MT	Description	Energy range [MeV]
3		Reaction cross sections	
	2	(z,z0)	(0.00, 3.00)
	28	(z,np)	(0.00, 20.00)
	650	(z,d_0)	(0.00, 20.00)
6		Energy-angle distributions for emitted particles	
	2	(z,z0)	
	28	(z,np)	
	650	(z,d_0)	

Table 114: CP2020 library, file: `t-002_He_003.endf`

MF	MT	Description	Energy range [MeV]
3		Reaction cross sections	
	2	(z,z0)	(0.00, 2.00)
	16	(z,2n)	(0.00, 20.00)
6		Energy-angle distributions for emitted particles	
	2	(z,z0)	
	16	(z,2n)	

Table 115: ENDF/B-VII.1 library, file: `t-001_H_003.endf`

MF	MT	Description	Energy range [MeV]
3		Reaction cross sections	
	2	(z,z0)	(0.00, 2.00)
	16	(z,2n)	(0.00, 20.00)
6		Energy-angle distributions for emitted particles	
	2	(z,z0)	
	16	(z,2n)	

Table 116: CP2011 library, file: `t-001_H_003.endf`

MF	MT	Description	Energy range [MeV]
3		Reaction cross sections	
	2	(z,z0)	(0.00, 20.00)
	16	(z,2n)	(0.00, 20.00)
6		Energy-angle distributions for emitted particles	
	2	(z,z0)	
	16	(z,2n)	

Table 117: ENDF/B-VIII.0 library, file: `t-001_H_003.endf`

MF	MT	Description	Energy range [MeV]
3		Reaction cross sections	
	2	(z,z0)	(0.00, 2.00)
	16	(z,2n)	(0.00, 20.00)
6		Energy-angle distributions for emitted particles	
	2	(z,z0)	
	16	(z,2n)	

Table 118: CP2020 library, file: `t-001_H_003.endf`

MF	MT	Description	Energy range [MeV]
3		Reaction cross sections	
	2	(z,z0)	(0.10, 14.00)
	50	(z,n_0)	(8.39, 14.00)
	51	(z,n_1)	(12.23, 14.00)
6		Energy-angle distributions for emitted particles	
	2	(z,z0)	
	50	(z,n_0)	
	51	(z,n_1)	

Table 119: CP2011 library, file: `t-002_He_004.endf`

MF	MT	Description	Energy range [MeV]
3		Reaction cross sections	
	2	(z,z0)	(0.14, 20.00)
6		Energy-angle distributions for emitted particles	
	2	(z,z0)	

Table 120: ENDF/B-VIII.0 library, file: `t-002_He_004.endf`

MF	MT	Description	Energy range [MeV]
3		Reaction cross sections	
	2	(z,z0)	(0.10, 20.00)
	50	(z,n_0)	(8.39, 20.00)
	51	(z,n_1)	(12.28, 20.00)
	52	(z,n_2)	(14.65, 20.00)
	600	(z,p_0)	(13.18, 20.00)
	650	(z,d_0)	(10.98, 20.00)
6		Energy-angle distributions for emitted particles	
	2	(z,z0)	
	50	(z,n_0)	
	51	(z,n_1)	
	52	(z,n_2)	
	600	(z,p_0)	
	650	(z,d_0)	

Table 121: CP2020 library new evaluation, file: `t-002_He_004.endf`

B Codes Used to Produce Evaluated Data

Name: C5TOEDA

- Purpose: Data-handling
- Author: M. Paris
- Description: Convert C5 formatted data from EXFOR-CSISRS database (http://www.nndc.bnl.gov/exfor/) to EDA-native formatted observable data file (EDA5 expected filename: DATA); features include handling of integrated and total cross sections and unpolarized differential cross section angular distributions (equivalently, excitation functions) and conversion of laboratory reference frame angular distributions to center-of-mass frame angular distributions at relativistic kinematics; depends on Perl modules (written by M. Paris): EXFOR ::X4TOOLS, EXFOR::C4TOOLS, NUCLEI::NUCPROPS, LORENTZ::LAB2CM, LORENTZ::RELLAB2CM
- Current version: v1.0.1
- Language: Perl5
- Lines (approx.): 1k
- License: NA
- Version control: https://github.com/mwparis/c5toeda
- External collaborators/funding: NCSP

Name: EDA6

- Purpose: Development code; primarily used for generating input decks for EDA5
- Author: M. Paris
- Description: modern FORTRAN (Fortran2018) EDA development code; object-oriented code development project; permits integration of new physics models to allow evaluations to go to higher projectile energies by direct incorporation of break-up spectra, currently handled by post-processing auxiliary codes (SPECT code by Hale) into the fit; EDA6 is primarily used to currently to adapt existing EDA5 parameter decks to include more resonance parameters and for generating `MF=2, MT=151` representations of existing evaluations; features interoperability with C/C++ for full integration with NJOY 21 and public release of EDA verification code, VEDA
- Current version: v1.0.0
- Language: Fortran2019
- Lines (approx.): 4.3k
- License: BSD (planned)
- Version control: NA
- External collaborators/funding: NA

Name: EDAF90

- Purpose: Post-processing; graphical representation; NJOY interface capability
- Authors: R. MacFarlane, M. Paris

- Description: modern Fortran (Fortran90/95) implementation of EDA; original code development by R. MacFarlane; modification for modern compilers/platforms by M. Paris in FY2020 (as part of CPT L2 Milestone); EDAF90 represents integration between light-element evaluation work and NJOY21 processing (to continuous-energy and multigroup library formats) and graphical representations of data; EDAF90 generates NJOY16/NJOY21 input decks; permits comparison of evaluated cross sections (in applications and graphically) between previous evaluations and library formats (evaluated cross section vs. experimental data); facilitates resonance parameter (`MF=2, MT=151`) representations of the evaluated cross sections
- Current version: v5.1.1
- Language: Fortran90
- Lines (approx.): 28k
- License: NA
- Version control: NA
- External collaborators/funding: NA

- EDA5: General multi-channel, multi-level R-matrix code for analyzing all types of measured data for reactions in light nuclei.
  - Current version (eda5) is operating in stable, production mode. Dates back to FY05 [earlier versions of EDA go back to 1972]. Programming language: F77. Lines = 18670 . No license; developed in-house. Prospect - newer, more modern version (eda6) is under development by M. Paris.

- SPECT: Calculates spectra for 3-body breakup reactions from a single-level, single-channel resonance model, and converts them to ENDF-6 format.
  - Current version (spect2bi) is operating in stable, production mode. Dates back to FY19 [earlier versions of SPECT go back to 2003]. Programming language: F77. Lines = 640. No license; developed in-house. Prospect - needs to be generalized to a multi-level, multi-channel resonance model that makes full use of the R-matrix parameters we have found for describing reactions in light systems. The theory has been developed, but the numerical implementation will be challenging.

- ENDFOR: Converts EDA5 calculations of cross sections to ENDF-6 format.
  - Current version (endfori) is operating in stable, production mode. Dates back to FY16 [earlier versions of ENDFOR go back to 2002]. Programming language: F77. Lines = 395. No license; developed in-house. Prospect - may be replaced by newer ENDF-formatting toolkit if its capabilities are duplicated.

- STEEP: Calculates Maxwellian-averaged reaction rates, lab spectra for outgoing particles.
  - Current version (stpm8i) is operating in stable, production mode. Dates back to FY19 [earlier versions of STEEP go back to 1976]. Programming language: F77. Lines = 3230. No license; developed in-house. Prospect - may be incorporated into NJOY processing code.

- NDIOUT: Converts STEEPM calculations to NDI-formatted files.
  - Current version (ndiout7) is operating in stable, production mode. Dates back to FY07 [earlier versions of NDIOUT go back to 2004]. Programming language: F77. Lines = 263. No license; developed in-house. Prospect - may be incorporated into NJOY processing code.
- COVAR: Uses calculated derivatives and parameter covariances from eda5 to produce evaluated cross-section covariances in ENDF-6 format.
  - Current version (covar2) is operating in stable, production mode. Dates back to FY17 [earlier versions of COVAR go back to 2008]. Programming language: F77. Lines = 140. No license; developed in-house.
- ANGCOV: Uses calculated derivatives and parameter covariances from EDA5 to produce covariances for evaluated Legendre coefficients in ENDF-6 format.
  - Current version (angcov2a) is operating in stable, production mode. Dates back to FY17 [earlier versions of ANGCOV go back to 2010]. Programming language: F77. Lines = 283. No license; developed in-house.

References

[1] Gerald M. Hale, D. Kent Parsons, and Morgan White. *ACE Library CP2011 Charged Particles Incident on Light Isotopes*. Memorandum XCP-5: MCW-12-004(U). Los Alamos National Laboratory, Oct. 20, 2011.

[2] Gerald M. Hale and Morgan White. *NDI MG Library CP2011 Charged Particles Emissions from Neutrons Incident on Light Isotopes*. Memorandum XCP-5: MCW-12-005(U). Los Alamos National Laboratory, Oct. 24, 2011.

[3] Charles M. Snell and Morgan White. *DEDX2011 Continuous Slowing Down Data Library*. Memorandum XCP-5: MCW-12-003(U). Los Alamos National Laboratory, Oct. 20, 2011.

[4] ASC/PEM/Nuclear Data Project. *Charged particle nuclear data / milestones*. https://xcp-stash.lanl.gov/projects/CPND/repos/milestones. Dec. 2019.

[5] G.M. Hale and D.C. Dodder. "R-matrix analysis of light-element reactions for fusion applications". In: *Nuclear cross sections for technology: proceedings of the international conference*. Ed. by J.L. Fowler and C.H. Johnson and C.D. Bowman. 1979, pp. 650–658.

[6] G.M. Hale, D.C. Dodder and J.C. DeVeaux. "Charged-particle elastic cross sections". In: *Nuclear Data for Science and Technology*. Ed. by K.H. Böckhoff. 1983, pp. 326–330.

[7] M. Paris, G. Hale, A. Hayes-Sterbenz and G. Jungman. "R-matrix Analysis of Reactions in the ^{9}B Compound System". In: 120.0 (2014), pp. 184–187.

[8] D.A. Brown et al. "ENDF/B-VIII.0: The 8th Major Release of the Nuclear Reaction Data Library with CIELO-project Cross Sections, New Standards and Thermal Scattering Data". In: *Nucl. Data Sheets* 148 (2018), pp. 1–142. DOI: 10.1016/j.nds.2018.02.001.

[9] A.J. Koning, S. Hilaire and M.C. Duijvetijn. "TALYS-1.0". In: *International Conference on Nuclear Data for Science and Technology 2007*. 2008. DOI: https://doi.org/10.1051/ndata:07767.

[10] A.J. Koning and D. Rochman and J.-Ch. Sublet and N. Dzysiuk and M. Fleming and S. van der Marck. "TENDL: Complete Nuclear Data Library for Innovative Nuclear Science and Technology". In: *Nucl. Data Sheets* 155 (2019), pp. 1–55. DOI: https://doi.org/10.1016/j.nds.2019.01.002. URL: http://www.sciencedirect.com/science/article/pii/S009037521930002X.

[11] A. Trkov, M. Herman, and D.A. Brown. *ENDF-6 Formats Manual*. Report BNL-203218-2018-INRE. National Nuclear Data Center. Oct. 2019.

[12] R.E. MacFarlane et al. *The NJOY Nuclear Data Processing System, Version 2016*. LA-UR-17-20093. Los Alamos National Laboratory. Dec. 2016. URL: http://www.njoy21.io.

[13] C. Snell. *Monte Carlo CP/CP cross sections, scatters and RIF's*. Memorandum XCP-8. Los Alamos National Laboratory, 2011. URL: https://xcp-stash.lanl.gov/projects/CPND/repos/milestones/browse/cp2011/doc/memos/snell-acereacs.pdf.

[14] C. Snell. *Neutron/CP scatters and reactions-in-flight*. Memorandum XCP-8. Los Alamos National Laboratory, 2011. URL: https://xcp-stash.lanl.gov/projects/CPND/repos/milestones/browse/cp2011/doc/memos/snell-ndineutcp.pdf.

[15] C. Snell. *Thermonuclear burn 'TN' reaction data*. Memorandum XCP-8. Los Alamos National Laboratory, 2011. URL: https://xcp-stash.lanl.gov/projects/CPND/repos/milestones/browse/cp2011/doc/memos/snell-data3_dedx_tn_ndi_ace.pdf.

[16] Harold H. Rogers. *Thermonuclear Burn: Charged-Particle Transport: Part I*. Research Note X2: RN 00-015(U). Los Alamos National Laboratory, May 23, 2000. URL: https://xcp-stash.lanl.gov/projects/CPND/repos/milestones/browse/cp2011/doc/memos/aux/rogers-tn_burn_cpt_part_1-2000.pdf.

[17] Harold H. Rogers. *Thermonuclear Burn: Charged Particle Transport: Part II*. Research Note X2: RN 00-016(U). Los Alamos National Laboratory, May 24, 2000. URL: https://xcp-stash.lanl.gov/projects/CPND/repos/milestones/browse/cp2011/doc/memos/aux/rogers-tn_burn_cpt_part_2-2000.pdf.

[18] Harold H. Rogers. *Thermonuclear Burn: Charged Particle Transport: Part III*. Research Note X2: RN 01-004(U). Los Alamos National Laboratory, Feb. 9, 2001. URL: https://xcp-stash.lanl.gov/projects/CPND/repos/milestones/browse/cp2011/doc/memos/aux/rogers-tn_burn_cpt_part_3-2001.pdf.

[19] Harold H. Rogers. *Thermonuclear Burn: Charged Particle Transport: Part IV*. Research Note X2: RN 01-035(U). Los Alamos National Laboratory, June 21, 2001. URL: https://xcp-stash.lanl.gov/projects/CPND/repos/milestones/browse/cp2011/doc/memos/aux/rogers-tn_burn_cpt_part_4-2001.pdf.

[20] Lowell S. Brown, Dean L. Preston and Robert L. Singleton. "Charged particle motion in a highly ionized plasma". In: *Phys. Rept.* 410 (2005), pp. 237–333.

[21] V.V. Zerkin and B. Pritychenko. "The experimental nuclear reaction data (EXFOR): Extended computer database and Web retrieval system". In: *Nuclear Instruments and Methods in Physics Research Section A: Accelerators, Spectrometers, Detectors and Associated Equip-*

ment 888 (2018), pp. 31–43. ISSN: 0168-9002. DOI: https://doi.org/10.1016/j.nima.2018.01.045. URL: https://www.nndc.bnl.gov/exfor/.

[22] D. Wiarda, M. L. Williams, C. Celik, and M. E. Dunn. "AMPX-2000: A cross-section processing system for gener- ating nuclear data for criticality safety applications". In: *International Conference on Nuclear Criticality Safety (ICNC 2015)*. 2015.

[23] Bret R. Beck. "FUDGE: A Program for Performing Nuclear Data Testing and Sensitivity Studies". In: *AIP Conference Proceedings* 769.1 (2005), pp. 503–506. URL: https://aip.scitation.org/doi/abs/10.1063/1.1945057.

[24] C. M. Mattoon and B. R. Beck. "Designing a new structure for storing nuclear data". In: *The European Physical Journal A* 51.12 (Dec. 24, 2015), p. 183. URL: https://doi.org/10.1140/epja/i2015-15183-y.

[25] D.E. Cullen. *PREPRO 2019: 2019 ENDF/B Pre-processing Codes*. Report IAEA-NDS-220. Aug. 20, 2019.

[26] J. M. Campbell, J. C. Comly, S. C. Frankle, and R. C. Little. *A Nuclear Data Interface for the ASCI Codes(U)*. Report LA-UR-98-5428. Oct. 1, 1998.

[27] Thomas G. Saller. *Release of NDI 2.1.4α*. Memorandum CCS-2:20-003. Jan. 15, 2020.

[28] Brian S. Triplett, Morgan C. White and Samim Anghaie. "Development of a Test System for Verification and Validation of Nuclear Transport Simulations". In: *International Conference on the Physics of Reactors*. PHYSOR. Kursaal Conference Center, Interlaken, Switzerland, 2008.

[29] *ENDF-6 Formats Manual, Erratum*. An error in the n-body phase space distriubtion (LAW=6), Sec. 6.2.7 in the 2012 ENDF-6 manual, was corrected by G. Hale 2016 ENDF-6 manual, Sec. 6.2.8. 2016.

[30] M.B. Chadwick et al. "ENDF/B-VII.0: Next Generation Evaluated Nuclear Data Library for Nuclear Science and Technology". In: 107.12 (2006). Evaluated Nuclear Data File ENDF/B-VII.0, pp. 2931–3060.

[31] Philip R. Page and Gerald M. Hale. "8Be Nuclear Data Evaluation". In: *AIP Conference Proceedings* 769.1 (2005), pp. 390–393. DOI: 10.1063/1.1945030. URL: https://aip.scitation.org/doi/abs/10.1063/1.1945030.

[32] Philip R. Page. "New broad Be-8 nuclear resonances". In: *Phys. Rev. C* 72 (2005), p. 054312. DOI: 10.1103/PhysRevC.72.054312.

[33] D. Kent Parsons. *Release of the CP2011 Charged Particle Cross Section Library for MCNP6*. Memorandum XCP-5: 13-018. Los Alamos National Laboratory, June 6, 2013.

[34] D. Kent Parsons. *Release of the CP2011 Charged Particle Cross Section Library for MCNP6*. Report LA-UR-14-23361. Los Alamos National Laboratory, 2014.

[35] Gerald M. Hale. *R-matrix evaluation of ^{6}Li system*. Private communication. 2013.

[36] Toshihiko Kawano. "DeCE: the ENDF-6 data interface and nuclear data evaluation assist code". In: *Journal of Nuclear Science and Technology* 56.11 (2019), pp. 1029–1035.

[37] C.J. Werner. *MCNP6.2 Release Notes*. report LA-UR-18-20808. Los Alamos National Laboratory, 2018.

[38] Wim Haeck. XCP-5/LANL, Private communication. 2020.

[39] Mark G. Gray. XCP-5/LANL, Private communication. 2019.

[40] Skip Kahler. T-2/LANL, Private communication. 2011.
[41] Gerald M. Hale. *R-matrix evaluation of ^{7}Li system*. Private communication. 2011.
[42] Gerald G. Ohlsen. "Polarization transfer and spin correlation experiments in nuclear physics". In: *Rep. Prog. Phys.* 35 (1972), pp. 717–801.
[43] A. M. Lane and R. G. Thomas. "R-Matrix Theory of Nuclear Reactions". In: *Rev. Mod. Phys.* 30 (2 Apr. 1958), pp. 257–353. DOI: 10.1103/RevModPhys.30.257.
[44] M. Paris, W. Haeck, G. Hale and Ian Thompson. *Proposal to CSEWG Clarification of R-Matrix Limited format Relativistic flag KRL for LRF=7 formatting*. https://indico.bnl.gov/event/6642/contributions/31557/. 2019.
[45] A.D. Carlson et al. "Evaluation of the Neutron Data Standards". In: 148 (2018). Special Issue on Nuclear Reaction Data, pp. 143–188. ISSN: 0090-3752. DOI: https://doi.org/10.1016/j.nds.2018.02.002. URL: http://www.sciencedirect.com/science/article/pii/S0090375218300218.
[46] Satoshi CHIBA et al. "Double-Differential Neutron Emission Cross Sections of 6Li and 7Li at Incident Neutron Energies of 4.2, 5.4, 6.0 and 14.2 MeV". In: *Journal of Nuclear Science and Technology* 22.10 (1985), pp. 771–787. URL: https://doi.org/10.1080/18811248.1985.9735728.
[47] Chad Forrest and others. Private communication. 2020.
[48] Gerald M. Hale. T-2/LANL, Private communication. 2020.
[49] R. J. S. Brown et al. "Elastic Scattering of Deuterons by He^3". In: *Physical Review* 96.1 (1954), p. 80. DOI: 10.1103/PhysRev.96.80. URL: http://dx.doi.org/10.1103/PhysRev.96.80.
[50] J. E. Brolley et al. "Hydrogen-Helium Isotope Elastic Scattering Processes at Intermediate Energies". In: *Physical Review* 117 (1960), p. 1307. DOI: 10.1103/PhysRev.117.1307. URL: http://dx.doi.org/10.1103/PhysRev.117.1307.
[51] T. A. Tombrello, R. J. Spiger, and A. D. Bacher. "Deuteron Elastic Scattering from He^3 and H^3". In: *Physical Review* 154.4 (1967), p. 935. DOI: 10.1103/PhysRev.154.935. URL: http://dx.doi.org/10.1103/PhysRev.154.935.
[52] N. Jarmie and J. H. Jett. "Various Cross Sections for $A \leq 3$ Nuclei". In: *Physical Review, Part C, Nuclear Physics* 10.1 (1974), p. 54. DOI: 10.1103/PhysRevC.10.54. URL: http://dx.doi.org/10.1103/PhysRevC.10.54.
[53] B. Jenny et al. "Analyzing-Power and Cross-Section Measurements for ^{3}He(d,d)^{3}He Scattering". In: *Nuclear Physics, Section A* 324.1 (1979), p. 99. DOI: 10.1016/0375-9474(79)90080-0. URL: http://dx.doi.org/10.1016/0375-9474(79)90080-0.
[54] Gerald M. Hale. T-2/LANL, Private communication. 2001.
[55] Wim Haeck. *Charged particles with a LAW=5 and LIDP=1*. XCP-5/LANL, 2019. URL: https://github.com/njoy/NJOY2016/issues/138.
[56] G.M. Hale. "Formats and related issues: Error in `LAW=6` phase-space distributions". In: *Cross Section Evaluation Working Group*. Ed. by D. Brown, M. Herman, A. Sonzogni, M. Chadwick, A. Kahler, Y. Danon, D. Smith, M. Dunn and G. Nobre. Meeting Minutes. 2016, p. 31.

[57] C.L. Dunford. *ENDF utility codes release 7.01/02*. Report. Brookhaven National Laboratory, 2005.

[58] D.R. Harris, D.E. Dei, A.A. Husseiny, Z.A. Sabri and G.M. Hale. *The STEEP4 code for Computation of Specific Thermonuclear Reaction Rates from Pointwise Cross Sections*. Report LA-6344-MS. Los Alamos Scientific Laboratory, 1976.

[59] D. Kent Parsons. *The Rules of CHECKACE – a Suite of Checking Codes for MCNP ACE Cross Section Files*. Memorandum XCP-5:15-032. Apr. 16, 2015.

[60] Joann Campbell and D. Kent Parsons. *The Rules of CHECKMG – a Checking Code for NDI XS Data Tables*. Memorandum XCP-5:11-008(U). Feb. 16, 2011.

[61] Gerald M. Hale. *Resonance model for the three-body final state of the t + t reaction*. T-2/LANL, Private communication. 2016.

[62] Mark G. Gray. *The Algebraic Structure of the Multigroup Approximation*. Memorandum X-1:09-084(U). Los Alamos National Laboratory, Dec. 9, 2009.

[63] Morgan White. *KERMA Data By Reaction For ^{6}Li (U)*. Memorandum XCP-5: MCW-10-001(U). Los Alamos National Laboratory, Jan. 5, 2010.

[64] Mark G. Gray. *Kerma Enhancements in NDI*. Memorandum XCP-5:11-004(U). Los Alamos National Laboratory, Jan. 5, 2011.

[65] Mark G. Gray. *Energy Non-conservation with NDI Multi-temperature Multigroup Total KERMA Data*. Memorandum XCP-5:15-010. Los Alamos National Laboratory, Jan. 20, 2016.

[66] Clell J. Solomon and Charlie Snell and Joann Campbell. *Comparison of Tabulated and Calculated KERMAs in the NDI CP2011 Data*. Memorandum XCP-2:19-008. Los Alamos National Laboratory, Nov. 18, 2019.

[67] Clell J. Solomon, Charlie Snell and Joann Campbell. *Apparent Discrepancies Between Multigroup CP2011 and Transport Libraries*. Memorandum XCP-2:19-006Rev1. Los Alamos National Laboratory, June 18, 2019.

[68] Ian Thompson and Caleb Mattoon. *ENDF/B sets for CP2020*. Private communication. 2020.

[69] R.J. Howerton, R.E. Dye and S.T. Perkins. "Evaluated Nuclear Data Library". In: *An Integrated System for Production of Neutronics and Photonics Calculational Constants*. UCRL-50400. 1981.

[70] Clell J. Solomon, Joann Campbell, Jon Dahl, Hye Young Lee and Ian Thompson. *ASC-PEM L2 Milestone 7174 Committee Review*. Report. Los Alamos National Laboratory, 2020.

[71] D. Kent Parsons, Cecile Toccoli, and Jeremy L. Conlin. "Verification of the Re-Released ENDF/B VIII.0 Based Thermal Scattering Libraries". In: *Winter 2020 Meeting, American Nuclear Society*. 2020.

[72] D. E. Cullen, L. F. Hansen, E. M. Lent, and E. F. Plechaty. *Thermal scattering law data: Implementation and testing using the Monte Carlo neutron transport codes cog, mcnp and tart*. Report UCRL-ID-153656. 2003.

[73] J.L. Conlin and D.K. Parsons. *Release of Continuous Representation for $S(\alpha, \beta)$ ACE Data*. Report LA-UR-14-21878. 2014.

[74] Mark Paris and Patrick Talou. *ASC-PEM-Nuclear Physics: FY20 L2 Milestone on CPT Libraries (MRT #7127)*. Memorandum. Oct. 1, 2019. URL: https://xcp-stash.lanl.

gov/projects/CPND/repos/milestones/browse/cp2020/doc/plans/L2-CPT-FY20-plan-to-MFrancois.pdf.

[75] Neudecker, Denise et al. "Template for estimating uncertainties of measured neutron-induced fission cross-sections". In: *EPJ Nuclear Sci. Technol.* 4 (2018), p. 21. DOI: 10.1051/epjn/2018026. URL: https://doi.org/10.1051/epjn/2018026.

MWP : MWP